QUARK OFF-SHELLNESS EFFECT ON PARTON DISTRIBUTIONS

Dissertation zur Erlangung des Doktorgrades
der Naturwissenschaftlichen Fakultät
der Justus-Liebig-Universität Gießen
Fachbereich 7 - Mathematik und Informatik, Physik, Geographie

Vorgelegt von

Olena Linnyk

aus Vinnytsya, Ukraine

· Gießen 2006 ·

Dekan: Prof. Dr. Volker Metag
I.Berichterstatter: Prof. Dr. Ulrich Mosel
II. Berichterstatter: PD Dr. Stefan Leupold
Tag der mündlichen Prüfung: 15.09.2006

QCD nowadays has a split personality. It embodies "hard" and "sof" physics, both being hard subjects and the softer the harder.

Y. L. Dokshitzer

Contents

iii

Acknowledgments

Being forever indebted to my whole family for sharing every day of my live, I especially thank my father for his wisdom and kindness, my mother for motivation and support and my dear sister for inspiration and understanding.

Chapter 1

Introduction

Hadron physics studies strongly interacting matter in terms of its building blocks, quarks and gluons. An important step towards this goal is a description of the internal structure for the proton and neutron. The proton is a stable (life time $> 2.1 \cdot 10^{29}$ years [1]) particle occurring in all atomic nuclei. It is the positively charged core of the hydrogen atom, which is the most abundant element in the universe. Indeed, hydrogen and helium (the nucleus of which consists of two protons and two neutrons) make up about 80% and 20% of all the matter in the universe respectively [2, 3]. Consequently, protons account for most of the mass in matter. The proton is a composite system consisting of quarks and gluons. Our research aims to improve the current understanding of the proton structure.

Quantum chromodynamics (QCD) is the theory of strong interaction with quarks and gluons as elementary degrees of freedom. Protons and neutrons are held together in nuclei by the residual effects of the strong force, just as molecular Van-der-Waals forces are residual effects of Coulomb's law. QCD is a quantum field theory based on the local interaction and local gauge SU(3) symmetry principles [4]. The proton is interpreted as a solution of QCD with given quantum numbers. However, a mathematical description of proton structure by directly solving QCD could not be achieved so far. The reason is that the infinite number of degrees of freedom (usual for quantum field theories) and the non-linear interaction of gluons (specific to non-Abelian QCD) lead to enormous complications.

In the quest of gaining better insight into the structure of the proton, we apply methods, that have proven useful in the investigation of nuclear structure, namely, the electron scattering analysis, assumptions of factorization,

and the spectral function method widely used in many-body calculations. At the same time, we take into account the specific properties of the quark interaction dictated by QCD. Fortunately, due to the asymptotic freedom property of QCD, the strong coupling becomes small at very high energy exchange. In this limit, one can apply perturbation theory to describe high energy quark (gluon) scattering. On the other hand, the experimental evidence shows that it is more favorable to create a cloud of quark-antiquark pairs, thus creating additional hadrons, than to extract a single quark from the parent hadron. This prevents one from using quarks and gluons as asymptotic scattering states, as stated by the confinement hypothesis. Philosophically, this makes application of perturbation theory to hadron scattering impossible [5]. In practice though, one relates the perturbative quark (gluon) scattering sub-processes to the observables by the factorization method, explained below.

The factorization assumption states that in high energy hadronic processes like deep inelastic scattering (DIS), Drell-Yan high mass lepton pair production, jet production, *etc.* the soft and hard sub-processes can be disentangled. The hard part can be calculated using the well established methods of perturbative QCD (pQCD). The perturbative expansion is applicable for this quantity, because due to asymptotic freedom, the coupling constant α_S is small at the large characteristic momenta of the hard scattering sub-diagram. The hard part of the cross section is process-dependent and contains information on the kinematics rather than on the structure of the participating hadron. The soft part is process independent and describes the quark and gluon properties in the bound state. However, calculating this part of the cross section from the QCD lagrangian is extremely complicated due to the infinite number of strongly interacting degrees of freedom. One extracts the soft part from a measurement of some high energy process and verifies it by predicting a different process.

The described factorization of soft and hard parts of the cross section is analogous to plane wave impulse approximation (PWIA) for the quasi-elastic $(e, e'p)$ scattering in nuclear physics. There, the approximation of quasi-free constituent nucleons is valid, if the binding energy is small as compared to the energy transfer. In the theory of nuclei, initial (ISI) and final state interaction (FSI) effects are known to be essential for understanding of semi-exclusive observables. Measurements, in which the energy and momentum of the nucleon can be determined from the final state kinematics, offer an opportunity to

study these effects beyond the PWIA and thus to probe the nucleon interaction in nuclei [6,7]. This is usually done by employing the concept of the spectral function [8]. Bound nucleons or those that interact in the initial or final state can no more be described by asymptotic, free, on-the-mass-shell states. In other words, the energy-momentum relation for the probed nucleon is not given by a simple formula $\epsilon^2 - \vec{p}_N^2 = M_N^2$. Such particles are termed off-shell and their wave functions are written as a combination of all possible free states with weighing factors, which appear in the cross section as a spectral function. The physical meaning of the nucleon spectral function $\mathrm{Sp}(\epsilon, \vec{p}_N)$ is the probability to probe a nucleon with a given energy-momentum relation.

The initial and final state quark interaction effects on hard scattering cross sections in hadron physics have recently attracted a lot of attention. The essential role of final state interactions in the interpretation of the measured DIS structure functions has been stressed in [9–11]. In several other calculations [12–15], non-collinear kinematics, *i.e.,* non-vanishing primordial transverse momenta of the quarks in the nucleon, were considered. The authors of [16,17] pointed out that a single gluon exchange in the initial state can produce a large effect in πp scattering in the framework of a quark-diquark model. On the other hand, as we will show in chapter 4, the quark off-shellness effects in DIS and the Drell-Yan process have the same order of magnitude as those of the intrinsic transverse momentum [18,19]. A consistent treatment of both is necessary in order to go beyond the PWIA in hard reactions.

In Chapter 3, the formalism is developed to study these effects and apply it to calculate the cross sections of deep inelastic ep scattering and the Drell-Yan pair production in $pp \to l^+l^-X$, $pA \to l^+l^-X$, $\bar{p}p \to l^+l^-X$. Our aim is to investigate observables and kinematical regions, for which collinear factorization and low-order perturbative QCD no longer work and where we thus need to model nonperturbative effects, *i.e.* go beyond the PWIA.

The analogy to nuclear physics suggests that the triple differential Drell-Yan cross section, which is a more exclusive observable than the DIS cross section, is more sensitive to the ISI. The results of our calculations confirm this expectation. By taking into account both the finite width and the non-collinearity of quarks, both being generated by ISI, we reproduce the experimentally measured fully inclusive DIS cross section and the triple-differential cross section of the Drell-Yan process very well.

Our success in describing the transverse momentum distribution of the

Drell-Yan lepton pairs $d\sigma/dM^2 dx_F dp_T$ is particularly interesting, since the collinear pQCD result for this triple differential cross section disagrees with the experiment by a large factor. In leading order of pQCD, a delta function at zero transverse momentum is predicted. Among the next-to-leading order (NLO) contributions to the dilepton (l^+l^-) cross section, the gluon Compton scattering can generate large transverse momentum p_T. However, this only exists in the region of very high p_T: $p_T \geq \sqrt{M}$, where M is the mass of Drell-Yan pair. In contrast, the major part of the measured pairs lies in the interval $0 < p_T < \sqrt{M}$, which, at NLO of pQCD, can be attributed only to gluon Bremsstrahlung. But the average p_T generated by $\bar{q}q \rightarrow \gamma^* g$ is too low to explain experimental data. Another problem of pQCD calculations is that the p_T spectrum of the Drell-Yan pairs has a singularity at $p_T = 0$ in every order. Phenomenologically regularized Sudakov resummation of the whole series [20] can be done on the level of the double differential cross section. However, accounting for the non-collinearity of quarks in the intrinsic-k_T approach [21] is necessary to bring calculations to qualitative agreement with data on triple differential cross section. Still, none of the aforesaid models is able to reproduce simultaneously the magnitude and shape of the experimentally observed p_T-distribution. In contrast, as we will demonstrate below in Section 4.3, the data can be successfully described by a model, which allows for off-shell quarks.

Chapter 2 of the thesis is dedicated to the basic definitions and known results concerning electron scattering in general, DIS in particular, and the Drell-Yan process.

The parton model, intrinsic-k_T approach, parton distributions in QCD (including the unintegrated and polarized ones) are explained. In the end of the chapter, we enlist some of the open problems of the standard approaches.

We propose a new model using phenomenological quark virtuality distribution in Chapter 3. The chapter starts with a discussion of factorization in hard scattering processes. Reviewing the Wigner function and its relation to the parton distributions in Section 3.2, we introduce an unintegrated k_T-dependent parton distribution (with a single parameter D) and a fully unintegrated ones, incorporating a quark off-shellness distribution (with a single parameter Γ). In Section 3.4 and 3.5, we formulate the cross sections of DIS and the Drell-Yan process in the intrinsic-k_T approach and in our model, which take into account the fact that the quarks inside the nucleon are off-shell.

Chapter 4 covers the results of our studies aimed at understanding the role

of quark off-shellness in hard scattering processes. Using formulas derived in Chapter 3 we calculate the DIS cross section at different values of the model parameters (intrinsic k_T dispersion and quark width) and compare it to the leading order result of pQCD (the parton model) in Section 4.1. The Drell-Yan process calculated in the framework of the same two models is presented in Section 4.2.

We fit experimental data on the Drell-Yan process with pp and pA initial state in Sections 4.3.1 and 4.3.2. As the result of the fits, we show the importance of the initial state interaction in Drell-Yan process, extract the value of the quark width in the proton, confirm the values of the quark transverse momentum dispersion stated in [22], and study Γ variation with M.

We find the exact evolution of the perturbatively generated part of the transverse momentum of the Drell-Yan pair $(p_T)_{pert}$ with the centre of mass energy $\sqrt{s}$ and M in the NLO of pQCD in Section 4.4.

Section 4.5 is dedicated to the explanation of the phenomenological K-factor in our model by accounting for the quark primordial transverse momentum and off-shellness.

Looking at the Drell-Yan cross section in our model in the limit of $s \to \infty$ as a series in $1/s$ in Section 4.6 gives an insight into the twist structure of the phenomenological corrections due to the intrinsic k_T and of those due to the off-shellness of quarks.

The Drell-Yan process at $\sqrt{s} = 5.5$ GeV and $M \leq 4$ GeV will be measured in the scope of the experiment PANDA [23] at FAIR, the future GSI facility. Our successful description of the data at different M and the study of p_T-variation with $\sqrt{s}$ enables us to extrapolating our parameters to the values of $\sqrt{s}$ and M relevant for PANDA. We present a prediction of the Drell-Yan cross section differential in M, x_F and p_T in PANDA kinematics and compare our prediction to the predictions in the intrinsic-k_T approach and in the generator PYTHIA [24] in Section 4.7. We discuss the results and conclude in Chapter 5.

Chapter 2

Background

2.1   Electron scattering

One of the most powerful tools for studying the structure of sub-atomic objects is high energy electron scattering. Since the electron-photon interaction is perfectly described by quantum electrodynamics (QED) [25], electron scattering is a well understood tool to probe the structure of a target. Moreover, the electron final state interaction is negligible due to the relative weakness of the electromagnetic coupling and the point-like nature of the electron. This allows a clean separation of the scattering mechanism and the structure of the object under investigation.

The magnetic moment and charge density distribution of the target can be extracted from a fully inclusive measurement, in which only the scattered electron is detected. However, in order to resolve the complete four-dimensional space-time structure of the target, an inclusive measurement does not suffice, and one has to detect the final state of the target in this case (for example, knock-out reactions, meson production, virtual Compton scattering) [26, 27]. Additionally, one can study photon, neutrino or hadron induced processes [28], providing complimentary information to that obtained from electron scattering, since they access correlations, which do not couple to the (virtual) photon. Nevertheless, electron scattering remains the process of choice in the investigation of nuclear and hadron structure, because it is well understood and easier to deal with experimentally. In this thesis, we concentrate on the question of hadron structure as probed by an unpolarized virtual photon, *i.e.*, in electron scattering and in lepton pair production.

The electron's stability and availability lead to its use in the historical
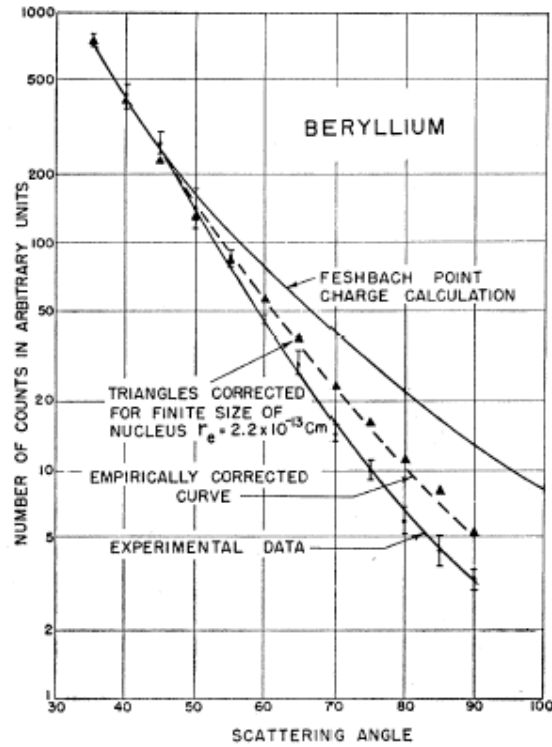
Figure 2.1: Historical proof of a non-vanishing nuclear radius by the Hofstadter group [29].

experiment by R. Hofstadter and collaborators. In this experiment, the nuclear radius has been measured for the first time in 1953. Fig. 2.1 is taken from the original paper by R. Hofstadter *et al.* [29] and presents the cross section of the inclusive process $e\text{Be} \to e'X$ as a function of the electron scattering angle. The experimental data are compared to calculations assuming a point-like nature of the nuclei (solid curve) and to calculations corrected to take into account the finite nuclear size (dashed curve). The data favor the assumption that the nuclear radius $r \geq 2.2 * 10^{-13}$ cm

This evidence of non-vanishing nuclear radius was based on QED calculations of the angular distribution of the scattered electrons in case of a structureless target. At leading order in the electromagnetic coupling, the scattering is modelled by the exchange of a single virtual photon (having 4-momentum q) between the incident electron and the target (nucleon or nucleus) [30], as seen in Fig. 2.2. For a spin $\frac{1}{2}$ target, the angular distribution of the scattered
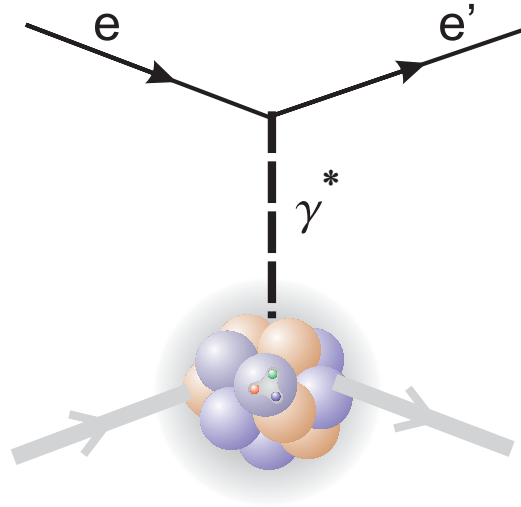
Figure 2.2: Electron scattering in the Born approximation.

electrons is given by the Rutherford cross section [30]

$$\left(\frac{d^2\sigma}{d\Omega}\right)_M = \frac{4Z\alpha^2 E'^2 \cos^2(\theta/2)}{Q^4}, \tag{2.1}$$

where $\alpha \equiv e^2/4\pi$ is the fine structure constant, E' is the energy of the scattered electron, $Q^2 \equiv -q^2$ the momentum transfer, Z the charge of the target in the units of electron charge. Additionally taking into account the target recoil, one arrives at the Mott cross section [31, 32]

$$\left(\frac{d^2\sigma}{d\Omega}\right)_R = \frac{4Z\alpha^2 E'^2}{Q^4} \left(\cos^2(\frac{\theta}{2}) + \frac{q^2}{2m_p^2}\sin^2(\frac{\theta}{2})\right) \tag{2.2}$$

of elastic electron scattering off another point-like charged particle with spin $\frac{1}{2}$ and mass m_p.

The dependence of the lepton scattering cross section on $Q^2 \equiv -q_\mu q^\mu$ also provides evidence of the target structure. As one can see in Fig. 2.3(a), the probability of elastic eC scattering falls rapidly with the momentum transfer. In contrast, fro a point-like target, the elastic scattering cross section does not change with Q^2 (*cf.* the scaling in DIS, Sect. 2.3.1). Thus, the elastic eC scattering data implies finite radius of the target charge distribution. This reflects a decreasing probability for the target to remain intact (in the ground state) after the interaction [33]. On the other hand, the probability of inelastic scattering remains roughly constant with energy. The same behaviour is found,

(a) $e\,C \to eX$ (b) $ep \to eX$
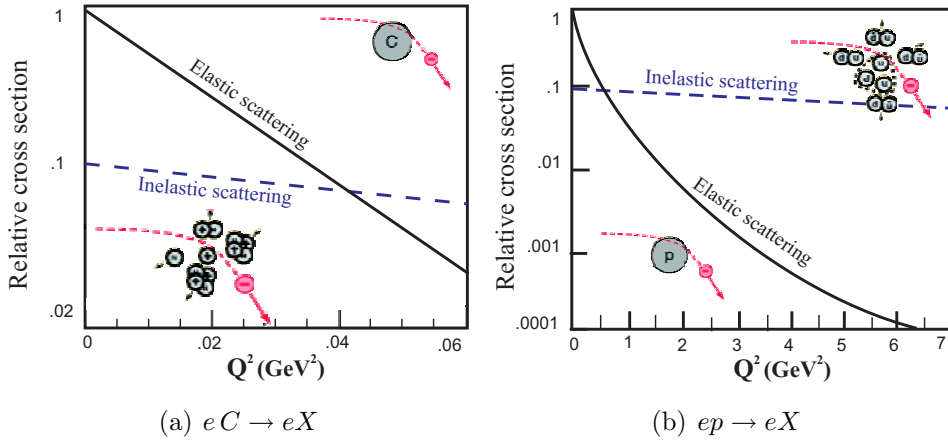
Figure 2.3: Electron scattering off carbon nuclei and off the proton [34].

at much higher energy, in ep scattering, see Fig. 2.3(b).

In the fully inclusive case, the event kinematics in such a process are determined by Q^2 and the Bjorken variable $x_{Bj} \equiv Q^2/2M_N\nu$ [26], where ν is the energy transfer in the target rest frame, and M_N is the nucleon's mass. Selecting different kinematics, we can examine different scattering processes off a nuclei with the mass number A:

- at $x_{Bj} \sim A$, the electron interacts with the entire nucleus, elastic scattering occurs,

- as x_{Bj} decreases from A and energy loss increases, the nucleus is being excited,

- near $x_{Bj} \sim 1$, the quasi-elastic scattering is dominant, the electron knocks out a single nucleon from a nucleus,

- at $x_{Bj} < 1$, the struck nucleon is excited into a resonance state or broken up completely, depending on Q^2.

The study of the proton structure in electron scattering has led to the experimental proof of the existence of quarks and gluons of QCD [35].The discovery of the anomalous magnetic moment of the proton in the experiment of Otto Stern et al [36,37] revealed for the first time the compositeness of the nucleon [25], while the ep scattering measurement at SLAC [38] showed that the proton constituents have quantum numbers of quarks [5].

2.2   Hadron tensor. Structure functions. Form factors

In this section, we briefly review, how one can obtain *quantitative* information on the target structure from electron scattering experiments. We derive unpolarized and polarized scattering cross sections and define electron scattering form factors and structure functions. The line of derivation in this section is based mainly on [26], but the metric has been changed from pseudo-Euclidean to Minkowski for the sake of consistency throughout the thesis.

The first non-vanishing term of the QED perturbative expansion for the scattering matrix $\hat{S}$ gives the following expression called the Born amplitude [26, 39]

$$\hat{S} = 1 + e \int \mathrm{d}^4 x A^\mu(x) \hat{J}_\mu(x), \tag{2.3}$$

where A_μ is the 4-vector potential of the electromagnetic field generated by the electron and satisfies the Maxwell equation [35, 39]

$$(\triangle - \frac{\partial}{\partial t^2}) A_\mu = -4\pi j_\mu, \tag{2.4}$$

where j_μ is the electron current. Plugging the free lepton current

$$j_\mu = -ie(\bar{u}_{\sigma'}(\vec{k}')\gamma_\mu u_\sigma(\vec{k})) \exp\{iq_\nu x^\nu\} \tag{2.5}$$

in (2.4), we obtain the Möller potential [40]

$$A_\mu(x) = -\frac{4\pi ie}{q^2}(\bar{u}_{\sigma'}(\vec{k}')\gamma_\mu u_\sigma(\vec{k})) \exp\{iq_\nu x^\nu\}, \tag{2.6}$$

where $q \equiv k' - k$, $q^2 \equiv q_\mu q^\mu$, u represents the asymptotic (plane wave) state of the electron, which is indexed by the electron momentum k and spin σ [39]. The incoming electron momentum and spin are (k, σ) and the outgoing values are (k', σ'). The bar denotes Dirac conjugation. Then, the scattering matrix is

$$\hat{S} = 1 - i\frac{4\pi e^2}{q^2}(\bar{u}_{\sigma'}\gamma_\mu u_\sigma) \int \mathrm{d}^4 x \hat{J}^\mu(x) \exp\{iq_\nu x^\nu\}. \tag{2.7}$$

The matrix element S_{fi}, which is defined as $S_{fi} \equiv \langle \vec{P}', f | \hat{S} | \vec{P}, i \rangle$ and gives the probability amplitude of the scattering between an initial state i with the

target momentum $\vec{P}$ and a final state f with target momentum $\vec{P}'$, is

$$S_{fi} = \frac{4\pi e^2}{q^2} \left(\bar{u}_{\sigma'}\gamma_\mu u_\sigma\right) 2\pi\delta(\omega + E_i - E_f)\langle\vec{P}', f| \int d\vec{r}\, e^{i\vec{q}\vec{r}}\hat{J}_\mu(\vec{r})|\vec{P}, i\rangle. \qquad (2.8)$$

After the integration over the center of mass motion [26],

$$\begin{aligned}
S_{fi} &= \frac{4\pi e^2}{q^2}\left(\bar{u}_{\sigma'}\gamma_\mu u_\sigma\right)(2\pi)^4\delta(\omega + E_i - E_f)\delta(\vec{P} + \vec{q} - \vec{P}') \\
&\times\langle f| \int d\vec{r}\, e^{i\vec{q}\vec{r}}\hat{J}_\mu(\vec{r})|i\rangle,
\end{aligned} \qquad (2.9)$$

where $\omega \equiv k'^0 - k^0$.

Since the scattering amplitude M_{fi} is defined through [25, 30]

$$S_{fi} \equiv (2\pi)^4\delta(\omega + E_i - E_f)\delta(\vec{P} + \vec{q} - \vec{P}')M_{fi}, \qquad (2.10)$$

then

$$M_{fj} = \frac{4\pi e^2}{q^2}\left(\bar{u}_{\sigma'}\gamma_\mu u_\sigma\right)J_{\mu fi}(\vec{q}). \qquad (2.11)$$

Finally, the differential cross section for electron scattering is

$$d\sigma_{fi} = (2\pi)^4|M_{fi}|^2\delta(\omega + E_i - E_f)\delta(\vec{P} + \vec{q} - \vec{P}')\frac{d\vec{k}'}{(2\pi)^3}\prod_{j=1}^{N}\frac{d\vec{p}_j}{(2\pi)^3}, \qquad (2.12)$$

where N is the number of particles in the final hadron state. $N = 1$ corresponds to elastic scattering. The DIS cross section is given by the same formula, integrated over all possible final states. This corresponds to an energy transfer, which is big enough to "break" the nucleon.

In case of unpolarized scattering, the cross section (2.12) can be decomposed into a product of the lepton tensor $L_{\mu\nu}$ and the hadron tensor $W^{\mu\nu}$

$$\frac{d\sigma}{d\Omega dE'} = \frac{\alpha^2}{q^4}\frac{E'}{E}L_{\mu\nu}W^{\mu\nu}, \qquad (2.13)$$

where

$$\begin{aligned}
W_{\mu\nu} &= \frac{1}{8\pi P^2}\sum_{N,s}\int\prod_{n=1}^{N}\frac{d\vec{p}'_n}{2E'_n(2\pi)^3}(2\pi)^4\delta^4(P + q - \sum_n p'_n) \\
&\times\sum_X\langle p, s|J_\mu^\dagger|X\rangle\langle X|J_\nu|p, s\rangle, \quad (2.14)
\end{aligned}$$

with P the initial momentum of the target, s its spin, and

$$L_{\mu\nu} = 4\left(k_\mu k'_\nu + k_\nu k'_\mu - g_{\mu\nu}(k_\alpha k'_\alpha + m_e^2)\right), \tag{2.15}$$

where m_e is electron mass. The decomposition (2.13) exists, because for every matrix $\hat{O}_\mu$ the following is true [25]

$$\frac{1}{2}\sum_{\sigma,\sigma'} |(\bar{u}_{\sigma'}(\vec{k'})\gamma^\mu u_\sigma(\vec{k}))\hat{O}_\mu|^2 = \frac{1}{4EE'}\eta^{\mu\nu}\hat{O}_\mu\hat{O}_\nu^\dagger, \tag{2.16}$$

where

$$\eta_{\mu\nu} = \frac{1}{2}Sp\{\gamma_\mu(m+\gamma^\alpha k_\alpha)\gamma_\nu(m+\gamma^\beta k'_\beta)\}. \tag{2.17}$$

Rewriting the hadron current in terms of its components

$$\langle X|J|Ps\rangle \equiv J_{fi} = (\rho, \vec{J}) \tag{2.18}$$

and introducing structure functions W_1 and W_2 as

$$W_1 = \langle \vec{J}_{if}^* \cdot \vec{J}_{fi}\rangle, \quad W_2 = \langle \rho_{if}^* \cdot \rho_{fi}\rangle, \tag{2.19}$$

we can write the cross section for the unpolarized scattering of a massless lepton on a hadron in the target rest frame in terms of W_1, W_2 [26]

$$\frac{d^2\sigma}{d\Omega dE'} = \frac{4\alpha^2 E'^2}{Q^4}\left[2W_1(Q^2, x_{Bj})\sin^2(\theta/2) + W_2(Q^2, x_{Bj})\cos^2(\theta/2)\right]. \tag{2.20}$$

The structure functions W_1, W_2 are scalar functions of two independent variables: the energy transferred $Q^2 \equiv -q^2$ and the Bjorken variable

$$x_{Bj} \equiv Q^2/(2P \cdot q). \tag{2.21}$$

If one takes the relativistic limit, in which the lepton can be considered massless, the lepton's helicity conservation allows to easily calculate the polarized scattering by using again (2.13), but implying the following for the lepton tensor [26]

$$L_{\mu\nu} = 2k^\mu k'^\nu + 2k'^\mu k^\nu + g^{\mu\nu}q^2 \mp 2i\epsilon^{\mu\nu\lambda\rho}k_\lambda k'_\rho, \tag{2.22}$$

(choose $\mp$ for the helicity $\pm 1/2$). In this case, two more components of $W_{\mu\nu}$ contribute to the cross section

$$W_{\mu\nu} = (\frac{q_\mu q_\nu}{q^2} - g_{\mu\nu})W_1 + (P_\mu - \frac{P\cdot q}{q^2}q_\mu)(P_\nu - \frac{P\cdot q}{q^2}q_\nu)W_2$$

$$+i\epsilon_{\mu\nu\lambda\rho}\frac{q^\lambda}{\sqrt{P^2}}(s^\rho M^2 G_1 + (P\cdot q s^\rho - s\cdot q P^\rho)G_2) \qquad (2.23)$$

The spin dependent structure functions $G_1(Q^2, x_{Bj})$, $G_2(Q^2, x_{Bj})$ can be measured through the difference of polarized cross sections

$$\frac{d^2\sigma(\uparrow\uparrow)}{d\Omega dE'} - \frac{d^2\sigma(\uparrow\downarrow)}{d\Omega dE'} = \frac{4\alpha^2}{Q^4}\frac{E'}{E}[(E + E'\cos\theta)M_T G_1(Q^2, x_{Bj})$$

$$- Q^2 G_2(Q^2, x_{Bj})], \qquad (2.24)$$

where $d\sigma(\uparrow\uparrow)/d\sigma(\uparrow\downarrow)$ denotes the cross section of polarized scattering, in which the electron and target spins are parallel/antiparallel; M_T is the target mass.

Dimensionless structure functions F_1, F_2, g_1, g_2 are sometimes used instead of W_i, G_i [5]

$$F_1 = M_T W_1, \quad F_2 = \nu W_2, \qquad (2.25)$$

$$g_1 = M_T^2 \nu G_1, \quad g_2 = M_T \nu^2 G_2, \qquad (2.26)$$

where ν is the energy transfer in the target rest frame. In case of elastic scattering $(x_{Bj} = A)$, the structure functions are directly related to Sachs electric and magnetic form factors G_E and G_M as [5]

$$F_1(elastic) = M_T \tau G_M^2(Q^2)\delta\left(\nu - \frac{Q^2}{2M_T}\right), \qquad (2.27)$$

$$F_2(elastic) = \frac{2\tau M_T}{1+\tau}(G_E^2(Q^2) + \tau G_M^2(Q^2))\delta\left(\nu - \frac{Q^2}{2M_T}\right), \qquad (2.28)$$

where $\tau \equiv Q^2/(2M_T)$. Let us recall the definition of Dirac and Pauli form factors F_D and F_P [26,39]

$$\langle P'|J_\mu|P\rangle = \bar{u}(P')\left(\gamma_\mu F_D(Q^2) + \frac{i\sigma_{\mu\nu}q^\nu}{2M_T}F_P(Q^2)\right)u(P), \qquad (2.29)$$

and their relation to the Sachs form factors [26]

$$\begin{aligned} G_E(Q^2) &= F_D(Q^2) - (Q^2/4M_T^2)F_P(Q^2), \\ G_M(Q^2) &= F_D(Q^2) + F_P(Q^2). \end{aligned} \qquad (2.30)$$
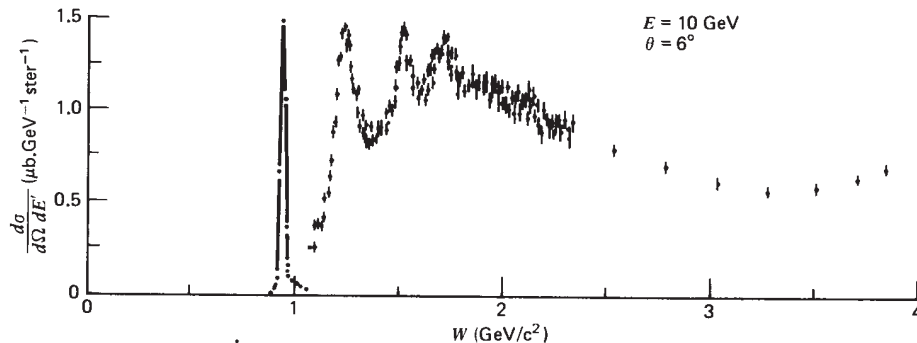
Figure 2.4: The $ep \to eX$ cross section as a function of the missing mass W. $W^2 = (p + q)^2 = M^2 + 2M\nu - Q^2$. The elastic peak has been reduced by a factor of 8.5. The illustration is taken from [42].

Concluding this section, let us note the importance of exclusive measurements in the study of composite targets. Point particles are fully defined by their quantum numbers, such as electrical charge and magnetic moment. On the other hand, one needs more information in order to describe composite systems. The Q^2-dependent form factors (for example, $G_E(Q^2)$ and $G_E(Q^2)$) carry information on the charge and magnetic moment distribution of the target, which can be related to its density profile and fully describe a spherically symmetrical system [26]. The structure functions, accessible in electron scattering cross sections differential in Q^2 and x_{Bj}, provide more information on the structure of the target, which is, in general, not spherical. For instance, one can reconstruct the 3-dimensional density distribution of quarks in the proton [41] from high energy ep scattering, in which the proton is probed as a bound state of quarks and gluons. Studying an even more exclusive observable, *e.g.* the triple differential cross section of the Drell-Yan process (Sect. 2.4), we are able to access the double unintegrated, 4-dimentional parton distributions, which carry information on the interaction of quarks in the proton [19].

2.3 Deep inelastic scattering (DIS)

2.3.1 Definitions

Electron-hadron scattering is qualitatively different in the following three energy regions [27] (see Fig. 2.4):
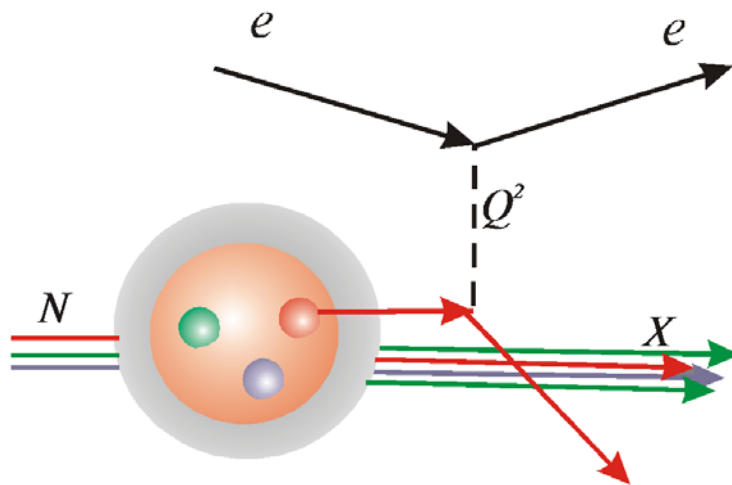
Figure 2.5: Deep inelastic scattering in the parton model picture is a single quark knock-out.

- elastic peak $(W \approx M_N)$,

- resonance region $(M_N \leq W \leq 2 \text{ GeV})$,

- deep inelastic region $(W \geq 2 \text{ GeV})$.

In the high energy regime of electron nucleon scattering, called Deep Inelastic Scattering (DIS), the quarks and gluons are the relevant degrees of freedom. In the regime of $Q^2 \gg 1 GeV^2$ and $0 < x_{Bj} < 1$ the electron primarily interacts with a single quark as illustrated in Fig. 2.5. Indeed, at these energies, the virtual photon has a wave length < 1 fm due to Heisenberg's uncertainty principle [43]. This suggests that the electron probes only the correlations of sizes smaller than the nucleon radius. At least, this qualitative argument is true in the Breit frame, in which the virtual photon is space-like

$$q = (E, q_x, q_y, q_z) = (0, 0, 0, -2x_{Bj}P_{Br}), \quad (2.31)$$

where P_{Br} is the nucleon's momentum in this frame. However, in the target rest frame DIS in the limit of $Q^2 \to \infty$ probes not the small spatial distances (or times), but the correlations confined to the light cone. We return to this point in 2.3.3.

Note that $0 \leq x_{Bj} \leq 1$ is always satisfied in inelastic eN scattering. Indeed, in the target rest frame,

$$x_{Bj} = -\frac{q^2}{2(P \cdot q)} = -\frac{q^2}{2(\vec{0}, M_N)(\vec{q}, \nu)} = -\frac{q^2}{2M_N \nu}, \quad (2.32)$$

where M_N is the nucleon mass. The energy transfer ν is defined as $\nu \equiv E_e - E'_e$ with E_e, E'_e being the electron energy before and after the interaction. The positivity of ν can be shown from the energy conservation as following

$$E_e + M_N = E'_e + E'_N = E'_e + \sqrt{M_N^2 + \vec{P'}^2}; \quad (2.33)$$

$$\nu = \sqrt{M_N^2 + \vec{P'}^2} - M_N \geq 0. \quad (2.34)$$

Also, $-q^2 \geq 0$, since

$$-q^2 = -(k' - k)^2 = (k' \cdot k) - m_e^2 \approx (k' \cdot k) \geq 0. \quad (2.35)$$

Therefore, $x_{Bj} \geq 0$. On the other hand, due to the structureless nature of the lepton, the invariant mass of final hadron state $(P + q)^2$ cannot be less than the squared mass of the initial hadron M_N^2

$$(P + q)^2 \geq M_N^2. \quad (2.36)$$

Consequently,

$$M_N^2 + 2(P \cdot q) + q^2 \geq M_N^2, \quad (2.37)$$

$$2(P \cdot q) \geq -q^2, \quad 1 \geq -\frac{q^2}{2(P \cdot q)} \quad (2.38)$$

$$x_{Bj} \leq 1. \quad (2.39)$$

Bjorken, using current algebra, found [44] that W_1 and W_2 defined in (2.20) should satisfy the scaling laws in the limit, when $Q^2 \to \infty$ and $\nu \to \infty$ simultaneously, leaving x_{Bj} finite. The proton structure function $W_2(Q^2, \nu)$ was first measured in the deep inelastic regime at SLAC in 1968. The data [38], indeed, exhibited scaling: W_2 was a function of only one scalar variable – the Bjorken variable $x_{Bj} = \frac{Q^2}{2P \cdot q}$ – independently of the momentum transfer Q^2. W_1 was not measured in this experiment, because of a relative $\tan^2(\theta/2)$ suppression ($\theta = 6^o - 10^o$, $\tan^2(\frac{10^o}{2}) = 7.6 \times 10^{-3}$), *cf.* (2.20).

The measurable structure functions are the Lorentz-invariant coefficients of the hadron tensor [5]

$$
\begin{aligned}
W^{\mu\nu} &= \left(\frac{q^\mu q^\nu}{q^2} - g^{\mu\nu} \right) W_1(\nu, q^2) \\
&+ \left(P^\mu - \frac{P \cdot q}{q^2} q^\mu \right) \left(P^\nu - \frac{P \cdot q}{q^2} q^\nu \right) \frac{W_2(\nu, q^2)}{M_N^2},
\end{aligned} \tag{2.40}
$$

defined for DIS as a fully inclusive process as (*cf.* (2.14))

$$
W_{\mu\nu} \equiv \frac{1}{4\pi} \sum_X (2\pi)^4 \delta^4(P + q - p_X) \langle P|J_\mu(0)|X\rangle \langle X|J_\nu(0)|P\rangle. \tag{2.41}
$$

2.3.2   Relation to virtual Compton scattering

By using $(2\pi)^4 \delta^4(P + q - p_X) = \int d^4y\, e^{i(P+q-p_X)y}$, one can transform (2.41) as [42]

$$
\begin{aligned}
W_{\mu\nu} &= \frac{1}{4\pi} \sum_X \int d^4y\, e^{i(q+P-p_X)\cdot y} \langle P|J_\mu(0)|X\rangle \langle X|J_\nu(0)|P\rangle && (2.42) \\
&= \frac{1}{4\pi} \sum_X \int d^4y\, e^{iq\cdot y} \langle P|e^{iP\cdot y} J_\mu(0) e^{-ip_X\cdot y}|X\rangle \langle X|J_\nu(0)|P\rangle && (2.43) \\
&= \frac{1}{4\pi} \sum_X \int d^4y\, e^{iq\cdot y} \langle P|J_\mu(y)|X\rangle \langle X|J_\nu(0)|P\rangle && (2.44) \\
&= \frac{1}{4\pi} \int d^4y\, e^{iq\cdot y} \langle P|J_\mu(y) J_\nu(0)|P\rangle_c, && (2.45)
\end{aligned}
$$

where the subscript 'c' denotes 'connected' and means that the vacuum transitions $\langle 0|J_\mu(y)J_\nu(0)|0\rangle \langle P|P\rangle$ are excluded.

We can rewrite (2.41) as

$$
W_{\mu\nu} = \frac{1}{4\pi} \sum_X (2\pi)^4 \big[\, \delta^4(P + q - p_X) \langle P|J_\mu(0)|X\rangle \langle X|J_\nu(0)|P\rangle \tag{2.46}
$$

$$
+ \delta^4(P - q - p_X) \langle P|J_\nu(0)|X\rangle \langle X|J_\mu(0)|P\rangle \big], \tag{2.47}
$$

since the both delta functions cannot be satisfied simultaneously [45]. Further rewriting the second term in (2.47) analogously to (2.42)-(2.45), we obtain that
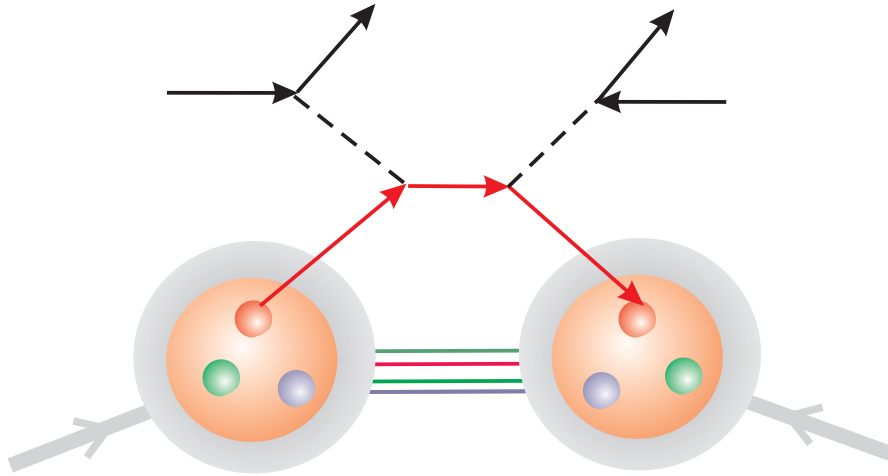
Figure 2.6: Virtual Compton scattering.

the hadron tensor can be written as a commutator of currents

$$W_{\mu\nu} = \frac{1}{4\pi} \int d^4y e^{iq \cdot y} \langle P | [J_\mu(y) J_\nu(0)] | P \rangle_c. \tag{2.48}$$

Formula (2.48) illustrates that the virtual photon probes a correlation of quark currents in the target with the space-time separation y.

On the other hand, the amplitude of forward virtual Compton scattering represented by diagram 2.6 is [46]

$$T_{\mu\nu} = i \int d^4y e^{iq \cdot y} \langle P | \mathrm{T}(J_\mu(y) J_\nu(0)) | P \rangle. \tag{2.49}$$

The hadron tensor (2.48) is connected with the Compton amplitude by [42]

$$W_{\mu\nu} = \frac{1}{2\pi} Im\, T_{\mu\nu}. \tag{2.50}$$

The imaginary part of $T_{\mu\nu}$ is related to its discontinuity and is depicted in Fig. 2.7 by means of a unitarity cut [39]. In the limit of high Q^2, factorization theorem [47] dictates that the interaction of the active quark, on which the photon is scattered, with the rest of the target hadron can be neglected. In this case, the active quark is considered free, and the diagram presented in Fig. 2.7 is called the 'hand-bag' diagram.
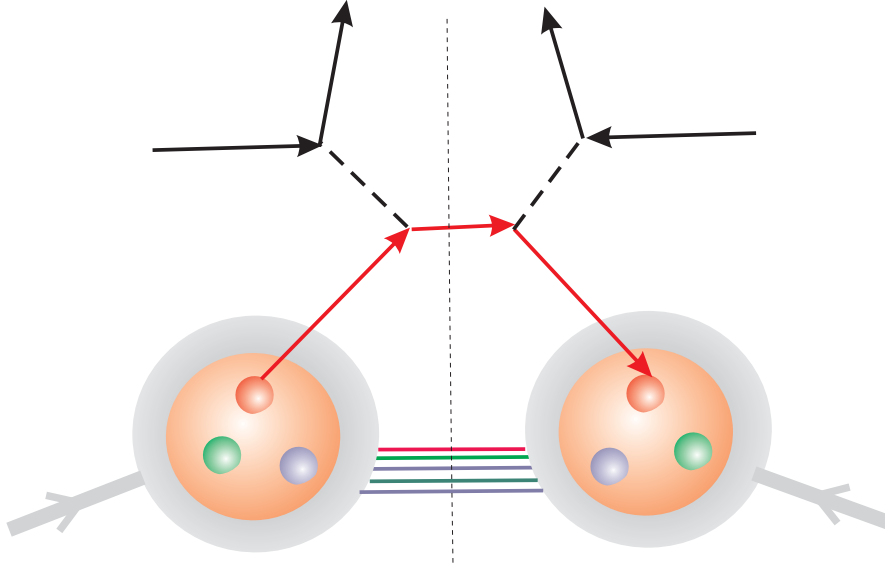
Figure 2.7: Imaginary part of the virtual Compton scattering amplitude proportional to the DIS cross section in leading order of Q^2.

2.3.3 Time-space region probed in the Bjorken limit

In the Bjorken limit ($Q^2 \to \infty$ at fixed x_{Bj}), the correlation probed in the target becomes light-like, but may extend to very large spatial distances (and times) [42]. To see this, let us consider the hadron tensor measured in DIS, which is given by formula (2.45). The separation y between the points, at which the currents J_μ and J_ν act, represents the space-time resolution of the probe in the deep inelastic scattering process.

Let us consider deep inelastic electron - nucleon scattering in the nucleon rest frame (M_N is the nucleon mass). The light cone components of the photon momentum are

$$(q_+, q_-, \vec{q}_T) = (-M_N x_{Bj}, \frac{Q^2}{M_N x_{Bj}}, \vec{0}), \qquad (2.51)$$

see App. A for the definition of light cone coordinates. As $Q^2 \to \infty$ with $x_{Bj} \equiv Q^2/P \cdot q$ finite and fixed, $q_- \to \infty$. As a consequence, the integral in (2.45) should vanish due to the fast oscillating exponent, unless

$$y_+ \to 0. \qquad (2.52)$$

At the same time, y_- is finite and even large y_- can contribute to $W_{\mu\nu}$ in some

cases. To be precise, the restriction on y_- is [42] :

$$|y_-| < \left| \frac{1}{q_+} \right| = \frac{1}{M_N x_{Bj}}. \tag{2.53}$$

In case of a fully inclusive process, one has the following condition due to causality:

$$y^2 = y_- y_+ - \vec{y}_T^2 \geq 0 \;\; \Rightarrow \;\; \vec{y}_T \to \vec{0}. \tag{2.54}$$

Thus, DIS in the Bjorken limit is a light-cone $(y^2 \to 0)$ dominated process.

2.3.4   Parton model

The first model that was able to describe DIS data [38], was the Feynman parton model [28]. In this model, the ep cross section is factorized as follows

$$d\sigma = \sum_i e_i^2 f_i(x_{Bj}) \otimes d\hat{\sigma}(x_{Bj}), \tag{2.55}$$

where the sum runs over all relevant parton flavors, e_i is the charge of the ith type of parton in units of the proton charge e. $d\hat{\sigma}$ is the elementary cross section for a parton-electron scattering, $f_i(x_{Bj})$ are parton distribution functions, x is the earlier introduced Bjorken variable. The parton distributions have in this model a probabilistic interpretation: they represent the probability to find a parton of a given flavor with the momentum fraction x_{Bj} of the hadron momentum inside a hadron. The experimental evidence that the partons have spin 1/2 and no structure led to their identification with the quark degrees of freedom of QCD [5].

After the introduction of QCD, the factorization assumption (2.55) has been proven [47] and an operator representation for parton distributions has been found (see Sect. 2.5). Moreover, a logarithmic evolution of structure functions with Q^2 has been explained [48–50]. This success, together with the prediction of the Drell-Yan process cross section [51], was crucial for the establishment of QCD as the theory of strong interaction.

2.4   Drell-Yan process

The parton model of Feynman (Sect. 2.3.4) was used by S. D. Drell and T. M. Yan to predict the cross section of the process $pp \to \gamma^* + X \to$
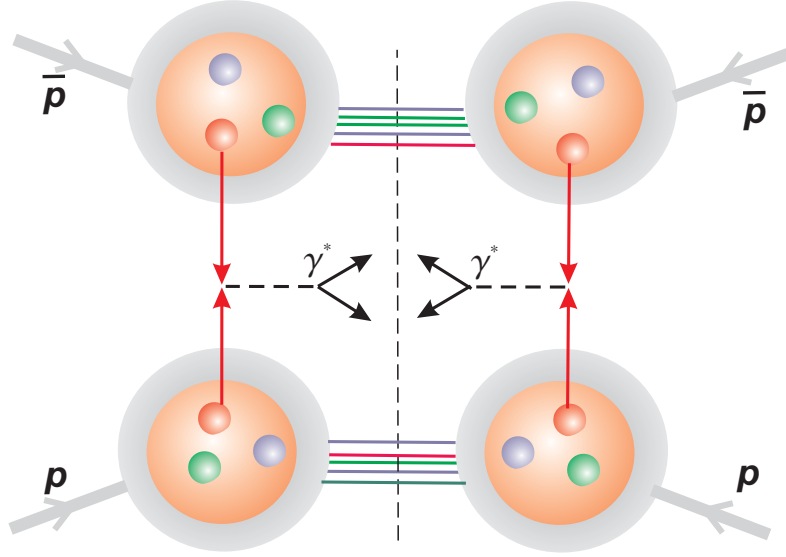
Figure 2.8: Parton model mechanism for heavy lepton pair production in high energy hadron-hadron collision.

$\mu^+\mu^- + X$ [51]. The partonic interpretation of this process is the following. A quark from one proton annihilates with an antiquark from the Dirac sea of the other proton and forms a highly virtual photon (see Fig. 2.8). The other quarks and gluons inside the target and the projectile are spectators. In the parton model, it is assumed that the active quark and antiquark behave as free particles. This assumption is justified by the fact that, viewed on the light cone, the process takes place on a very short time scale and the partons do not have time to interact.

The factorization formula in this case includes the annihilation cross section $\hat\sigma$, and two parton distribution functions – one for each of the interacting partons –

$$\left(\frac{d^2\sigma_q}{dM^2 d\bar{x}_F}\right)_{parton} = \sum_i e_i^2 [f_i(x_1)\bar{f}_i(x_2) + \bar{f}_i(x_1)f_i(x_2)] \otimes \left(\frac{d^2\hat\sigma_q(x_1,x_2)}{dM^2 d\bar{x}_F}\right)_{LO} \quad (2.56)$$

where the subprocess $eq \to eq$ cross section at leading order pQCD (and neglecting the quark and electron masses) is given by a simple expression [28]

$$\left(\frac{d^2\hat\sigma_q(x_1,x_2)}{dM^2 d\bar{x}_F}\right)_{LO} = \frac{4\pi\alpha^2 e_q^2}{9M^4}\frac{x_1 x_2}{x_1 + x_2}, \quad (2.57)$$
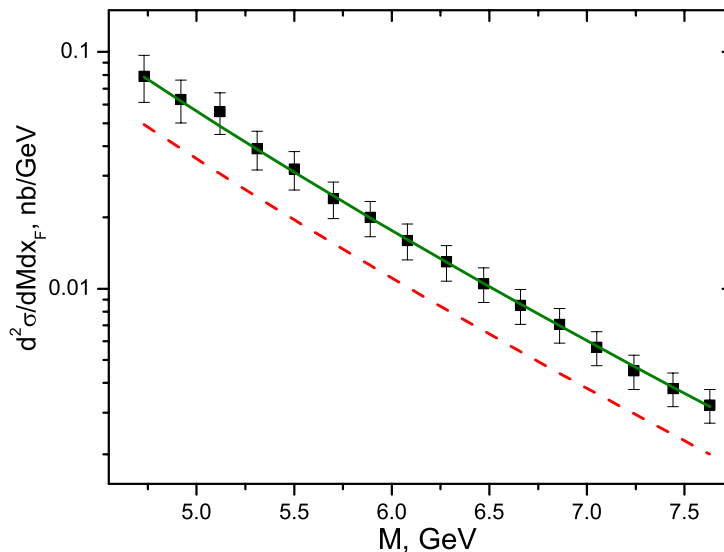
Figure 2.9: Parton model prediction for a double differential Drell-Yan cross section (dashed line) at $\sqrt{s} = 20$ and $x_F = 0.1$ as compared to experiment E439 [52]. Solid line is the result scaled up with a factor $K = 1.6$.

with x_1 and x_2 are defined by the relations

$$x_1 x_2 s = M^2, \tag{2.58}$$

$$x_1 - x_2 = \bar{x}_F. \tag{2.59}$$

Above, $\bar{x}_F \equiv 2p_z/\sqrt{s} \approx x_F$, where $x_F \equiv p_z/(p_z)_{max}$ is the Feynman variable of the produced virtual photon with momentum p and invariant mass M (see the discussion of (3.53) for details on x_F definition).

We plot the result of the parton model using parton distribution functions fitted to DIS data in [53], for the Drell-Yan process cross section as compared to data of experiment E439 [52] in Fig. 2.9. The dependence of the Drell-Yan process cross section on the invariant mass of the produced pair is predicted with a very good accuracy over two orders of magnitude. However, the magnitude of the cross section is underestimated and an additional parameter - an overall scaling factor (the so-called K-factor) is necessary in order to describe the data. Nevertheless, this is a definite success, given the simplicity of the parton model.

Note that Drell-Yan dileptons have vanishing transverse momentum in this

model:

$$\left(\frac{d^3\sigma}{dM^2 dx_F dp_T^2}\right)_{LO} = \sum_q \Phi_q(x_1, x_2) \left(\frac{d^2\hat{\sigma}_q}{dM^2 dx_F}\right)_{LO} \delta\left(p_T^2\right). \qquad (2.60)$$

Indeed, in the parton model mechanism for the Drell-Yan pair production (Fig. 2.8), the initial state has no transverse momentum, while the virtual photon in the final state does not interact with the remnants; therefore, the lepton pair gains no transverse momentum. This prediction disagrees with data (see Chapter 4).

2.5   Parton distributions in QCD

2.5.1   Collinear parton distributions

Factorization, analogous to the one of parton model, has been proven for DIS and the Drell-Yan process in the reference frame, in which the hadrons move infinitely fast [47]. In this hypothetical frame, the quarks are collinear with the hadron they form. The twist expansion has been used to show that the collinear factorization in DIS case holds also in the realistic frames up to corrections proportional to the inverse powers of the hard scale of the process [54].

   At leading twist (leading power of the hard scale), the quark structure of hadrons is described by three distribution functions:

1. The unpolarized quark distribution function $f(x)$, representing the probability of finding a quark with a fraction x of the hadron light cone momentum, regardless of its spin orientation. The formula for this distribution in terms of quark field operator ψ is [55]

$$f(x) = \int \frac{d\xi^-}{4\pi} \, e^{ixp^+\xi^-} \langle P|\bar{\psi}(0)\gamma^+\psi(0, \xi^-, \vec{0}_T)|P\rangle; \qquad (2.61)$$

2. The longitudinal polarization distribution $\Delta q(x)$ that measures the net helicity of a quark in a longitudinally polarized hadron [55]

$$\Delta q(x) = \int \frac{d\xi^-}{4\pi} \, e^{ixp^+\xi^-} \langle Ps|\bar{\psi}(0)\gamma^+\gamma^5\psi(0, \xi^-, \vec{0}_T)|Ps\rangle; \qquad (2.62)$$

3. The transversity $\delta q(x)$ (first introduced in [56]), which is the distribution

of transversely polarized quarks in a transversely polarized hadron [55]

$$\delta q(x) = \int \frac{d\xi^-}{4\pi} e^{ixp^+\xi^-} \langle Ps|\bar{\psi}(0)\gamma^+\gamma^1\gamma^5\psi(0, \xi^-, \vec{0}_T)|Ps\rangle, \qquad (2.63)$$

where $\{\gamma\}$ are Dirac gamma matrixes [28], $\gamma^+ = \gamma^0 + \gamma^3$, the direction of the hadron momentum defines '3' axis. We used light cone gauge, in which the gluon field satisfies $A_g^+ = 0$ and the formulas look simpler. Note that the transverse spin (*i.e.* the quark spin density along '1' axis) and transversity have, by convention, different Lorentz structure [57]. Indeed, the former is $\psi^\dagger\sigma^{23}\psi \equiv \bar{\psi}\gamma^1\gamma^5\psi$, while the latter is defined by $\bar{\psi}\sigma^{23}\psi \equiv \bar{\psi}\gamma^0\gamma^1\gamma^5\psi$, where $\sigma^{\mu\nu}$ are Dirac-Pauli matrices, $\bar{\psi} \equiv \psi\gamma^0$, $\gamma^5 \equiv \gamma^0\gamma^1\gamma^2\gamma^3$. They coincide for a free spinor (for which $\bar{\psi} = \psi^\dagger$), but not for a bound, off-shell particle like quark (see [57] for details). That is why Jaffe and Ji [58] advocated the name 'transversity' in stead of 'transverse polarization of quarks'. The definition of transversity is chosen so that it changes with the same factor as helicity, when the system is Lorentz-boosted along the z-axis [57].

The evolution of the aforesaid distributions with the factorization scale Q^2 is governed by the Dokshitzer-Gribov-Lipatov-Altarelli-Parisi (DGLAP) equations [48–50] that follow from perturbative QCD (pQCD). However, it is impossible to calculate matrix elements (2.61)-(2.63) at fixed (Q^2, x) in pQCD. The parton distributions are modelled at some low factorization scale using low energy effective theories with parameters, fitted to data after a DGLAP evolution to experimentally relevant values of Q^2.

Several parametrizations of parton distributions exist today, for example, GRV [53], MRST [59], CTEQ [60]. All of them were fitted to high statistics DIS data, but differ slightly in describing other processes, such as charmonium production [61]. An advantage of GRV94 parametrization is that the DGLAP evolution is approximated by a function of Q^2 with very good accuracy for $x_{Bj} > 10^{-8}$. This makes a solution of the DGLAP integral equation set at each Q^2 unnecessary and saves computer power. This parametrization is used in our analysis presented in the following Chapters.

2.5.2 Unintegrated parton distributions

The conventional pQCD approach to the calculation of hard scattering cross sections assumes that the partons are collinear and on-shell, *i.e.* both the

virtuality and transverse momenta of the quarks and gluons inside hadrons are neglected and the partonic four-momentum is replaced with its light cone projection $(k^+, 0, \vec{0})$. This approximation does not affect the cross section of fully inclusive processes like DIS, but it leads to unrealistic results for the cross sections of more exclusive processes. Intrinsic transverse momentum of quarks has been proven to be important for the interpretation of various cross sections and asymmetries [62].

To explore the effects of partonic transverse momenta, one needs to know the distribution of a parton's transverse momentum k_T, as well as x, *i.e.* the probability to find a parton with transverse momentum k_T and longitudinal momentum k^+ at given factorization scale μ. These distributions $f_i(x, k_T^2, \mu)$, first introduced in [63], are called "unintegrated parton distributions" and satisfy evolution equations, which depend on two hard scales: k_T and μ of the probe [64].

One possible way to obtain such a distribution [65] is to consider the DGLAP evolution, generated by a Bremsstrahlung type emission of *strongly k_T-ordered* partons, combined to the Balitsky-Fadin-Kuraev-Lipatov (BFKL) evolution equation [66–69], valid for very small x. In the DGLAP approach, the parton k_T is assumed to be entirely perturbatively generated and its effect is reduced to the change of hard scales at which the partons are probed (due to the enforcement of the strong ordering) towards small x. In the region of small x, the BFKL equations are applied and predict a Gaussian distribution of k_T. Approximately, the k_T distributions is $\delta(0)$ at x above some limiting value and a Gaussian in the region of small x. The limiting value is extracted from experiment. The parameters of the Gaussian quark distribution are related to the unintegrated gluon distribution. However, the unintegrated distribution of gluons cannot be obtained in this approach. It has to be modelled, thus introducing additional parameters to be fitted to data.

An alternative opinion is that the nonperturbative component of the partonic k_T, *i.e.* the one that can not be generated by an evolution ladder, is also important [64] and should be modelled phenomenologically. The argumentation is as following. The DGLAP equations are valid only in the collinear factorization approximations, in which the intrinsic k_T is neglected. On the other hand, BFKL equations are applicable only at $x \rightarrow 0$; therefore, it is questionable that they can predict partonic k_T at final x. In the phenomenological approach, quark k_T is a result of both perturbative and nonperturbative

processes; its distribution is parametrized and fitted to experiment. For example, one uses a Gaussian in analogy to the small-x case, and extracts the dispersion from data.

The representation of the corresponding correlation functions in terms of quark and gluon fields is not as simple as in the case of usual parton distributions (formula (2.61)). One such representation is given in [70] and will be presented in Sect. 3.1. On the other hand, an unintegrated quark distribution can be defined as an integral of a matrix element of the quark Wigner function as it will be explained in Sect. 3.2. For example, in [64], the operator form of an unintegrated parton distribution is found as an integral of the parton correlation function, which is ultimately related to the quark Wigner function.

2.5.3 Parton correlation functions

The virtuality of quarks and gluons in the proton has attracted considerable attention recently. The importance of accounting for the virtuality (off-shellness) of partons in high energy processes was stressed, for instance, by O. Benhar [71] and, recently, by J. Collins and H. Jung [72]. As it will be shown in Sect. 4.2, by taking into account the virtuality distribution of partons, we can explain simultaneously DIS data, the K-factor type corrections to the magnitude of the transverse momentum distribution of Drell-Yan pairs as well as the shape of the double differential cross section of the Drell-Yan process $d\sigma/dMdx_F$.

The generalization of the usual parton distribution function, which depends on the virtuality and k_T of the quark in addition to its longitudinal momentum k^+, is sometimes called "fully unintegrated parton density" [72] or "parton correlation function" [64]. But the terminology is still not fixed, one of the reasons being that the gauge invariant definition of these distributions in terms of parton field operators is not known yet.

2.6 Open questions

The current understanding of high energy scattering experiments has led to a proof of QCD as the underlying fundamental theory of hadron structure. QCD agrees with the observation of the DIS cross section scaling in the Bjorken limit and describes the logarithmic scaling violations. Secondly, within the scope of QCD it was possible to predict the dependence of the Drell-Yan process cross section on the invariant mass of the produced pair and the Feynman variable.

Admittedly, the calculation of parton probabilities and quark wave functions inside the proton from first principles of QCD is still very much problematic and complex. However, the analysis of DIS, the Drell-Yan process and other observable cross sections allows to extract the quark properties from the data. In this way, the unpolarized quark distribution $f(x)$ defined in (2.61) was obtained with a good accuracy in a wide region of x [1]. The distribution $\Delta q(x)$ is known, too, although with larger error-bars. There are several experiments planned to access the transversity $\delta q(x)$.

If the quarks were perfectly collinear and on-shell, the distributions $f(x)$, $\Delta q(x)$ and $\delta q(x)$ would contain all the information on the internal dynamics of the nucleon. However, the quark transverse momentum is not always negligible. In particular, it is essential in understanding the semi-inclusive DIS, the transverse momentum distribution of Drell-Yan lepton pairs, low Q^2 and low x_{Bj} physics. A number of additional distribution functions arise, if the quark transverse momentum is not put to zero (see Section 3). As mentioned in Section 2.5, the definition of double unintegrated parton distributions (*i.e.* parton correlation functions, or off-shell parton distributions) in terms of parton field operators is not known. The evolution of these parton distributions has not been determined so far either. We propose a parametrization of the fully unintegrated parton distributions and obtain it's parameters from data. Evolution of the parameters with the hard scale is also studied.

Another open question is the understanding of less inclusive observables, such as the triple differential cross section of the Drell-Yan process

$$\frac{d^3\sigma}{dMdp_Tdx_F}, \tag{2.64}$$

azimuthal distribution of the Drell-Yan pairs, and large single spin asymmetries of a number of processes. Perturbative QCD fails to reproduce the p_T-distribution of Drell-Yan pairs in any fixed order of perturbative QCD [73]. Leading logarithm approximation is not applicable to the cross section $d^2\sigma/dM^2dp_T$, because of the presence of two scales (M, p_T). Summing an infinite number of $O(\alpha_S^n)$ diagrams by, for example, a regularized Sudakov method [74,75], allows to calculate this quantity. However, the result does not agree with the experiment quantitatively, because the higher twist (power M^2 suppressed) effects are not taken into account in the perturbative resummation. One needs to build models to calculate the higher twist corrections.

We tackle these problems by proposing a phenomenological model that yields a quantitative description of the triple differential Drell-Yan cross section (2.64) at moderate M^2, which could not be archived in any previously available approach [76]. From the fits to the triple differential cross section data, we reconstruct quark off-shellness and transverse momentum distributions in the proton and study their evolution with the hard scale. In the same time, the model agrees with DIS data and describes the inclusive, double-differential Drell-Yan process cross section without a need of a K-factor. As we show below, this success is caused by our accounting for higher twist effects.

It is also an open question, whether factorization still holds in the generalized case, in which the soft part of the cross section depends on the full quark momentum (k^+, k^-, k_T). Until such a factorization theorem is proven, we calculate measurable cross sections using a model that *assumes* generalized factorization. The predictive power of such a model has to be tested. For this purpose, we predict the triple differential cross section of the Drell-Yan process in the kinematical region relevant for PANDA [23] experiment at the future GSI facility [77].

Chapter 3

The model

3.1 Factorization in non-collinear off-shell case

The basic tool in the calculation of hard processes is the factorization into hard and soft physics. In the non-collinear case, the factorization formula for DIS is

$$d\sigma = \sum_i e_i^2 f_i(\xi, \vec{p}_\perp) \otimes d\hat{\sigma}(\xi, \vec{p}_\perp), \tag{3.1}$$

where the sum runs over all relevant parton flavors, e_i is the charge of the ith type of parton in units of the proton charge e. $d\hat{\sigma}$ is the elementary cross section for a given process, $f(\xi, \vec{p}_\perp)$ are unintegrated parton distributions defined as [70]:

$$f(\xi, \vec{p}_\perp) = \frac{1}{4\pi} \int d^4 y \langle N|\bar{\psi}(y)\gamma^+[y, 0]\psi(0)|N\rangle \delta(y^+) e^{i(\xi P^+ y^+ + p^- y^- - 2p_\perp y_\perp)/2}, \tag{3.2}$$

where $\xi \equiv p^+/P^+$ is the Nachtmann variable and p and P are momenta of the active parton and hadron, respectively;

$$[y, 0] \equiv \mathrm{P} \exp\left[\frac{ig}{2} \int_0^y d\tau A^+(\tau)\right] \tag{3.3}$$

is the gauge link operator introduced in order to preserve gauge invariance. In [78], the factorization in the form (3.1) was proven in the leading power of the hard scale (photon virtuality in DIS and Drell-Yan process).

Note that the unintegrated distributions do not depend on p^- due to $\delta(y^+)$. In other words, the parton distributions measure the correlation of partons with equal light cone times ($y^+ = 0$). This reflects the fact that the struc-

ture functions, measured in the fully inclusive DIS, depend only on p^+ in the Bjorken limit. Indeed, because of the conditions (2.52) and (2.54), the hadronic part of the DIS cross section (2.45) is a function of a single variable $p^+ \equiv x_{Bj} P^+$.

However, the factorization formula (3.1) is valid only in the scaling limit, *i.e.*, at the leading power as $Q^2 \rightarrow \infty$. At moderate Q^2 considerable p^--dependent corrections might be necessary to make predictions for semi-exclusive observables, *e.g.* Drell-Yan lepton pair production cross section and asymmetries. In this case, we propose the following factorization ansatz:

$$d\sigma = \sum_i e_i^2 q_i(\xi, \vec{p}_\perp, p^-) \otimes d\hat{\sigma}(\xi, \vec{p}_\perp, p^-). \tag{3.4}$$

The difference between (3.1) and (3.4) is precisely due to off-shellness effects that we aim to study. Indeed, for a free quark the minus component of its momentum is fixed by the on-shell condition:

$$p^2 = p^+ p^- - \vec{p}_\perp^2 = \xi P^+ p^- - \vec{p}_\perp^2 = 0 \tag{3.5}$$

(we put the current quark mass to zero). Note that in the intrinsic-k_T approach $p_\perp \neq 0$ and, therefore, $p^- \neq 0$. However, p^- in this case is not an independence variable; it is fixed by $p^- = p_\perp^2 / p^+$ as a consequence of (3.5).

In contrast, since the partons are bound in the nucleon, they are off-shell. Condition (3.5) no longer holds. For instance, $p^- \neq 0$ even when $p_\perp = 0$. Moreover, p^- can vary at fixed $(p^+, p_\perp)$: all the four components of the parton momentum are independent. Therefore, the cross section must be calculated using a quark off-shellness distribution. Such a distribution is an integral of the quark Wigner function, which will be introduced in Section 3.2. Unfortunately, calculating this distribution from QCD presents great difficulties. Therefore, we use a phenomenological model parametrization (Section 3.3) with two parameters, which we extract from experimentally measured cross sections (Section 4.3.1).

The partonic cross section is calculated using the rules of pQCD. We calculated the pQCD differential cross section for an electron scattering off a virtual quark and that for the annihilation of an off-shell quark-antiquark pair into a pair of dileptons. Also, by performing the calculations in different gauges, we checked that both these off-shell partonic cross sections are gauge invariant

(due to the on-shell leptons) making the modification of the vertex by Ward's identity unnecessary.

The analysis of the off-shell kinematics and the obtained cross sections are separately given below for DIS and the Drell-Yan process. The case of electron scattering (see Section 3.4) is simpler and serves as an introduction to the calculation of the Drell-Yan pair transverse momentum distribution in Section 3.5.

3.2   Wigner function

A pure quantum state is defined by a set of quantum numbers n and a corresponding wave function, for instance $\psi_n(r)$. A closed quantum system is always in a particular quantum state, therefore it can always be characterized by a wave function. On the other hand, a subsystem of a bigger quantum system can be in a mixed state, for which a wave function does not exist. The correlated particles of the Einstein-Podolsky paradox [80] are examples of such systems. Mixed quantum systems can be described by a more general quantity: the density matrix [43]

$$\rho(r, r') \equiv \sum_n \omega_n \psi_n(r) \psi_n^*(r'). \tag{3.6}$$

In contrast to density matrix of statistical physics [81], ρ is not a probability. Although a wave function ψ is a probability density and the diagonal elements $\rho(r, r)$ give probabilities of different states, non-diagonal elements $\rho(r, r')$ of the density matrix are, in general, not positive definite and cannot be interpreted as probabilities.

A relativistic generalization of a wave function is an operator field. In this case, ρ is also generalized to an operator $\hat{\rho}$. However, it is more convenient to use instead a relativistic Wigner function $\hat{W}_\Gamma(r, p)$, which is an operator with the Lorentz and spinor structure defined by a Clifford algebra member Γ. For instance, if $\psi(r)$ is a quark field, the quark Wigner function is defined as follows

$$\hat{W}_\Gamma(r, p) \equiv \int d^4\eta\, e^{i\eta \cdot p} \bar{\psi}(r - \eta/2) \mathcal{L}^\dagger \, \Gamma \, \mathcal{L} \, \psi(r + \eta/2), \tag{3.7}$$

where $\mathcal{L}$ is the gauge link operator that serves to preserve the gauge invariance of W. For $\eta_0 > 0$, $\mathcal{L} = 1$ in the light cone gauge, in which $A_g^+ = 0$.

(a) vacuum

(b) correlated state

(c) four photon Fock state

(d) Schrödinger cat

$$|\Psi\rangle = |\alpha\rangle + |-\alpha\rangle$$
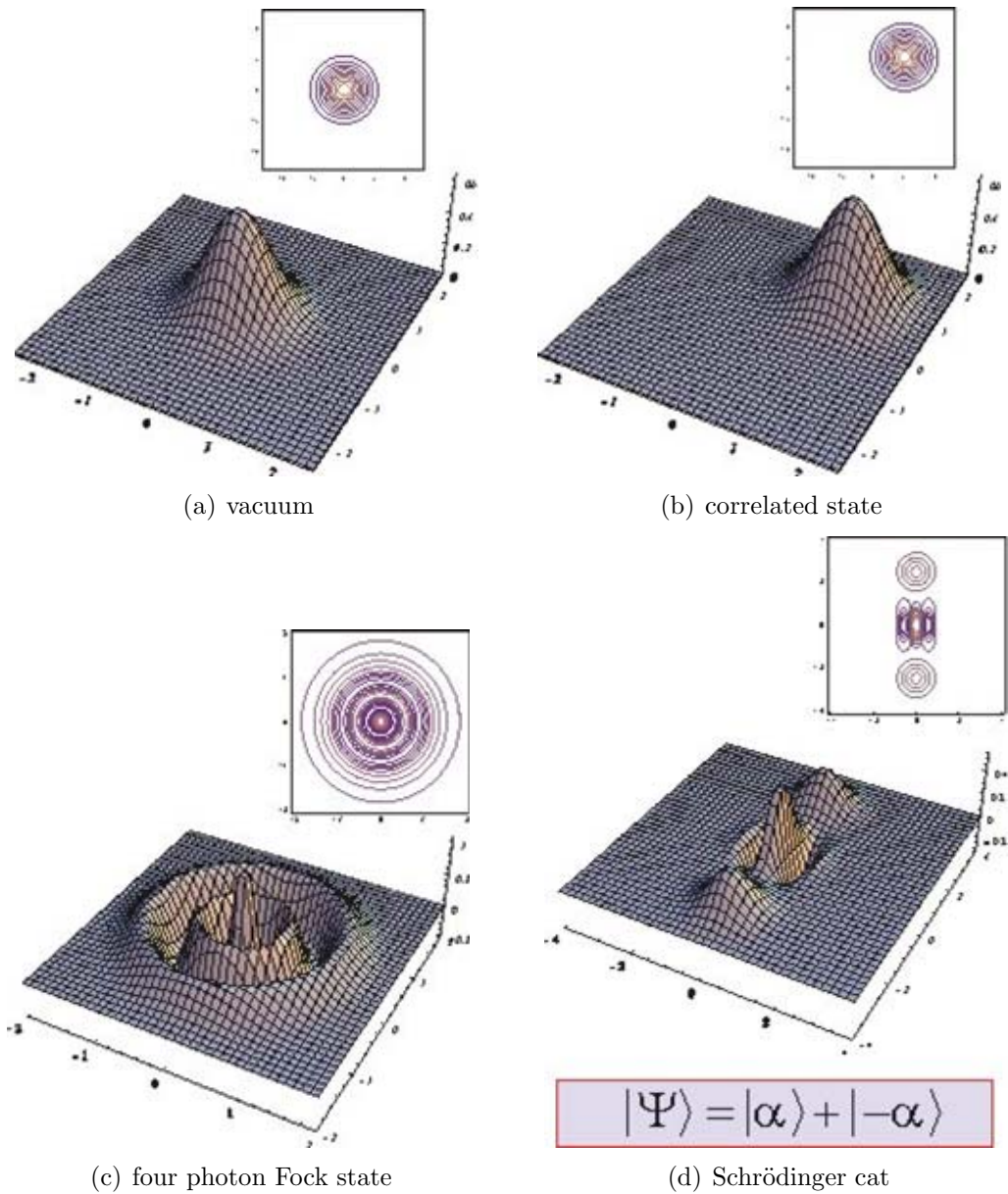
Figure 3.1: Wigner functions of multi-photon systems versus polarization and energy (the illustrations is from [79]). (a) a state with no photons. (b) a system with polarization and energy strongly correlated. (c) a Fock state of four identical photons. (d) "Schrödinger cat" system, *i.e.*, a superposition of a state and an anti-state.

The concept of Wigner function is widely used in quantum information theory [82], which deals with systems of photons [79]. Since photon ensembles have only two coordinates (for instance, polarization and energy), one can plot calculated Wigner functions for different states on a three-dimensional plot. For example, the Wigner functions of the following systems are plotted in Fig. 3.2 [79]

- vacuum [83]: there are no photons, both coordinates fluctuate around zero (Fig. 3.1(a));

- a coherent state [84], for which the two coordinates strongly correlate (Fig 3.1(b));

- a Fock state [83] of four photons with the same energy and polarization (Fig. 3.1(c));

- a "Schrödinger cat" state [79], which is a superposition of a state and an anti-state with an equal weight (Fig. 3.1(d)).

For example, for a mixture of a Fock state with 1 photon and a vacuum state

$$\alpha|1\rangle + (1 - \alpha)|0\rangle, \tag{3.8}$$

Wigner function is given by [83]

$$W(X, P) = \frac{2}{\pi} \left(4\alpha(X^2 + P^2) + 1 - 2\alpha\right) \exp\{-2(X^2 + P^2)\}. \tag{3.9}$$
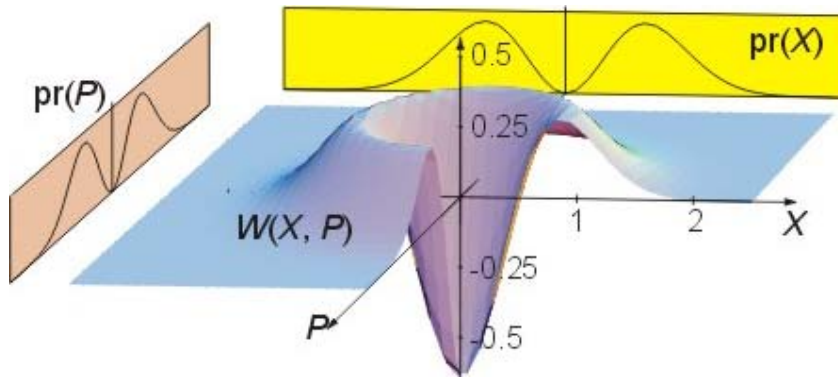

Figure 3.2: Wigner function for a single particle state [79].

Just like the quantum mechanical density matrix, the Wigner function of a quantum system is not positive definite. Interference of quantum fluctuations

Integral of $W(\vec{p}, x_\mu)$	Process
$q(x) = \int \frac{d^2 p_T}{(2\pi)^2} \int \frac{d^3 r}{(2\pi)^3} \int \frac{dp^-}{(2\pi)} W_{\gamma^+}(\vec{r}, p)$	DIS $\gamma^* p \to X$
$q(x, p_T) = \int \frac{d^3 r}{(2\pi)^3} \int \frac{dp^-}{(2\pi)} W_{\gamma^+}(\vec{r}, p)$	Drell-Yan $\bar{p}p \to \gamma^* X$
$f(r, x) = \int \frac{d^2 k_T}{(2\pi)^2} \int \frac{dp^-}{(2\pi)} W_{\gamma^+}(\vec{r}, p)$	virtual Compton scattering $\gamma^* p \to \gamma p$
$f(b_\perp, x, p_T) = \int \frac{dz}{2\pi} \int \frac{dp^-}{(2\pi)} W_{\gamma^+}(\vec{r}, p)$	double boson production $\gamma^* p \to V_1 V_2 p$
$q(x, p_T, p^-) = \int \frac{d^3 r}{(2\pi)^3} W_{\gamma^+}(\vec{r}, p)$	Drell-Yan $\bar{p}p \to \gamma^* X$

Table 3.1: Parton distributions measured in high energy processes as integrals of quark Wigner function. $V_i \in \{\gamma, W^\pm, Z^0\}$.

leads to negative values of W at zero (P, X) in Fig. 3.2, which illustrates a single particle state $(\alpha = 1)$. This reflects Heisenberg uncertainty principle, due to which the quantum-complementary [85] variables of W can not be measured simultaneously. However, integration of W over X yields a positive definite distribution of P (displayed in Fig. 3.2 as $pr(P)$) and vice versa. This is a general property of Wigner functions. Summarizing, integrals of Wigner function are measurable and can be interpreted as probability distributions, e.g. $pr(P)$ is a momentum distribution.

Let us define the matrix elements of the quark Wigner function in the basis of nucleon wave functions as

$$W_\Gamma(\vec{r}, p) = \langle P | \hat{W}_\Gamma(r, p) | P \rangle, \qquad (3.10)$$

$$W(S)_\Gamma(\vec{r}, p) = \langle P, S | \hat{W}_\Gamma(r, p) | P, S \rangle, \qquad (3.11)$$

where P is the nucleon's momentum, S its spin. The time dependence has been omitted due to energy conservation.

Because of the uncertainty principle, it is impossible to extract $W_\Gamma(\vec{r}, p)$ from a single measurement. On the other hand, one can access integrals of it in various processes. We list some of the measurable integrals and the processes, in which they can be accessed, in the table 3.1.

Parton distribution functions are Wigner function matrix elements integrated over all the variables except p^+ and are measurable in DIS. Polarization properties of the quarks inside the proton are studied by looking at Wigner functions with different Dirac structure. For example, the helicity distribution

is given by (*cf.* (2.62))

$$
\begin{aligned}
\Delta q(x) &= \int \frac{d^2 p_T}{(2\pi)^2} \int \frac{d^3 r}{(2\pi)^3} \int \frac{dp^-}{(2\pi)} W(S)_{\gamma^+ \gamma^5}(\vec{r}, p) \\
&= \int \frac{d\xi^-}{4\pi} e^{ixp^+ \xi^-} \langle Ps|\bar{\psi}(0)\gamma^+ \gamma^5 \psi(0, \xi^-, \vec{0}_T)|Ps\rangle.
\end{aligned} \tag{3.12}
$$

Transversities [86] are (*cf.* (2.63))

$$
\begin{aligned}
\delta q(x) &= \int \frac{d^2 p_T}{(2\pi)^2} \int \frac{d^3 r}{(2\pi)^3} \int \frac{dp^-}{(2\pi)} W(S)_{\gamma^+ \gamma^1 \gamma^5}(\vec{r}, p) \\
&= \int \frac{d\xi^-}{4\pi} e^{ixp^+ \xi^-} \langle Ps|\bar{\psi}(0)\gamma^+ \gamma^1 \gamma^5 \psi(0, \xi^-, \vec{0}_T)|Ps\rangle
\end{aligned} \tag{3.13}
$$

and

$$
\begin{aligned}
h(x, \vec{p}_T) &= \int \frac{d^3 r}{(2\pi)^3} \int \frac{dp^-}{(2\pi)} W_{\gamma^+ \gamma^1 \gamma^5}(\vec{r}, p) \tag{3.14} \\
&= \int \frac{d\xi^-}{4\pi} e^{i(xp^+ \xi^- + \vec{p}_T \cdot \vec{\xi}_T)} \langle P|\bar{\psi}(0)\gamma^+ \gamma^1 \gamma^5 \psi(0, \xi^-, \vec{\xi}_T)|P\rangle. \tag{3.15}
\end{aligned}
$$

In the scope of this thesis, we are most interested in the one distribution that depends on p^-, and, therefore, on the off-shellness of the quark, since the off-shellness m^2 and p^- are related by $m^2 = p^- p^+ - \vec{p}_T^2$,

$$
q(x, p_T, p^-) = \int \frac{d^3 r}{(2\pi)^3} W_{\gamma^+}(\vec{r}, p). \tag{3.16}
$$

3.3 Model for the quark virtuality distribution

A model for the virtuality distribution can be built analogically to nuclear physics based on a concept of spectral function [71, 87]. In nuclear physics, the spectral function method is used widely. The on-shell condition for the nucleon reads $P^2 = M_N^2$, where M_N is the nucleon mass in vacuum. Thus, only 3 components of the on-shell nucleon's 4-momentum are independent. In case of an interacting nucleon, P^2 is no longer fixed and its distribution (spectral function) is given by the details of the interaction. All four components of the off-shell nucleon's momentum are independent. Thus, a hadron is said to be off-shell, if its momentum squared is different from the free hadron mass, *i.e.*

when it is virtual.

The distribution of P^2 is given by the nucleon spectral function. The concept was first introduced by Källen and Lehmann and is explained, for instance, in [46]. Spectral function of a nucleon is defined by [46]

$$\rho(P^2) = (2\pi)^3 \sum_\alpha \delta^4(P - P_\alpha) |\langle 0|\phi(0)|\alpha\rangle|^2, \qquad (3.17)$$

where $\phi(x)$ is an interacting nucleon field, $\{|\alpha\rangle\}$ is a full set of nucleon asymptotic states. As stated by the confinement hypothesis, quarks have no asymptotic states. Therefore, the quark spectral function in the Källen-Lehmann sense does not exist. Instead, we introduce a phenomenological distribution of the quark off-shelness and dub it the quark spectra function in our model.

Partons in the nucleon are always virtual. For example, in the parton model, the parton momentum squared is $p^2 = (x_{Bj}P)^2 = x_{Bj}^2 M_N^2$, which is usually far from the current quark mass squared ($= 0$ in our calculations). We call a parton off-shell, if the parton's momentum has four independent components. In this case the parton off-shellness p^2 is not fixed and should be integrated over. This differs from the "trivial off-shellness" of the parton model, in which the quark is virtual, but it's off-shellness is fixed (to $x_{Bj}^2 M_N^2$). More realistically, one should include the transverse motion of partons. Then, for a free parton, $p^- = p_\perp^2/p^+$. In our calculations, p^- is not fixed by p^+ or $p_\perp^2$. Instead, we integrate over all kinematically allowed p^-.

In the following, we additionally assume that the dependence of q, defined in (3.16), on p^- factorizes from the $p_\perp$-dependence:

$$d\sigma = \sum_i e_i^2 \tilde{f}_i(\xi, \vec{p}_\perp) \otimes d\hat{\sigma}(\xi, \vec{p}_\perp, m) \otimes \mathrm{A}(m), \qquad (3.18)$$

cf. (3.4). In (3.18), $d\hat{\sigma}(\xi, \vec{p}_\perp, m)$ is the off-shell partonic cross section, and $m \equiv \sqrt{p^2}$ is the parton's off-shellness related to p^- via $m^2 = p^+ p^- - \vec{p}_\perp^2$. We choose

$$\tilde{f}_i(\xi, \vec{p}_\perp) = f_i(\xi, \vec{p}_\perp). \qquad (3.19)$$

Identifying $\tilde{f}_i(\xi, p_\perp)$ with the usual parton distribution functions means that we apply a quasi-particle picture, in which all effects involving more than one parton are encoded in the virtuality distribution $A(m)$. The latter has a width caused by parton-parton interactions (see *e.g.* [88] and references therein).

In our calculations, a Breit-Wigner parametrization for the parton virtual-

ity distribution A(m) is applied:

$$A(m) = \frac{1}{\pi} \frac{\Gamma}{m^2 + \frac{1}{4}\Gamma^2}. \tag{3.20}$$

The width Γ of partons is considered constant at each hard scale (Q^2 in DIS, M^2 in Drell-Yan). We find the value of Γ by comparing the calculated cross sections to the data. For simplicity we use the same $A(m)$ for all parton types. Note that we considered only the region $m > 0$. (3.20) is normalized as

$$\int_0^\infty A(m)dm = 1. \tag{3.21}$$

We choose Breit-Wigner parametrization on analogy with the nucleon spectral function in nuclear physics [27]. This distribution is also often called the Lorentzian function due to its application in geometry and statistics [89]. Note that as $\Gamma \to \infty$, $A(m) \to \delta(m)$. Moments of the Lorentzian function do not exist

$$\int_0^\infty m^n A(m) = \infty, \text{ for all natural } n. \tag{3.22}$$

Therefore, we cannot define the average off-shellness $\langle m^2 \rangle$. However, Γ/π can be understood as the measure of quark off-shellness, because

$$\lim_{a \to \infty} \int_0^a \frac{m^2}{a} A(m) = \frac{\Gamma}{\pi}. \tag{3.23}$$

Summarizing, we propose to parametrize a fully unintegrated parton distribution as a product of the unintegrated distribution and a Breit-Wigner quark off-shellness distribution

$$q(\xi, \vec{p}_\perp, p^-) = f_i(\xi, \vec{p}_\perp)A(\sqrt{p^- \xi P^+ + \vec{p}_\perp{}^2}). \tag{3.24}$$

3.4   DIS cross section formula

3.4.1   Collinear approximation

The factorization formula (3.1) for DIS gives

$$\frac{d\sigma}{d\hat{t}d\hat{u}} = \sum_i e_i^2 \int\limits_0^1 d\xi \int d\vec{p}_\perp f_i(\xi, \vec{p}_\perp) \frac{d\hat{\sigma}}{d\hat{t}d\hat{u}}, \tag{3.25}$$

where s, t, u are the Mandelstam variables, the parton quantities are labeled with hats.

Ignoring the off-shellnesses of partons, the sub-process $qe \rightarrow q'e'$ cross section $d\hat{\sigma}/d\hat{t}d\hat{u}$ is equivalent to that of electron-muon scattering, when the electron and muon masses are neglected [32]:

$$\left(\frac{d\hat{\sigma}}{d\hat{t}d\hat{u}}\right)_{\text{on-shell}} = \frac{2\pi\alpha^2}{\hat{t}^2\hat{s}^2} \left(\hat{s}^2 + \hat{u}^2\right) \delta(\hat{s} + \hat{u} + \hat{t}), \tag{3.26}$$

with $\alpha = e^2/4\pi$, and the δ-function reflects the on-shell condition on the parton level:

$$\hat{s} + \hat{u} + \hat{t} = 0. \tag{3.27}$$

Let us consider the Bjorken limit ($Q^2 \rightarrow \infty$ with x_{Bj} -fixed, where q is the momentum transfer, $Q^2 \equiv -q^2$) in the rest frame of the nucleon. In this limit, one can neglect the transverse motion of partons compared to the "+"- component of the partonic momentum, *i.e.*, the partons are collinear with the hadron. In this case, the partonic and hadronic invariants are simply related:

$$\hat{t} = t, \quad \hat{s} = \xi s, \quad \hat{u} = \xi u. \tag{3.28}$$

From (3.27) and (3.28) one gets the constraint

$$\xi \rightarrow -\frac{t}{s+u} = -\frac{q^2}{2P \cdot q} \equiv x_{Bj}. \tag{3.29}$$

Therefore, the cross section of DIS in the Bjorken limit is

$$\left(\frac{d\sigma}{dtdu}\right)_{\text{LO}} = \sum_i e_i^2 x_{Bj} f_i(x_{Bj}) \left(\frac{2\pi\alpha^2}{t^2s^2} \frac{(s^2 + u^2)}{s+u}\right), \tag{3.30}$$

where

$$f_i(x_{Bj}) \equiv \int d\vec{p}_\perp f_i(x_{Bj}, \vec{p}_\perp),$$

"LO" stands for leading order of perturbative QCD. The formula (3.30) coincides with the parton model result [28].

3.4.2   Off-shell kinematics in DIS

In electron-nucleon DIS, photons of sufficiently high virtuality will interact with a single quark inside the nucleon and not with the nucleon as a whole. In
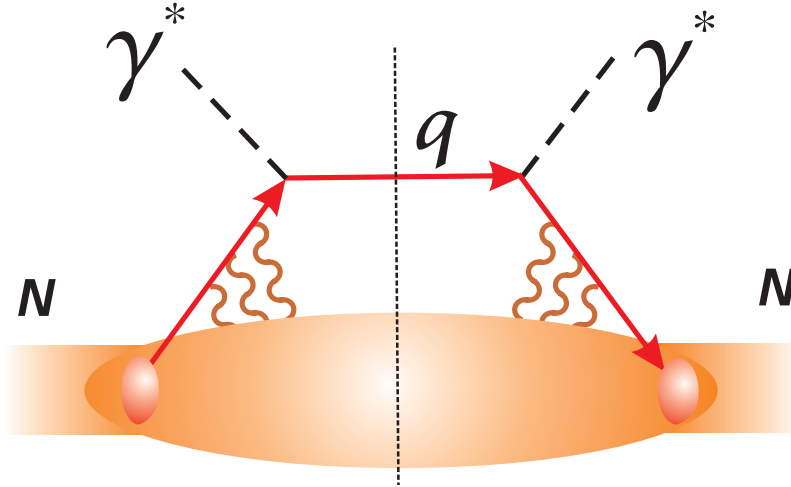
Figure 3.3: The handbag graph for DIS and the relevant initial state interactions that could build up a finite quark width.

this case, the process is described by a hand-bag diagram (see fig. 2.7), where the quark after the interaction with the electron is fixed to the mass shell by the unitarity cut. Physically, an on-shell quark in the final state fragments and, together with the hadron remnants (that move in the opposite light cone direction with respect to the active quark), forms the final high-mass hadronic state.

The active quark in the final state can acquire a small off-shellness and transverse momentum due to gluon exchange in the final state. However, such processes are additionally suppressed by Q^2. It can be interesting to study the FSI effect on DIS and fragmentation [9]. However, we are primarily interested in the fully unintegrated parton densities and, therefore, concentrate on the ISI. The quarks in the initial state are virtual already because they are bound and interact with each other (see fig. 3.3). Therefore, the '-' component of the initial quark momentum is not fixed, and DIS probes not the equal light cone time correlation, but the parton correlation function that we are after.

Let P be the four-momentum of the nucleon and p the momentum of the quark, which interacts with the virtual photon having momentum q. We denote the fraction of the nucleon's light cone momentum P^+ carried by the struck quark in the DIS scattering as

$$\xi \equiv p^+/P^+. \tag{3.31}$$

By demanding the outgoing quark to be on the mass-shell, one obtains:

$$0 = p_f^2 = (p+q)^2 = p^2 + 2p \cdot q + q^2 = p^2 + 2(p^+ q^- + p^- q^+ - \vec{p}_\perp \cdot \vec{q}_\perp) - Q^2, \quad (3.32)$$

where $Q^2 \equiv -q^2 \geq 0$. In a coordinate system, in which $q^+ = 0$,

$$0 = p^2 + 2(p^+ q^- - \vec{p}_\perp \vec{q}_\perp) - Q^2 = p^2 + \xi \frac{2P \cdot q}{Q^2} Q^2 - Q^2 + 2\xi \vec{P}_\perp \cdot \vec{q}_\perp - 2\vec{p}_\perp \cdot \vec{q}_\perp. \quad (3.33)$$

Using the definition of Bjorken variable $x_{Bj} = 2P \cdot q/Q^2$, the above equation 3.33 can be solved with respect to ξ:

$$\xi = x_{Bj} \frac{p^2 + Q^2 + 2(\vec{p}_\perp \cdot \vec{q}_\perp)}{Q^2 + 2x_{Bj}(\vec{P}_\perp \cdot \vec{q}_\perp)}. \quad (3.34)$$

One can see that as $Q^2 \to \infty$, ξ approaches x_{Bj} and so that the momentum fraction carried by the struck quark becomes determined by the momenta of the electron and the nucleon.

3.4.3 DIS cross section taking into account quark off-shellness

For finite Q^2, the fact that the partons are off-shell can generate large corrections to the formulas (3.27)-(3.30). We would like to point out the important analogies and differences to the on-shell case:

- The energy-momentum conservation reads (*cf.* (3.27))

$$\hat{s} + \hat{u} + \hat{t} = m^2, \quad (3.35)$$

  where $m^2 \equiv p^2$ denotes the virtuality of the struck parton.

- In case of an off-shell initial quark, we find the following relation between the partonic and hadronic variables

$$\hat{t} \quad = t = -Q^2, \quad (3.36)$$

$$\hat{s} \quad = \xi(s - M_N^2) + m^2, \quad (3.37)$$

$$\hat{u} \quad = Q^2 - \xi(s - M_N^2) = \xi(u + M_N^2) + Q^2(1 - \frac{\xi}{x_{Bj}}), \quad (3.38)$$

  which coincides with (3.28) in the Bjorken limit. We choose the z-axis

in the direction of the incoming electron's momentum.

• The hadron light cone momentum fraction carried by the struck parton ($\xi \equiv p^+/P^+$) is not equal to the Bjorken x_{Bj}, unless $Q^2 \to \infty$. The relation between x_{Bj} and ξ is

$$x_{Bj} = \xi \frac{Q^2}{Q^2 - m^2 - \xi(M_N^2 - \frac{m^2+\vec{p}_\perp^2}{\xi^2})\frac{Q^2}{s-M_N^2} + 2\vec{p}_\perp\vec{q}_\perp}. \tag{3.39}$$

Relation (3.39) yields a nonlinear equation for x_{Bj}, because $\vec{q}_\perp$ depends on x_{Bj} as follows:

$$\vec{q}_\perp{}^2 = Q^2(1 - \frac{Q^2}{s - M_N^2}(\frac{1}{2x_{Bj}} + \frac{M_N^2}{s - M_N^2})). \tag{3.40}$$

One can see that $\vec{q}_\perp{}^2 \leq Q^2$ and that it reaches its maximum at $s \gg Q^2/2x$. Due to (3.39), the ISI in DIS can be interpreted as a smearing of the parton momentum fraction ξ around its parton model value x_{Bj}. In the following three cases equation (3.39) simplifies:

– Taking the Bjorken limit:

$$x_{Bj} = \xi. \tag{3.41}$$

– Neglecting the transverse momentum of the struck parton inside the nucleon, but keeping $m^2 \neq 0$:

$$x_{Bj} = \xi \frac{Q^2}{Q^2 - m^2 - \xi(M_N^2 - \frac{m^2}{\xi^2})\frac{Q^2}{s-M_N^2}}. \tag{3.42}$$

– Taking into account both the parton's transverse momentum and off-shellness, but considering the limit $s \gg Q^2/2x$, $s \gg M_N^2$:

$$x_{Bj} = \xi \frac{Q^2}{Q^2 - m^2 + 2|\vec{p}_\perp|\sqrt{Q^2}\cos(\phi)}, \tag{3.43}$$

where ϕ is the azimuthal angle of the quark momentum. As Q^2 goes to infinity, equation (3.43) coincides with (3.41).

- The off-shell partonic cross section is

$$\left(\frac{d\hat{\sigma}}{d\hat{t}d\hat{u}}\right)_{\text{off-shell}} = \frac{2\pi\alpha^2}{\hat{t}^2\hat{s}^2}\left(\hat{s}^2 + \hat{u}^2\right)\delta(\hat{s} + \hat{u} + \hat{t} - m^2), \qquad (3.44)$$

where $\hat{u}$ and $\hat{s}$ depend on m^2 via (3.36) and (3.39).

The leading order expression for the Lorentz invariant DIS cross section (3.30) is modified by the ISI as follows:

$$\left(\frac{d\sigma}{dtd\hat{u}}\right)_{\text{ISI}} = \sum_i e_i^2 \int\limits_0^\infty dm\, A(m) \int\limits_0^1 d\xi \int d\vec{p}_\perp\, f_i(\xi, \vec{p}_\perp)\left(\frac{d\hat{\sigma}}{dtd\hat{u}}\right)_{\text{off-shell}}, \quad (3.45)$$

where we used $\hat{t} = t$ from (3.36).

In order to compare our calculations to the experiment or to the leading order cross section (3.30), we also need to change variables from partonic $\hat{u}$ to hadronic u or x_{Bj} (x_{Bj} is related to the hadronic Mandelstam variables (s, t, u) by (3.29)). We choose the following independent variables for the hadronic cross section

$$t,\ x_{Bj}. \qquad (3.46)$$

The partonic cross section $d\hat{\sigma}$ depends on

$$t,\ \hat{u},\ m^2,\ \xi,\ \vec{p}_\perp, \qquad (3.47)$$

with m^2, ξ and $\vec{p}_\perp$ being the integration variables.

Firstly, we transform $d\sigma/dtd\hat{u}$ of (3.45) to $d\sigma/dtdx_{Bj}$ as follows [1]

$$\left(\frac{d\sigma}{dtdx_{Bj}}\right)_{\text{ISI}} = \int_{-\infty}^{m^2} d\hat{u}\left(\frac{d\sigma}{dtd\hat{u}}\right)_{\text{ISI}}\delta(x_{Bj} - x_{Bj}(s, t, \hat{u})), \qquad (3.48)$$

where m^2 is the struck parton off-shellness, x_{Bj} as a function of the variables (3.47) is defined by (3.39). We note in passing that $(d\sigma/dtdx_{Bj})$ is negative, while $(d\sigma/dtd\hat{u})$ is positive. This is taken into account in (3.48) by the choice of integration boundaries.

---

[1] Alternatively, on can use the Jacobian method:

$$\frac{d\sigma}{dtdx_{Bj}} = \frac{\partial(t,\ \hat{u}\ )}{\partial(t, x_{Bj})}\frac{d\sigma}{dtd\hat{u}} = \frac{\partial\hat{u}}{\partial x_{Bj}}\frac{d\sigma}{dtd\hat{u}}.$$

Then, we obtain the hadronic cross section as an integral over the partonic one, using the equations (3.44), (3.45), (3.48),

$$
\left(\frac{d\sigma}{dtdx_{Bj}}\right)_{\text{ISI}} = \sum_i \frac{2\pi\alpha^2 e_i^2}{t^2} \int_0^\infty dm\, \text{A}(m) \int_0^1 d\xi \int d\vec{p}_\perp\, f_i(\xi, \vec{p}_\perp) \int d\hat{u}
$$
$$
\frac{(\hat{s}^2 + \hat{u}^2)}{\hat{s}^2}\, \delta\left(\hat{s}+\hat{u}+t-m^2\right) \delta(x_{Bj} - x_{Bj}(s, t, \hat{u}, \xi, m^2, \vec{p}_\perp)), \quad (3.49)
$$

where $\hat{s} = \xi(s - M_N^2) + m^2$. The integration over $\hat{u}$ can be done using one of the δ-functions.

The result is:

$$
\left(\frac{d\sigma}{dtdx_{Bj}}\right)_{\text{ISI}} = \sum_i \frac{2\pi\alpha e_i^2}{t^2} \int_0^\infty dm \int_0^1 d\xi \int d\vec{p}_\perp\, \text{A}(m) f_i(\xi, \vec{p}_\perp)
$$
$$
\times \left(1 + \frac{(Q^2 - \xi(s - M_N^2))^2}{(\xi(s - M_N^2) + m^2)^2}\right)
$$
$$
\times \delta\left(x_{Bj} - x_{Bj}(s, t, \hat{u}, \xi, m^2, \vec{p}_\perp)\right), \quad (3.50)
$$

where $x_{Bj}(s, t, \hat{u}, \xi, m^2, \vec{p}_\perp)$ is given by (3.39) and $\hat{u} = -t - \xi(s - M_N^2)$. The δ-function can be used to perform the integration over the azimuthal angle of the parton momentum. The remaining three integrations must be performed numerically. The limit $s \gg M_N^2, Q^2/2x$ was taken for simplicity. For the unintegrated parton distributions $f(\xi, \vec{p}_\perp)$ we use the factorized form (3.69) discussed in more detail in the next section. With these simplifications, the integrations can be done in Mathematica [90] program (within about 30 minutes per plot on Athlon2400). The results for DIS are presented in Section 4.1.

3.5   Drell-Yan process cross section formula

3.5.1   Off-shell kinematics in Drell-Yan

We applied the same technique to calculate the cross section of the Drell-Yan process ($pp \to X + l^+l^-$). In this case, an off-shell quark-antiquark pair annihilates into a pair of leptons (see Fig. 3.4). The virtuality of the quark (antiquark) coming from the target proton ($m_1^2 \equiv p_1^2$) and that of the antiquark (quark) coming from the projectile proton ($m_2^2 \equiv p_2^2$) are in general not equal. We assume for simplicity, however, that their distributions $A(m)$ are the same.
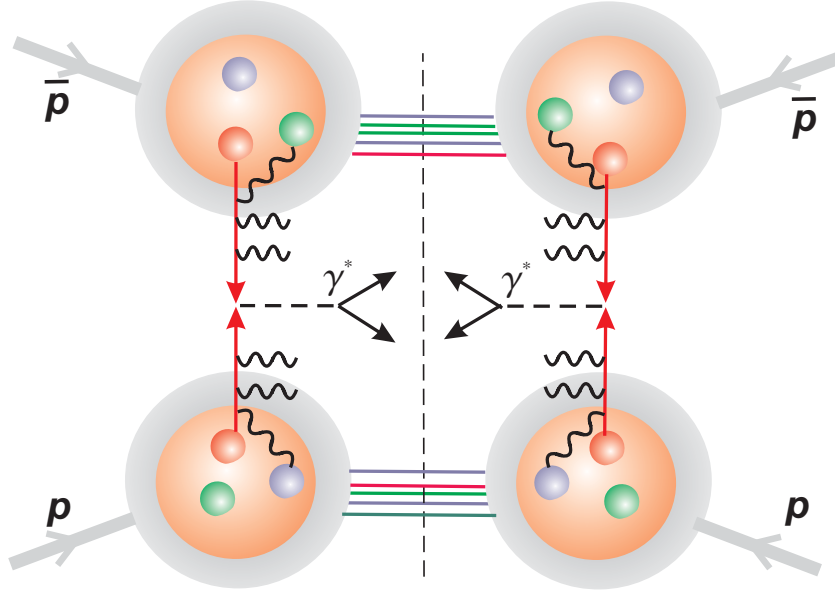
Figure 3.4: Relevant initial state interactions that can build up intrinsic transverse momentum and width of quarks in the proton. The Drell-Yan process.

The connection between the observables and partonic variables in case of two off-shell particles is more complicated. Moreover, the choice of proper partonic variables is frame dependent. We obtain the following kinematic equations in the hadron center of mass system

$$
\begin{aligned}
M^2 &= m_1^2 + m_2^2 + \xi_1\xi_2 P_1^- P_2^+ + \frac{(m_1^2 + \vec{p}_{1\perp}^2)(m_2^2 + \vec{p}_{2\perp}^2)}{\xi_1\xi_2 P_1^- P_2^+} - 2\vec{p}_{1\perp} \cdot \vec{p}_{2\perp}; \\
x_F &= \frac{\sqrt{s}}{s - M^2}\left(\xi_2 P_2^+ - \xi_1 P_1^- + \frac{(m_1^2 + \vec{p}_{1\perp}^2)}{\xi_1 P_1^-} - \frac{(m_2^2 + \vec{p}_{2\perp}^2)}{\xi_2 P_2^+}\right).
\end{aligned}
\tag{3.51}
$$

We use

$$
\xi_1 = p_1^-/P_1^-, \quad \xi_2 = p_2^+/P_2^+,
\tag{3.52}
$$

P_1 (P_2) is the 4-momentum of the target (projectile) hadron, $p_{1,2}$ denote momenta of the annihilating quark and antiquark, M^2 is the invariant mass squared of the produced leptons. s denotes the hadron center of mass energy squared. The Feynman variable is defined as $x_F \equiv p_z/(p_z)^{max}$, where $\vec{p}$ is the lepton pair momentum. In some works, for example [28], an approximate definition for the Feynman variable is used: $x_F \approx 2p_z/\sqrt{S}$. We used the exact

definition [1] that can be written in the hadron center of mass system as follows

$$x_F \equiv \frac{p_z}{(p_z)_{max}} = \frac{2p_z\sqrt{s}}{s - M^2}. \tag{3.53}$$

Experimentally observed Drell-Yan pairs have small M^2 compared to S, so the difference between the two definitions of x_F is small. However, in the Drell-Yan scaling limit, $M^2 \sim s$ and the difference is finite (see formulas (3.55) and 3.56 below).

One sees that the definition of ξ_2 is analogous to the DIS case, whereas the target's momentum fraction is defined as a ratio of minus-components. In some articles, alternative definitions are used: $\xi_1 = p_1^+/P_1^+, \xi_2 = p_2^+/P_2^+$. Our choice of ξ_i definitions is based on the behavior of the hadron momenta in the Drell-Yan scaling limit $(s \to \infty)$.

Let us consider the Drell-Yan scaling limit $(s \to \infty)$. The light cone components of hadron momenta in the center of mass system are

$$\left(P_1^{\mp}\right)^2 = \left(P_2^{\pm}\right)^2 = \frac{s}{2} - M_N^2 \pm \sqrt{\left(\frac{s}{2}\right)^2 - M_N^2 s}. \tag{3.54}$$

Thus, the plus-component of the projectile's momentum P_2^+ and the minus-component of the target's momentum P_1^- go to infinity $\sim \sqrt{s}$, while all the other components are negligible in the scaling limit.

With the chosen definitions of ξ_i, we get as a limit of (3.51):

$$M^2 = \xi_1\xi_2 s;$$
$$x_F = \frac{\xi_2 - \xi_1}{1 - \xi_1\xi_2}. \tag{3.55}$$

Applying approximate definition $x_F \approx 2p_z/\sqrt{s}$, we recover the well known parton model relations:

$$M^2 = \xi_1\xi_2 s;$$
$$x_F = \xi_2 - \xi_1. \tag{3.56}$$

This means that we can use $\xi_1 = p_1^+/P_1^+$, $\xi_2 = p_2^-/P_2^-$ as the arguments of the parton distribution functions in the factorization formula for the Drell-Yan process in the center of mass system.

In contrast, hadron light cone momenta scale differently in the target rest

frame:

$$P_2^\pm = \frac{s}{2M_N} - M_N \pm \sqrt{\left(\frac{s}{2M_N}\right)^2 - s}; \qquad P_1^\pm = M_N. \qquad (3.57)$$

The motion of the projectile is again confined to the light cone. However, there is no special direction for the target parton. Therefore, one needs to parameterize the "soft" properties of the target with more general distribution functions, which depend on the 4-momentum of the parton instead of a single scalar variable ξ. These functions $W(p)$ (partonic Wigner distributions) were introduced in Section 3.2.

M. Sawicki and J.P. Vary have considered the Drell-Yan process in the target rest frame within the non-collinear factorization framework in [91]. They used the analogous to DIS definitions of the both momentum fractions,

$$\xi_1 = p_1^+/P_1^+; \qquad \xi_2 = p_2^+/P_2^+; \qquad (3.58)$$

and found scaling violation. Indeed, in the target rest frame (3.51) transforms to

$$M^2 = m_1^2 + m_2^2 + \frac{\xi_1 M_N}{\xi_2 P_2^+}\left(m_2^2 + \vec{p}_{2\perp}^2\right) + \frac{\xi_2 P_2^+}{\xi_1 M_N}\left(m_1^2 + \vec{p}_{1\perp}^2\right) - 2\vec{p}_{1\perp}\cdot\vec{p}_{2\perp};$$

$$x_F = \frac{1}{w}\left(\xi_1 M_N + \xi_2 P_2^+ - \frac{(m_1^2 + \vec{p}_{1\perp}^2)}{\xi_1 M_N} - \frac{(m_2^2 + \vec{p}_{2\perp}^2)}{\xi_2 P_2^+}\right), \qquad (3.59)$$

with

$$w = \frac{\sqrt{s}}{2}\left(\frac{s}{2M_N^2} - 1 + \frac{M^2}{s}\right)\Big/\sqrt{\frac{s}{4M_N^2} - 1}, \qquad (3.60)$$

if we use the definitions (3.58).

Bearing in mind equations (3.57) and (3.59), we arrive at the following limiting values for M^2 and x_F:

$$M^2 = \frac{\xi_2}{\xi_1}\left(m_1^2 + \vec{p}_{1\perp}^2\right);$$

$$x_F = 2\xi_2. \qquad (3.61)$$

Hence, the variables (3.58) do not coincide with the Bjorken variables in the Drell-Yan scaling limit.

On the other hand, there are no scaling violations, is the definitions (3.52) are used. Contrary to the statement of [91], the relations (3.61) are not a

dynamics effect, but an artifact caused by the use of the alternative definitions (3.58).

The choice of (3.52) was based on the behaviour of the hadron momenta in the scaling limit. Indeed, the relations (3.54) imply that the Drell-Yan process becomes light-cone dominated in the scaling limit and, therefore, the operator product expansion method can be used in order to proof the factorization theorem (see [46] for detail). This does not hold in the target rest frame (*cf.* (3.57)). We conclude that k_T-factorization (3.1) is not applicable in the target rest frame, because the motion of the target parton is not confined to a light cone in the high S limit.

3.5.2   Drell-Yan cross section taking into account quark off-shellness

Using the Feynman rules for QCD derived, for instance, in [92], we find the perturbative QCD cross section of the off-shell quark-antiquark annihilation into a pair of leptons:

$$\frac{d\hat{\sigma}}{d\vec{p}'_1 d\vec{p}'_2} = \frac{e^4 e_q^2 \left[\hat{t}^2 + \hat{u}^2 - m_1^4 - m_2^4 + \hat{s}(m_1 + m_2)^2\right]}{16\pi \epsilon'_1 \epsilon'_2 \hat{s}^2 N_c \sqrt{(p_1 \cdot p_2)^2 - m_1^2 m_2^2}} \delta(p_1 + p_2 - p'_1 - p'_2), \quad (3.62)$$

where $\vec{p}'_{1,2}$ are the three-momenta of the leptons, $\epsilon'_{1,2}$ their energies, and e_q the parton charge in units of the proton charge. The color factor is $N_c = 3$.

The off-shell partonic cross section differential over the Drell-Yan process observables – mass M, Feynman variable x_F, and transverse momentum p_T of the lepton pair – is

$$\frac{d\hat{\sigma}}{dM^2 dx_F dp_T^2} = \int \frac{d\vec{p}'_1}{2\epsilon'_1} \frac{d\vec{p}'_2}{2\epsilon'_2} d\phi \ \kappa \left[\hat{t}^2 + \hat{u}^2 - m_1^4 - m_2^4 + \hat{s}(m_1 + m_2)^2\right]$$
$$\times \delta(p_1 + p_2 - p'_1 - p'_2)\delta(p - p'_1 - p'_2); \quad (3.63)$$

$$\kappa = \frac{\alpha^2 e_q^2 (S - M^2)}{\sqrt{S} E M^4 8 N_c \sqrt{(p_1 \cdot p_2)^2 - m_1^2 m_2^2}}, \quad (3.64)$$

where the integration over $\vec{p}'_1$ and $\vec{p}'_2$ is in the whole 3-dimensional space, and ϕ is from 0 to 2π.

After performing analytically the seven integrations over non-measured quantities, four δ-functions are integrated out and the remaining four preserve

the correct relation between the hadronic and partonic variables (*cf.* (3.51)):

$$
\frac{d\hat{\sigma}}{dM^2 dx_F dp_T^2} = \kappa' \left[2M^4 - M^2 \left(m_1^2 - 6m_1 m_2 + m_2^2 \right) - \left(m_1^2 - m_2^2 \right)^2 \right]
$$

$$
\times \delta \left(M^2 - m_1^2 - m_2^2 - \xi_1 \xi_2 P_1^- P_2^+ - \frac{\left(m_1^2 + \vec{k}_{1\perp}^2 \right) \left(m_2^2 + \vec{k}_{2\perp}^2 \right)}{\xi_1 \xi_2 P_1^- P_2^+} + 2\vec{k}_{1\perp} \vec{k}_{2\perp} \right)
$$

$$
\times \delta \left(x_F - \frac{\sqrt{s}}{s - M^2} \left\{ \xi_2 P_2^+ - \xi_1 P_1^- + \frac{\left(m_1^2 + \vec{k}_{1\perp}^2 \right)}{\xi_1 P_1^-} - \frac{\left(m_2^2 + \vec{k}_{2\perp}^2 \right)}{\xi_2 P_2^+} \right\} \right)
$$

$$
\times \delta \left(\left(\vec{k}_{1\perp} + \vec{k}_{2\perp} \right)^2 - p_T^2 \right), \tag{3.65}
$$

with

$$
\kappa' = \frac{2\alpha^2 e_q^2}{3M^4 N_c \sqrt{(k_1 \cdot k_2)^2 - m_1^2 m_2^2}}. \tag{3.66}
$$

In (3.65),

$$
\epsilon_1 \equiv \frac{1}{2} \left(\xi_1 P_1^- + \frac{(m_1^2 + \vec{k}_{1\perp}^2)}{\xi_1 P_1^-} \right), \quad \epsilon_2 \equiv \frac{1}{2} \left(\xi_2 P_2^+ + \frac{(m_2^2 + \vec{k}_{2\perp}^2)}{\xi_2 P_2^+} \right). \tag{3.67}
$$

Generalizing the ansatz (3.18) to the case of two off-shell partons in the initial state, we obtain the hadronic cross section by integrating over the masses and transverse momenta of quark and antiquark:

$$
\frac{d\sigma}{dM^2 dx_F dp_T^2} = \sum_i \int d\vec{p}_{1\perp} \int d\vec{p}_{2\perp} \int_0^\infty dm_1 \int_0^\infty dm_2 \int_0^1 d\xi_1 \int_0^1 d\xi_2 A(m_1) A(m_2)
$$

$$
\times f_i(Q^2, \xi_1, \vec{p}_{1\perp}) \bar{f}_i(Q^2, \xi_2, \vec{p}_{2\perp}) \frac{d\hat{\sigma}}{dM^2 dx_F dp_T^2}. \tag{3.68}
$$

The integration in (3.68) is 8-fold, $d\hat{\sigma}$ is given by equations (3.65) and (3.66), and

$$
\int d\vec{p}_\perp \equiv \int_0^\infty p_\perp dp_\perp \int_0^{2\pi} d\phi_{p_\perp}.
$$

The common parametrization for the unintegrated parton distributions is [12, 14, 93]

$$
f(Q^2, \vec{p}_\perp, \xi) = f(\vec{p}_\perp) \cdot q(Q^2, \xi), \tag{3.69}
$$

where

$$
f(\vec{p}_\perp) = \frac{1}{4\pi D^2} \exp\{-\frac{\vec{p}_\perp^2}{4D^2}\}, \tag{3.70}
$$

and $q(Q^2, \xi)$ is the conventional parton distribution. For the latter, we have used the latest parametrization by Glück, Reya, Vogt [53]. The mean primordial transverse momentum of partons is

$$< \vec{p}_\perp^2 >= 4D^2. \tag{3.71}$$

The Gaussian form of $f(\vec{p}_\perp)$ allows the analytical evaluation of the integrals over $\vec{p}_{1\perp}$ and $\vec{p}_{2\perp}$. Then, we are left with a four-dimensional integral to be done numerically (see App. B for details on numerics). In the special case of a constant spectral function width, one of the integrals over the off-shellness can be reduced to a superposition of special functions (incomplete elliptic integrals). However, it turned out to be faster to perform the integrals numerically than to evaluate these particular spectral functions.

3.5.3   Intrinsic-k_T approach as a limiting case

We will compare the result of our model, in which the partons in the proton have a finite width, with the experimental data and with the cross sections obtained by two other methods (perturbative QCD and the intrinsic-k_T approach).

In k_T-factorization, the formula

$$d\sigma = f(\xi_1, \vec{p}_{\perp 1}) f(\xi_2, \vec{p}_{\perp 2}) \otimes d\hat{\sigma}(\xi_1, \xi_2, \vec{p}_{\perp 1}, \vec{p}_{\perp 2}) \tag{3.72}$$

is used, where $d\hat{\sigma}$ is the Born cross section for the $q\bar{q}$ annihilation into a pair of leptons, $f(\xi, \vec{p}_\perp)$ is the unintegrated parton distribution defined in (3.2). A proof for the k_T-factorization in the Drell-Yan process is given in the leading twist in [62, 78]. In this case, the primordial transverse momenta of q and $\bar{q}$ have (in general, non-zero) values defined by these distributions in the same way as the usual integrated parton distributions define the large light cone fractions of the parton momenta (p^+ for the projectile parton and p^- for the target parton).

In [62, 78], the fourth component of the parton momentum (p^- for the projectile parton or p^+ for the target parton) is set to zero due to the following reason. For large hard scales M, the projectile parton momentum is $p_2 = (p_2^+, p_2^-, \vec{p}_{2\perp}) \sim M(1, \lambda^2, \vec{\lambda})$, where $\lambda = m_2/M$. The parameter λ is small for $M > 1$ GeV, since the parton off-shellness and transverse momentum are

related to the inverse of the confinement radius and are not expected to scale with M. Our results will show that this assumption is not reliable. In fact, the width of the quark off-shellness (m_2^2) distribution depends on the virtuality M^2 of the photon that probes it (see Sect. 4.3 and Sect. 4.6 for details).

A phenomenological 'intrinsic-k_T approach' has been developed on the basis of the k_T-factorization theorem. In this model, the unintegrated distributions are taken in the form (3.69), (3.70). An additional difference from [62, 78] is that the smaller light cone component of the parton momentum is put to its on-shell value: $p_2^- = \vec{p}_{2\perp}^2/p_2^+$, which is small, but not zero. This approach is well described in the literature [12, 14, 15, 21] and proves to be very useful for the calculation of cross sections and asymmetries of different processes.

The intrinsic-k_T approach is a limiting case of our model at $\Gamma \to 0$. The Drell-Yan process cross section in this approach can be obtained from (3.68) by putting all parton masses to 0 and dropping the mass integrations and spectral functions. In particular, the following kinematic relations are ensured by the δ-functions in this case:

$$M^2 = \xi_1 \xi_2 P_1^- P_2^+ + \frac{\vec{p}_{1\perp}^2 \vec{p}_{2\perp}^2}{\xi_1 \xi_2 P_1^- P_2^+} - 2\vec{p}_{1\perp} \cdot \vec{p}_{2\perp};$$

$$x_F = \frac{\sqrt{s}}{s - M^2} \left(\xi_2 P_2^+ - \xi_1 P_1^- + \frac{\vec{p}_{1\perp}^2}{\xi_1 P_1^-} - \frac{\vec{p}_{2\perp}^2}{\xi_2 P_2^+} \right). \tag{3.73}$$

In Section 4.2, we compare the cross section calculated in our model with off-shell partons to the result of the intrinsic-k_T approach. In order to perform such a comparison, we have calculated the Drell-Yan cross section in the intrinsic-k_T approach by using the full on-shell partonic cross section and the exact kinematics (3.73).

In the works [14,15], the Drell-Yan process was studied also in the intrinsic-k_T approach, but with an additional approximations of the collinear subprocess cross section and the approximate kinematical relations (3.56). We compare our model with this simplified version of the intrinsic-k_T approach in Sect. 4.2. We show in Sect. 4.6 that this approximation is equivalent to truncating the twist expansion at the leading term.

Chapter 4

Results

4.1 DIS cross section dependence on the model parameters D and Γ

The results of our calculations for the deep inelastic electron-proton scattering cross section using the formulas of the subsection 3.4.3 for a range of Γ as compared to the parton model (eq. (3.30)) are shown in fig. 4.1, where Γ is the width of parton off-shellness distribution (3.20). There is a moderate effect of the initial state interaction in DIS in the region of small Bjorken x_{Bj} and low momentum transfer Q^2. The cross section deviation reaches 45% at $Q^2 = 1$ GeV^2, if the parton spectral function width and mean transverse momentum are both equal to 300 MeV. In fig. 4.1, one can also see that the cross section calculated in our model differs from the LO even when the parton width is negligibly small (5 MeV). This effect is due to the non-vanishing intrinsic transverse momentum.

In order to separate the effects of the parton off-shellness from those of the intrinsic transverse momentum, we plot the relative difference between the result of our model with off-shell partons and the calculations taking into account only the intrinsic transverse motion (fig. 4.2), *cf.* subsection 3.5.3. To obtain the cross section in the latter approach, we have put Γ to zero in the formulas of section 3.4 thus forcing the parton on-shell. It is seen that this difference amounts to at most 10 % of the cross section 4.2.

The $Q^2 = 1$ GeV^2 value used in Fig. 4.2 is very low. As we will show in Section 4.6, the effect of parton off-shellness in of higher twist, *i.e.* Q^2-suppressed. Therefore, the deviation of the DIS cross section in our model
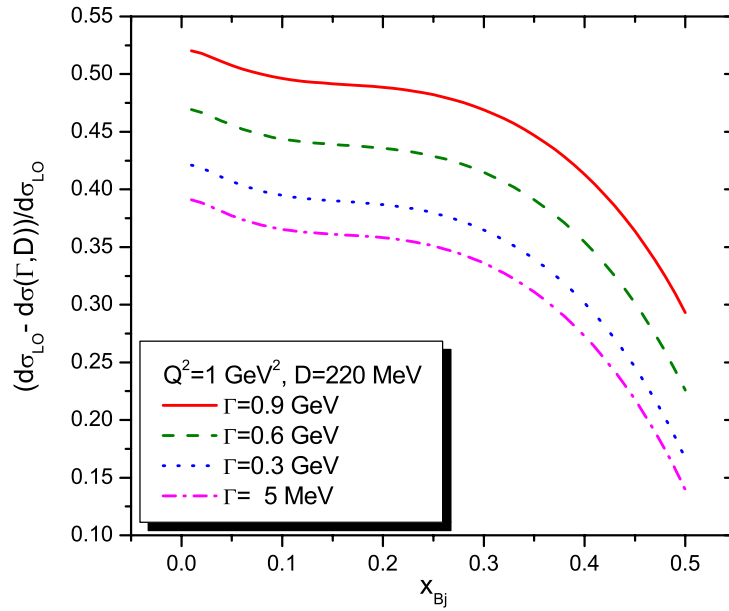
Figure 4.1: Relative deviation of the calculated DIS cross section from the leading order pQCD for the range of parton spectral function widths 5 MeV to 0.9 GeV. $Q^2 = 1$ GeV^2, $s \gg Q^2$.
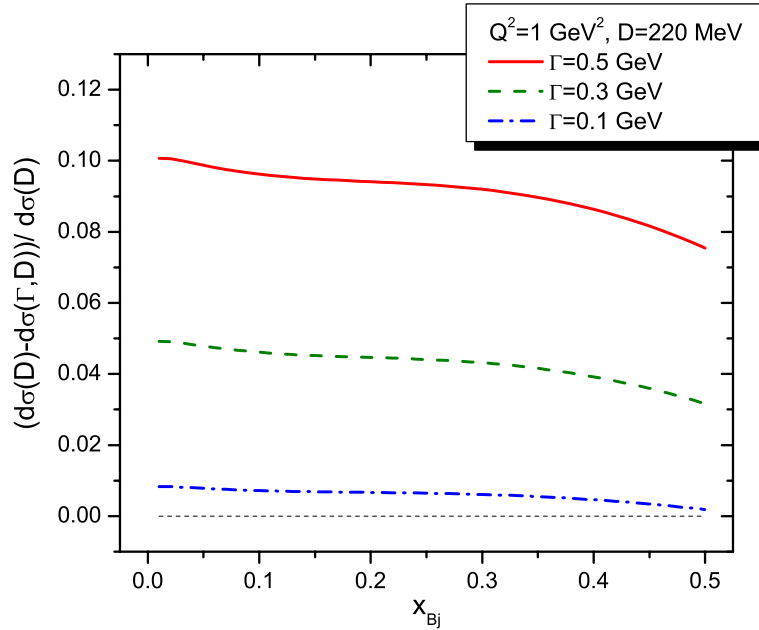

Figure 4.2: Relative deviation of the calculated DIS cross section from the result of calculations taking into account only intrinsic transverse momentum effects. $Q^2 = 1$ GeV^2, $s \gg Q^2$.
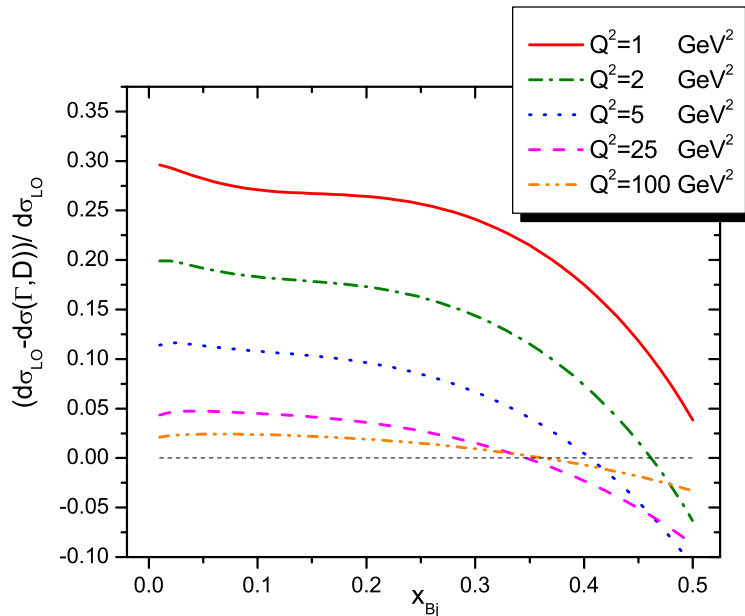
Figure 4.3: Relative deviation of the calculated DIS cross section from the leading order of pQCD for different Q^2. The spectral function width is fixed to $\Gamma = 0.2$ GeV and the transverse momentum dispersion to $D = 0.1$ GeV, $s \gg Q^2$.

from the intrinsic-k_T approach result is even lower at $Q^2 > 1$ GeV^2 relevant for experiments. The Q^2-suppression of parton virtuality and intrinsic transverse momentum effects in DIS is illustrated in fig. 4.3.

For values of Q^2 above 25 GeV^2, the initial state interaction in DIS gives at most a 5% deviation from the lowest order cross section (3.30). For most of the experimentally investigated values of Q^2, the ambiguity in the parton distribution function parameterizations due to the renormalization scale uncertainty is of the same order as the effect of parton off-shellness on DIS cross section.

In the region of $Q^2 \leq 25$ GeV^2, the difference is $30 - 40$ %, which should be observable. However, in order to make a quantitative comparison to the experiment at such low Q^2 and x_{Bj}, we would have to incorporate into our model other effects, such as resonance production and diffractive scattering [94–96].

We conclude that, using the model described in the present work, we cannot extract the value of the parton width in the nucleon from the DIS data. This is the result expected by the analogy to nuclear physics, because the DIS cross section is too inclusive. On the other hand, the DIS data do not contradict

the assumption of a finite parton width in the proton.

4.2 Drell-Yan process cross section dependence on D and Γ

In contrast to the DIS case, the effect of parton off-shellness on the transverse momentum distribution of the Drell-Yan lepton pairs is substantial. In this section, we present the Drell-Yan triple differential cross section calculated by the method described in Section 3.5. We compare the result of our model, in which the partons in the proton have a finite width, with the experimental data and with the cross sections obtained in two other approaches (LO pQCD and standard k_T-factorization).

Although the leading order (LO) of collinear perturbative QCD (pQCD) predicts the correct dependence of the double differential Drell-Yan cross section $d^2\sigma/dM^2dx_F$ on the hard scale M, it fails to reproduce

1. the magnitude of this cross section, the discrepancy being usually parametrized by a K-factor;

2. the average transverse momentum p_T of the dileptons;

3. the p_T-spectrum of Drell-Yan pairs, which is given by the triple differential cross section $d^3\sigma/dM^2dx_Fdp_T$.

Experimentally observed Drell-Yan lepton pairs have non-vanishing transverse momentum p_T, which can be as large as several GeV. Meanwhile, in the leading order approximation of pQCD, the cross section is proportional to $\delta(p_T)$. Indeed, in collinear QCD, both the transverse momentum and the light cone energy of quarks inside hadrons are neglected compared to the component of the quark momentum parallel to the hadron momentum. Thus, the initial state, *i.e.* the colliding quark and antiquark to be annihilated into a lepton pair, has no transverse momentum. Therefore, the final state has zero transverse momentum, too. Possible extensions of the LO pQCD are

a) addition of the NLO processes,

b) taking into account the quark transverse motion and off-shellness.

In the former case (a), the lepton pair can gain non-vanishing p_T, if it recoils against an additional jet in the final state. However, such processes are
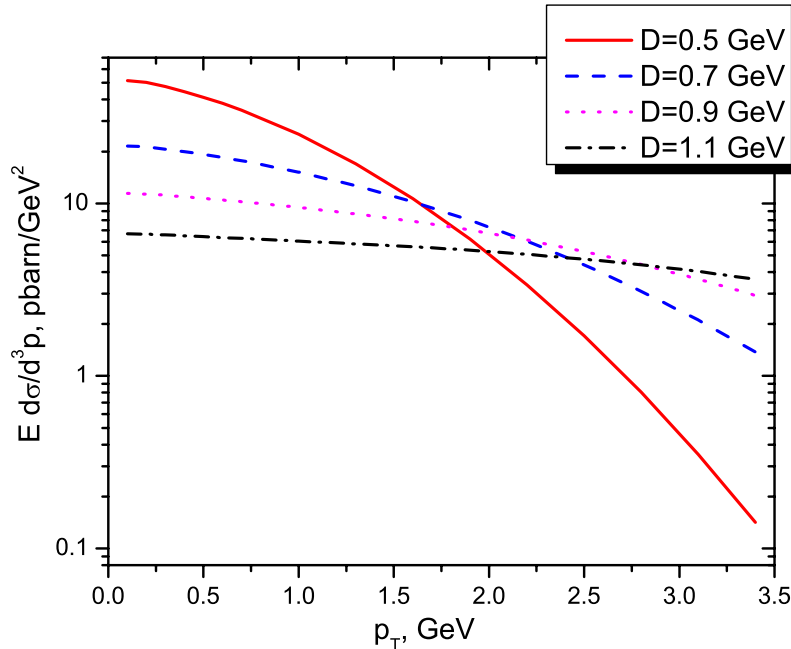
Figure 4.4: Transverse momentum distribution of the Drell-Yan lepton pairs in the intrinsic-k_T approach for different values of the parton primordial transverse momentum dispersion. $M = 4$ GeV, $x_F = 0.1$, $\Gamma = 0$.

suppressed by α_S. In case (b), the recoil transverse momentum is carried by hadron remnants, formed by the "spectator" partons.

The quark and gluon off-shellness can have a large effect for some observables, as will be shown in Sections 4.3, 4.5 and 4.7. In our model, both the double differential and triple differential cross section of the Drell-Yan process are very well reproduced in a wide energy range and with different hadrons in the initial state: pp, pA, $\bar{p}p$. As we will show in the present section, the triple differential Drell-Yan cross section is sensitive to both parameters of the model (D and Γ), thus allowing for a double fit (see Section 4.3). On the other hand, the study of the double differential cross section presented in the subsection 4.4 enables us to relate the model parameters to the phenomenological K-factor.

Calculations using LO pQCD and collinear factorization analogous to (3.1)

$$d\sigma = f(\xi_1)f(\xi_2) \otimes d\hat{\sigma}(\xi_1, \xi_2) \tag{4.1}$$

give a simple result for the triple differential Drell-Yan cross section (p_T-distribution of the dileptons) - a δ-function at zero p_T. This follows from
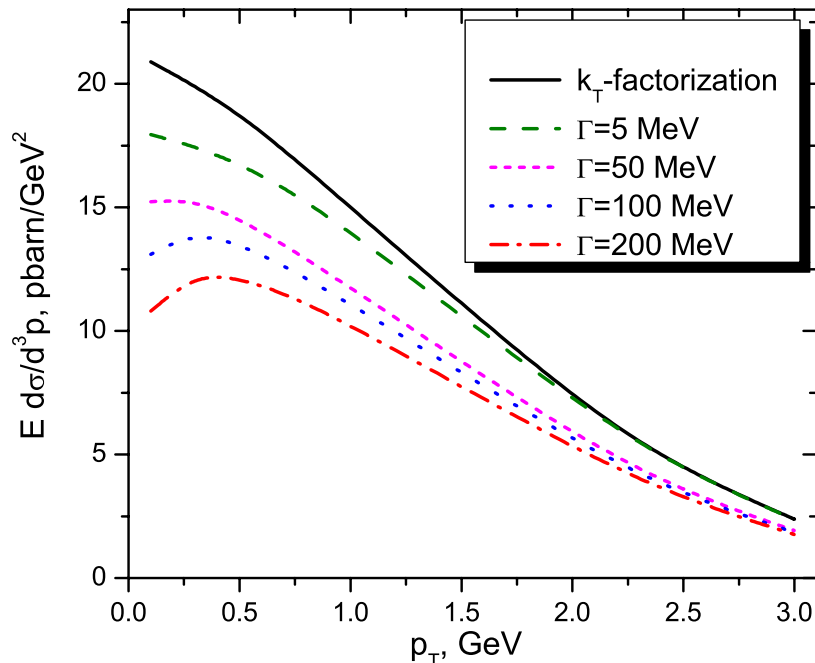
Figure 4.5: Transverse momentum distribution of the Drell-Yan lepton pairs in our model for different values of the parton spectral function width: from $\Gamma = 0$ (solid) to $\Gamma = 200$ MeV (dash-dot). $M = 4$ GeV, $x_F = 0.1$, $D = 0.7$ GeV.

the fact that the annihilating q and $\bar{q}$ in this approach are collinear with the corresponding hadrons, thus the $q\bar{q}$ pair has no transverse momentum in the hadron center of mass system. Therefore, the resulting lepton pair cannot gain any transverse momentum in this model. In contrast, the experimentally measured transverse momentum distribution of the dileptons extends to $p_T = 4$ GeV at a hard scale (the mass of the lepton pair M) as high as 8.7 GeV. Note that NLO corrections do not cure the disagreement with the data. The Drell-Yan pair p_T-distribution obtained in fixed order pQCD is divergent at $p_T = 0$. A resummation of an infinite series of diagrams is necessary to obtain a finite value for the triple differential Drell-Yan cross section at $p_T = 0$ in pQCD with on-shell partons [20].

In order to analyze the effect of a finite parton width and distinguish it from the effect of the intrinsic transverse momentum, we have performed the calculations in both the intrinsic-k_T approach and in our model allowing for off-shell partons. We used the formalism developed in Section 3.5 to calculate the cross section of the Drell-Yan process in the kinematics of the experiment E866 [76, 97] in the intrinsic-k_T approach and for a parton off-shellness distributed
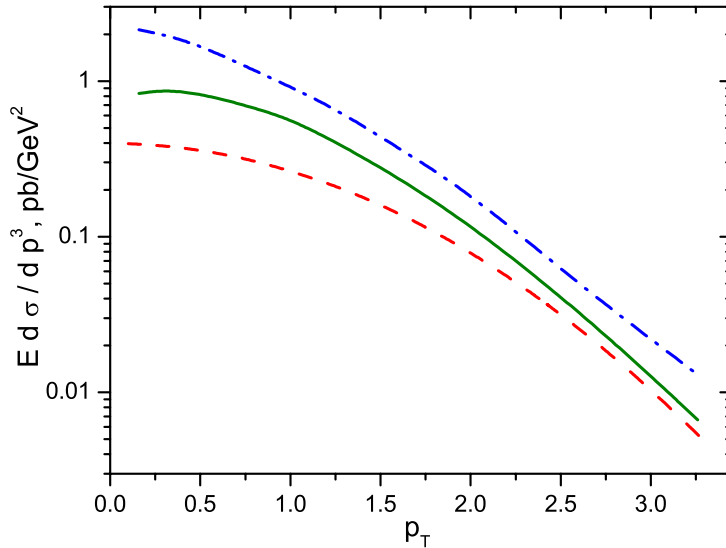
Figure 4.6: Drell-Yan cross section in three approaches: simplified intrinsic-k_T with collinear sub-process cross section (dash), full intrinsic-k_T (dash-dot), our model at $\Gamma = 225$ MeV (solid). Everywhere, $D = 550$ MeV, $\sqrt{s} = 40$ GeV, $M = 7.5$ GeV.

according to the Breit-Wigner spectral function (3.20).

We present the obtained cross section

$$\frac{d\sigma}{d\vec{p}} \equiv \frac{2}{\pi\sqrt{s}} \frac{d\sigma}{dx_F dp_T^2} \tag{4.2}$$

for different values of the parameters in figures 4.4 and 4.5. We illustrate in fig. 4.4 that the slope of the distribution mainly depends on the dispersion of the intrinsic transverse momentum (D), which is proportional to the primordial transverse momentum of the parton (see (3.71)). In the limit, in which the dispersion of the intrinsic transverse momentum (D) goes to zero, the leading order result of perturbative QCD, *i.e.* a sharp peak at $p_T = 0$, is restored.

On the other hand, the parton width variation leads to changes of the cross section magnitude and influences the behavior of the distribution in the region of low p_T (see Fig. 4.5). With increasing Γ, magnitude of the cross section decreases, the decrease being most pronounced at low p_T, which shifts the peak of the distribution to higher p_T. This indicates that some additional nonperturbative effects are included via a finite parton width. One can also see in Fig. 4.5 that our model approaches the result of the standard intrinsic-k_T

method as the parton width (Γ) goes to zero.

The formula (3.68) is often simplified by neglecting the dependence of $\hat{\sigma}$ on $\vec{k}_{T1}$ and $\vec{k}_{T2}$, for example in [22] and in PYTHIA [24]. In this case, the integration of $\hat{\sigma}$ can be done analytically. Summarizing, there are three phenomenological approaches to the Drell-Yan process beyond LO pQCD:

1. our model, accounting for both intrinsic transverse momentum ($D \neq 0$) and off-shellness ($\Gamma \neq 0$) of quarks;

2. intrinsic-k_T approach ($D \neq 0$), which is the limiting case of our model at $\Gamma = 0$;

3. simplified intrinsic-k_T approach ($\Gamma = 0$), in which the primordial transverse momentum is not zero ($D \neq 0$), but the non-collinearity of the $\bar{q}q \to l^+l^-$ sub-process cross section $d\hat{\sigma}$, *i.e.* its dependence on $\vec{k}_1$ and $\vec{k}_2$, is neglected.

We compare the effects of primordial k_T, non-collinearity of $d\hat{\sigma}$ and quark off-shellness by plotting the triple differential Drell-Yan cross section calculated in the three aforesaid phenomenological approaches in Fig. 4.6. The simplified intrinsic-k_T approach gives a Gaussian for the p_T-distribution (dash line). As we will show in Section 4.6, the approximation of $\Gamma = 0$ and collinear $d\hat{\sigma}$ is equivalent to restricting oneself to the leading order in the twist expansion, that is, in the case of the unpolarized Drell-Yan process, the expansion in powers of $1/M$. In Fig. 4.6, the importance of higher twist corrections in the Drell-Yan process is illustrated by the difference between the solid and dash lines.

The part of higher-twist effects incorporated in the full intrinsic-k_T approach changes the distribution considerably (*cf.* the dash and dash-dot curves in Fig. 4.6). On the other hand, additional higher twist effects, modelled by quark off-shellness and given by the difference between the dash-dot and solid curves, are of the same order. We conclude that higher twists in the Drell-Yan process can be large and that we have to take into account both non-collinearity and off-shellness of quarks in order to model them.

4.3   Analysis of Drell-Yan data on triple differential cross section

4.3.1   Fit to the data of experiment E866 on $pp \to \mu^+\mu^- X$

In figures 4.7-4.12, calculations both in the model with off-shell partons and in the standard k_T-factorization approach are compared to the data of the Fermilab experiment E866 for the continuum dimuon production in pp collisions at 800 GeV incident energy, corresponding to $\sqrt{s} = 40$ GeV. In this experiment, both the double differential Drell-Yan cross section $d\sigma/dM^2dx_F$ (data published in [97]) and the triple differential cross section $d\sigma/d\vec{p}$ (data published in [76]) were measured in a wide range of M and x_F (here, $\vec{p}$ is the lepton pair's momentum). The p_T-distribution was obtained in terms of the triple differential cross section averaged over the azimuthal angle of the lepton pair

$$E\frac{d\sigma}{d\vec{p}} \equiv \frac{2E}{\pi\sqrt{s}}\frac{d\sigma}{dx_F dp_T^2} = \frac{2E}{\pi\sqrt{s}}\int_{\text{bin}}\frac{d\sigma}{dx_F dp_T^2 dM^2}\, dM^2, \qquad (4.3)$$

where

$$E \equiv \sqrt{M^2 + p_T^2 + x_F^2(s - M^2)^2/(4s)}. \qquad (4.4)$$

The data points were averaged in several bins in M and x_F. The x_F binning is responsible for the wiggly structures both in the data and some of our calculations.

The result of the intrinsic-k_T approach is shown in figures 4.7 and 4.8 (solid line). The slope of the cross section can be reproduced by an appropriate choice of the single parameter (D) of the intrinsic transverse momentum distribution, given by (3.70). The optimal values for D are $500-600$ MeV, which correspond to

$$< p_\perp^2 >^{1/2} = 1.0 - 1.2 \text{ GeV}. \qquad (4.5)$$

A slightly smaller value for this parameter was obtained in [14, 15] from the analysis of the data of the experiment E744 on Drell-Yan cross section in pp collisions at 400 GeV incident energy:

$$< p_\perp^2 >^{1/2} = 0.8 - 1.0 \text{ GeV}. \qquad (4.6)$$

Still, the data are overestimated by a factor of $2-3$, depending on the mass of the Drell-Yan pair (M). Dashed lines in figures 4.7 and 4.8 illustrate
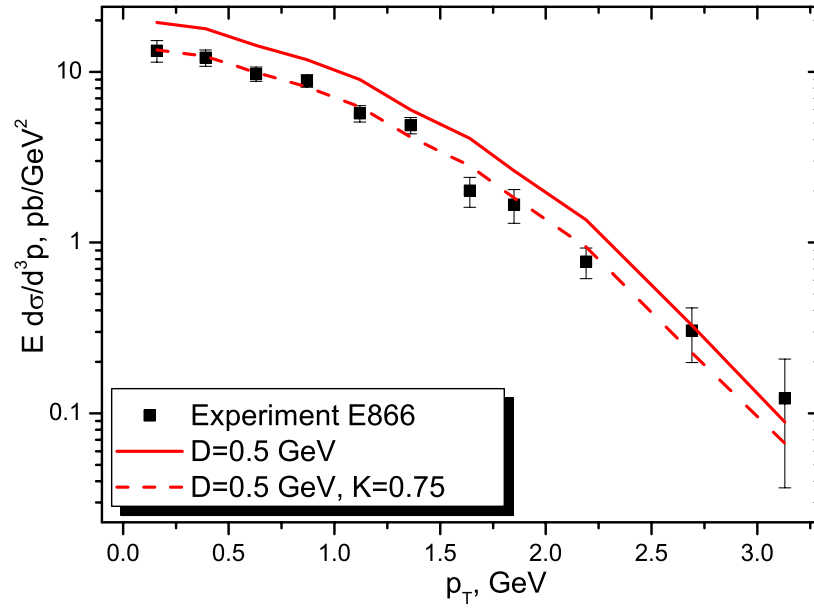
(a) $4.2 \leq M \leq 5.2$ GeV
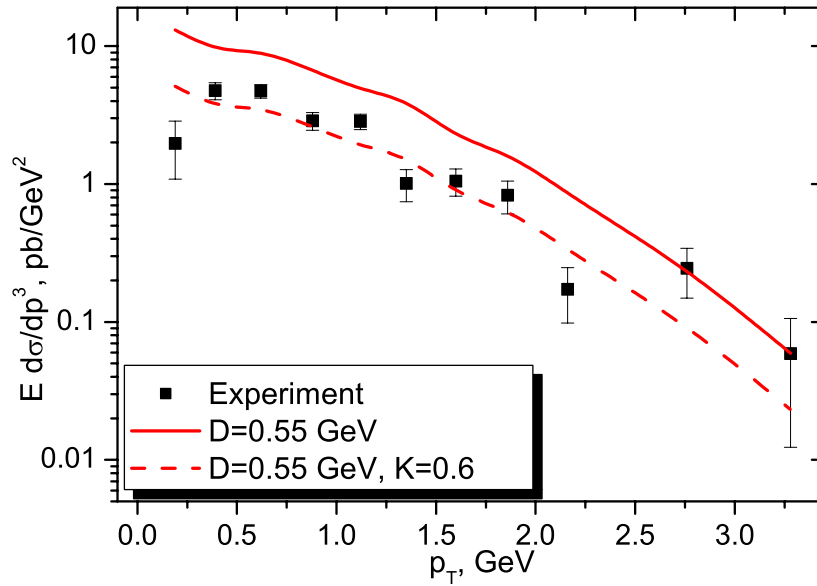

(b) $5.2 \leq M \leq 6.2$ GeV

Figure 4.7: Drell-Yan cross section in intrinsic-k_T approach (solid line) compared to the data of E866 [76]. An additional overall K-factor is necessary to reproduce the cross section amplitude (dashed line), $-0.05 \leq x_F \leq 0.15$.
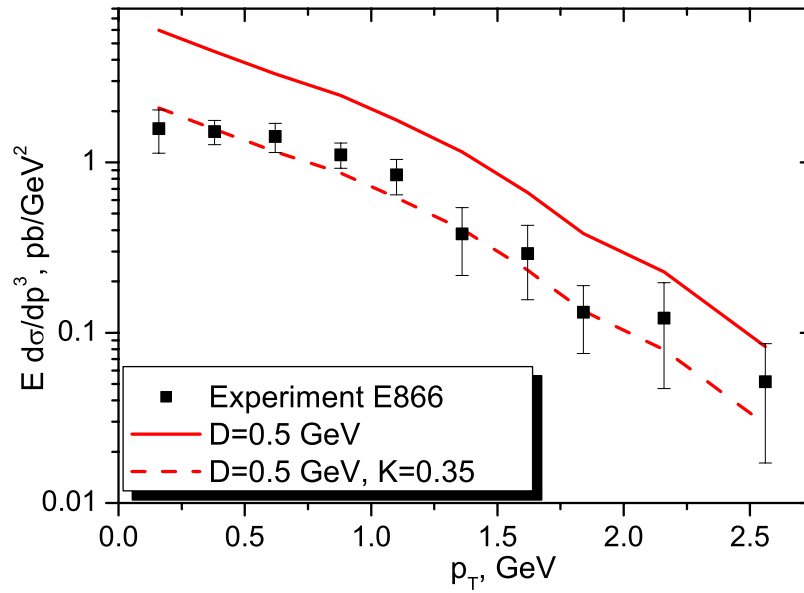
(a) $6.2 \leq M \leq 7.2$ GeV
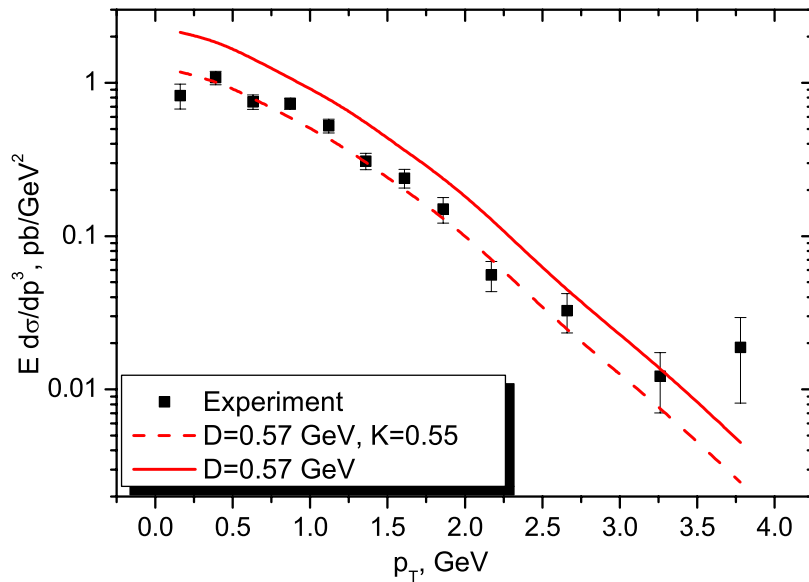

(b) $7.2 \leq M \leq 8.7$ GeV

Figure 4.8: Same as Fig. 4.7, but higher mass bins.

that the data can be fitted by introducing an additional overall factor (K). The discrepancy between the calculations and the data is larger for higher M. Thus, in the intrinsic-k_T approach, the magnitude of the cross section cannot be correctly reproduced. An additional overall K-factor is necessary that reflects the importance of higher order corrections to the Drell-Yan cross section.

In contrast, the calculations with a finite parton width yield not only the experimentally measured shape of the cross section but also its amplitude without any K-factor. The comparison of our results with the data is presented in figures 4.9-4.12. The values for the average parton primordial transverse momentum

$$< p_\perp^2 >^{1/2} = 0.9 - 1.1 \text{ GeV} \tag{4.7}$$

are compatible with those existing in the literature (4.6). Allowing for off-shell partons, we eliminate the need for any K-factor. Choosing Γ in the order of 100 MeV (*cf.* table 4.1 for details), both the amplitude and the slope of the cross section are well reproduced.

The dependence of the optimal values for the parameters (dispersion D and width Γ) on the mass of the Drell-Yan pair was obtained by fitting experimental data within different bins of M independently. The result is presented in figures 4.9-4.12 and in table 4.1. Note that the varying quality of the data in different mass bins leads to large uncertainties in the extraction of the width. In table 4.1 we present the average values and uncertainties for D and Γ. The latter have been obtained by analyzing the χ^2 values as a function of D and Γ.

We find that the optimal Γ increases with the hard scale (the mass of the Drell-Yan pair). The dependence of Γ on M indicates that, at higher scales, partons with broader spectral functions are probed. However, as we will shown in Sect. 4.6 by analyzing the $M^2 \to \infty$ limit, Γ decreases as $1/M$ with growing, asymptotically large M^2. The increase of Γ with M that we have obtained for $M = 4.2 - 7.8$ GeV must be due to relatively low hard scales and may be a consequence of phase space limitations arising as $M \to 0$. We did not study the dependence of our parameters on x_F.

The analysis of the data in the mass bin $6.2 \le M \le 7.2$ GeV calls for more discussion. As shown in Fig. 4.11, the best fit (dashed line) to this data set leads to values for both parameters (D=0.43 GeV, Γ=1.1 GeV), which are not in the trend set by the fits to the other three data bins (cf. table 4.1). Thus, we did not trust this fit and sought for more experimental input. For
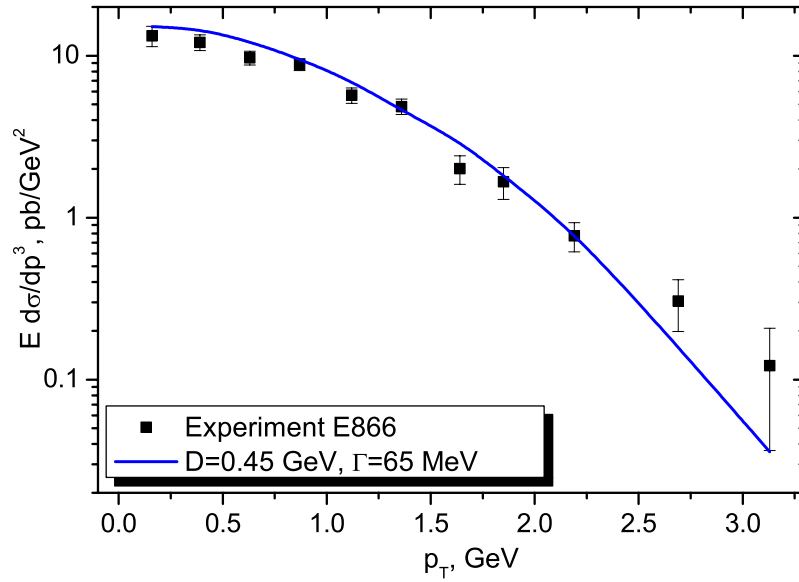
Figure 4.9: The Drell-Yan cross section as calculated in our model (solid line) compared to the data of the Fermilab experiment E866 for the continuum dimuon production in 800 GeV proton, $4.2 \leq M \leq 5.2$ GeV, $-0.05 \leq x_F \leq 0.15$. Only statistical errors shown.
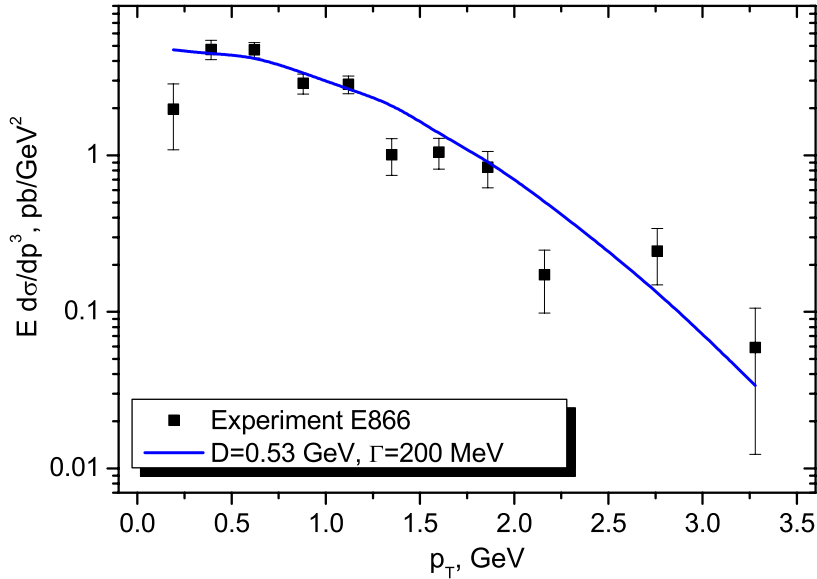
Figure 4.10: Same as fig. 4.9, only for a higher mass bin: $5.2 \leq M \leq 6.2$ GeV.
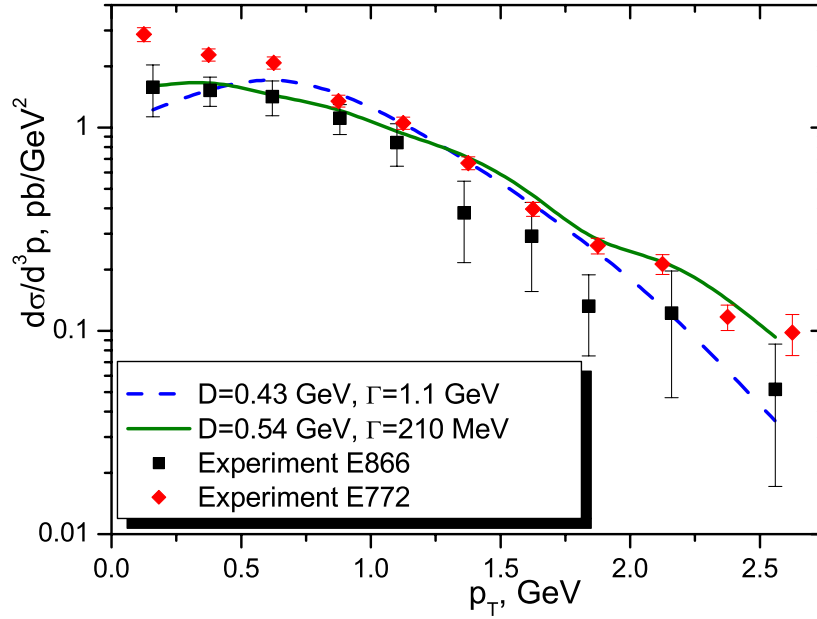
Figure 4.11: The Drell-Yan cross section as calculated in our model compared to the data of E866 on $pp \to \mu^+\mu^- X$, $6.2 \le M \le 7.2$ GeV, $-0.05 \le x_F \le 0.15$, and to the data of E772 on $pd \to \mu^+\mu^- X$, $6 \le M \le 7$ GeV, $0 \le x_F \le 0.3$. Only statistical errors shown. See main text for more details about the different lines.
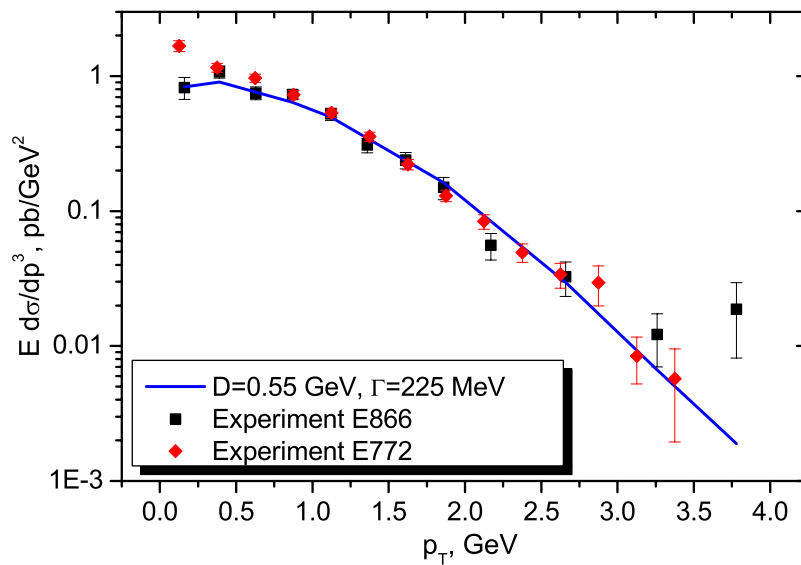
Figure 4.12: Same as fig. 4.11, only for a higher mass bin: $7.2 \le M \le 8.7$ GeV.

M	4.2-5.2	5.2-6.2	6.2-7.2	7.2-8.7
D	450 ± 100	530 ± 70	540^*	550 ± 60
Γ	65 ± 20	200 ± 75	210^*	225 ± 75

Table 4.1: Optimal parameters for different masses of the Drell-Yan pair, $-0.05 \leq x_F \leq 0.15$. All values are in MeV. Values denoted with stars are trend-average and not best-fit. See main text for details.

$p_T \geq 1$ GeV, the data of the experiments E866 on $pp \to \mu^+\mu^- X$ and E772 [98] on $pd \to \mu^+\mu^- X$ agree very well in all the mass bins, except the one of Fig. 4.11 (see Fig. 4.12, for example). Therefore, we compared our fit (dashed line) to the experimental data on the pd cross section from E772 in approximately the same mass range (Fig. 4.11). One can see that the calculations with $D = 0.43$ GeV and $\Gamma = 1.1$ GeV (dashed line) do not reproduce the high-p_T part of the pd cross section. On the other hand, if the trend-average values from table 4.1 are applied ($D = 0.54$ GeV, $\Gamma = 210$ MeV, solid line in Fig. 4.11), the cross section calculated in our model both describes the E866 data on the border of experimental error bars and reproduces the pd cross section of E772 at $p_T \geq 1$ GeV.

Allowing for a finite parton width and using a single-parameter form for the parton spectral function, we account for non-perturbative effects, including the K-factor. The result of the collinear factorization and fixed order pQCD (δ-peak at $p_T = 0$) is not reached in the experiment even at masses of lepton pairs as high as $M \sim 16$ GeV. There is one area of hard scales, where the intrinsic-k_T approach seems to reproduce the cross section with good accuracy: at low M the K-factor of the intrinsic-k_T approach is closer to 1. As the dilepton mass goes higher, the measured distribution is getting more sharply peaked. This suggests that the result of LO pQCD might be recovered at Drell-Yan pair masses, which are higher than those yet observed. On the other hand, our model allowing for off-shell partons with finite width works well for all hard scales M.

4.3.2 Reproduction of the data of experiments E605 and E772 on $pA \to \mu^+\mu^- X$

In Section 4.3.1, our model was compared to the data on the triple differential Drell-Yan cross section $d^3\sigma/dM^2 dx_F dp_T$ from experiment E866 [76] at
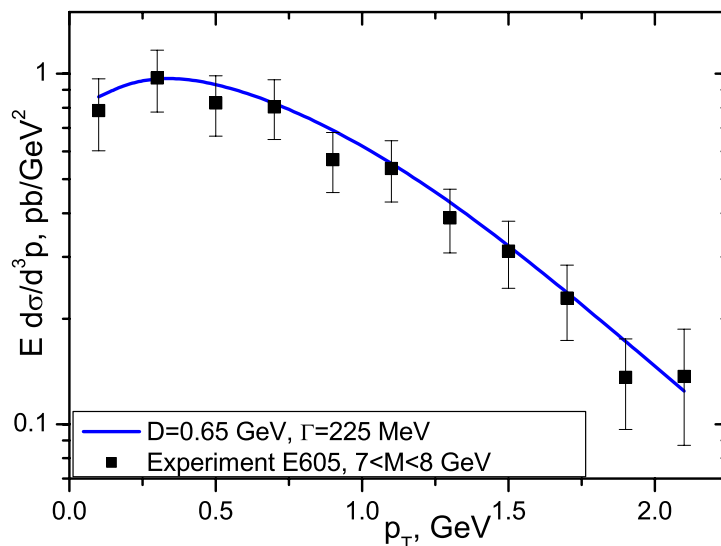
Figure 4.13: Prediction for the p_T spectrum of Drell-Yan dileptons in our model at $\sqrt{s} = 40$ and $x_F = 0.1$ as compared to the data of experiment E605 [99].

Fermilab in pp collisions at 800 GeV incident energy. Both the slope and magnitude of the p_T distribution of the Drell-Yan pairs were described well without the need for a K-factor. In particular, the experimentally measured p_T is reproduced in this model by fitting the model parameter D (the dispersion of the quark intrinsic transverse momentum). At $s = 1600$ GeV^2, we obtained $D = 0.5 \pm 0.18$ GeV. On the other hand, the detailed shape of the distribution turned out to be sensitive to the off-shellness, giving $\Gamma = 50 - 300$ MeV (depending on the mass bin) for this particular experiment.

The distribution of the transverse momentum of lepton pairs produced in the Drell-Yan process off *nuclei* $pA \rightarrow l^+l^-X$ also can be reproduced within this model. For example, in Fig. 4.13 the calculation for the transverse momentum spectrum of Drell-Yan dileptons of our model is compared to the data of the experiment E605 [99] on $p\,Cu$ collisions at $\sqrt{s} = 38.8$ GeV, $x_F = 0.1$. The cross section plotted in Fig. 4.13 is given by (4.3). The model parameters D, Γ used in the calculations were fitted to data on $pp \rightarrow l^+l^-X$ in the previous subsection and no readjustment was done for the pA case.

On the other hand, one can study nuclear effects in the Drell-Yan process, using higher accuracy data, for example, the pd Drell-Yan data from the experiment E772. See the comparison of our model result for the pp process
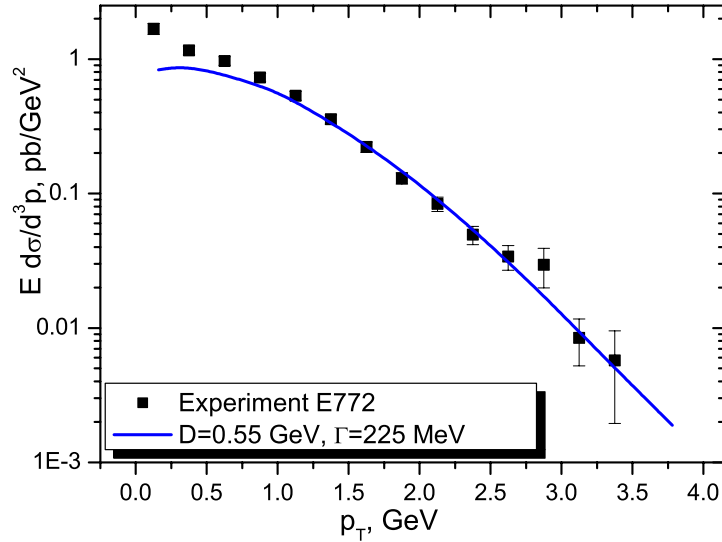
Figure 4.14: Prediction for the transverse momentum spectrum of Drell-Yan dileptons in a model, accounting for the intrinsic-k_T and off-shellness of quarks in the proton, as compared to the data of the experiment E772 [98] on $p\,d$ collision at $\sqrt{s} = 38.8$ GeV. Only statistical errors shown. The model parameters D, Γ were fitted to the data on $pp \to l^+l^-X$. $x_F = 0.1$.

compared to the pd cross section divided by $A = 2$ in Fig. 4.14. The discrepancy between the Drell-Yan pair production in pp and pd can be absorbed into the parametrization of nucleon parton distribution functions. However, it is naïve to assume that the effects of Fermi motion and binding of nucleons in nuclei is negligible. A model to account for these effects in pd Drell-Yan is suggested in [100].

4.4 Drell-Yan transverse momentum evolution with M and s in NLO pQCD

In this section, we study the average p_T of the Drell-Yan pairs produced in $\bar{p}p$ collisions in the scope of conventional perturbative QCD. Consequently, intrinsic transverse momentum and off-shellness of the quarks are neglected for the duration of the current section. Therefore, important features are missing and we do not expect to reproduce the experimental p_T.

At NLO of perturbative QCD, several diagrams contribute to the triple differential cross section, see Fig. 4.15. Among these, the vertex corrections do not generate transverse momentum. Therefore, we are interested in the gluon
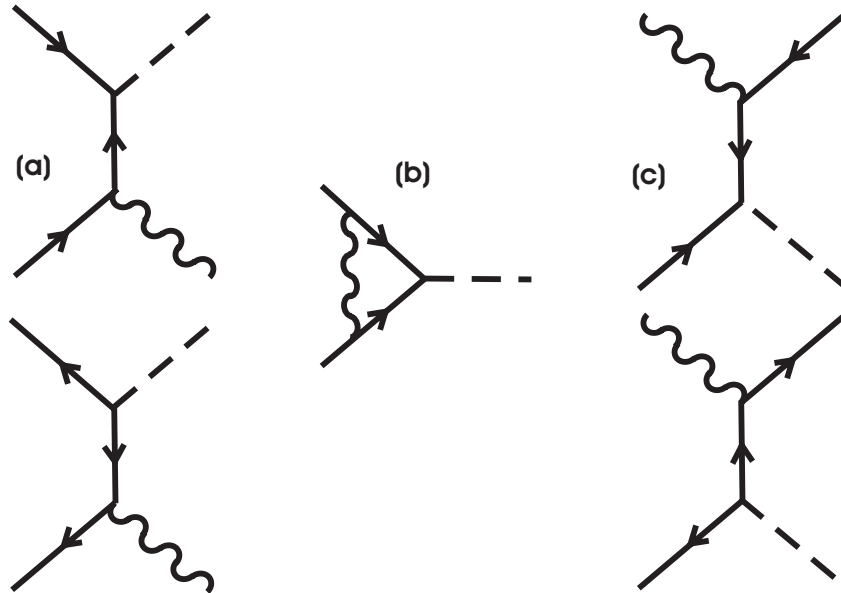
Figure 4.15: $O(\alpha_S)$ contributions to the Drell-Yan process: (a) gluon Bremsstrahlung, (b) vertex correction, (c) gluon Compton scattering. Virtual photons (dashed lines) split into lepton pairs, waved lines denote gluons, arrows denote quarks. In each diagram, time runs from left to right.

Bremsstrahlung and gluon Compton scattering. The pair with invariant mass M has a transverse momentum that relates to the scattering angle as [101]

$$p_T^2 = \frac{(\hat{s} - M^2)^2}{4\hat{s}} \sin^2 \Theta, \tag{4.8}$$

where $\hat{s} = x_1 x_2 s$ is the total squared energy of the colliding partons in terms of their momentum fractions in the collinear approximation, and Θ is the scattering angle of the outgoing lepton pair with respect to the incoming quark momentum in the quark centre of mass system.

In particular, the gluon Compton scattering contributes to the pairs with $p_T \gtrsim M$ [102], *i.e.* in the tail of the p_T distribution. On the other hand, the gluon Bremsstrahlung process generates the bulk of the Drell-Yan pairs with a non-vanishing perturbatively generated p_T. According to [101], the cross section of the process $\bar{q}q \rightarrow g + \mu^+\mu^-$ is

$$\frac{d^2\hat{\sigma}}{dM^2 d\cos\Theta} = \frac{8\alpha^2 e_q^2 \alpha_S}{27M^2} \frac{\hat{s} - M^2}{\hat{s}^2 \sin^2\Theta} \left\{ 1 + \cos^2\Theta + 4\frac{M^2\hat{s}}{(\hat{s} - M^2)^2} \right\}. \tag{4.9}$$

By convoluting the sub-process cross section (4.9) with parton distribu-
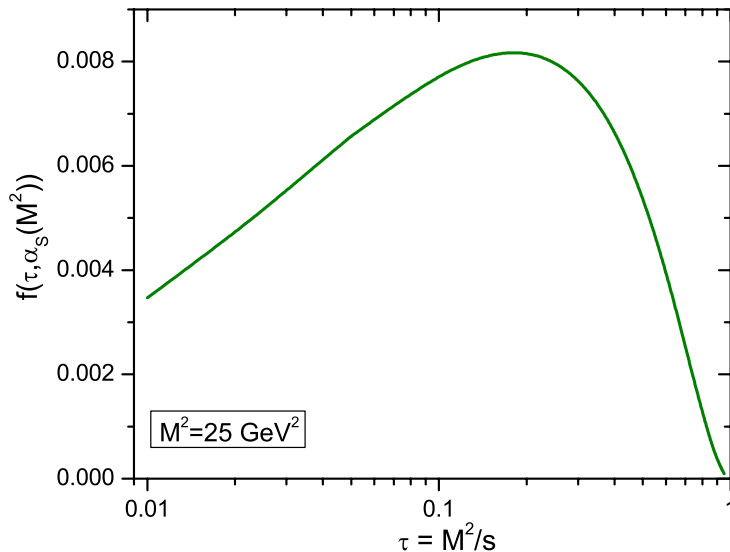
Figure 4.16: Function $f(\tau, \alpha_S)$ introduced in (4.11). This function governs the evolution of the p_T of Drell-Yan pairs with s and M^2 at NLO perturbative QCD.

tions, one expects to obtain the p_T distribution of the Drell-Yan pairs. Unfortunately, the resulting cross section is singular at $p_T = 0$ [73], so that the triple differential cross section cannot be described by NLO perturbative QCD. In order to be able to compare the NLO result with other approaches and with experiment, the authors of [101] and [103] proposed instead to calculate the average squared transverse momentum of Drell-Yan dileptons

$$\langle p_T^2 \rangle_{pert} = \frac{\int p_T^2 (d^2 \sigma_{NLO}/dp_T dM^2) dp_T}{d\sigma_{NLO}/dM^2}, \tag{4.10}$$

which is finite. In formula (4.10), $d\sigma_{NLO}$ is the double differential hadronic Drell-Yan cross section at the next-to-leading order.

The result is

$$\langle p_T^2 \rangle_{pert} = \alpha_S(M^2) s f(\tau, \alpha_S(M^2)), \tag{4.11}$$

where $\tau \equiv M^2/s$. Therefore, in the leading power of $\alpha_S(M^2)$, the mean squared p_T of Drell-Yan pairs is proportional to s, to α_S, and to a functional of parton distributions $f(\tau, \alpha_S)$ derived in [101]. Based on (4.11), it is sometimes concluded that $\langle \vec{p}_T^2 \rangle_{pert}$ scales linearly with s [22, 104, 105]. However, there is an additional nonlinear dependence on s in $f(\tau, \alpha_S(M^2))$ through its dependence
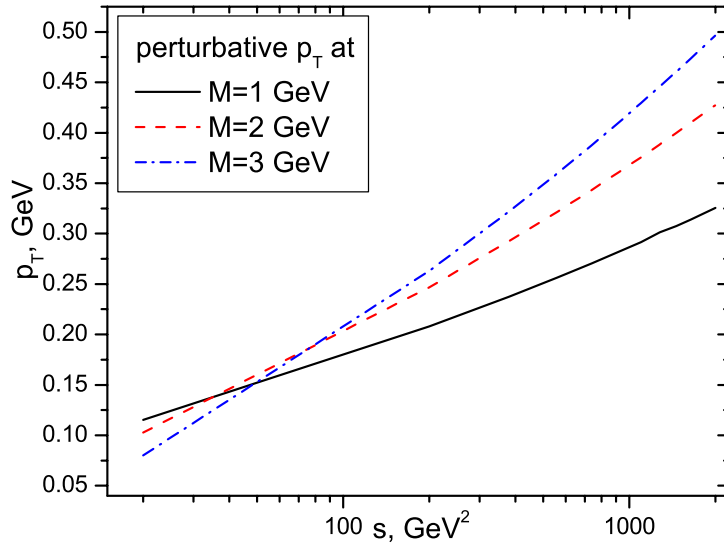
Figure 4.17: Evolution of the perturbative component of Drell-Yan pair transverse momentum $p_T \equiv \sqrt{\langle \vec{p}_T^2 \rangle_{pert}}$ with s at different values of M.

on $\tau \equiv M^2/s$. The dependence of f on α_S is introduced by the scaling violations in the parton distributions, while the dependence of f on τ arises from the gluon Bremsstrahlung cross section [101].

In order to determine the evolution of $\langle \vec{p}_T^2 \rangle_{pert}$ with M and $\sqrt{s}$, we have calculated the function $f(\tau, \alpha_S(M^2))$ numerically, using a recent parametrization [53] for parton distributions. The result is shown in Fig. 4.16. We see that only for a narrow region around $\tau \approx 0.2$, $f(\tau, \alpha_S)$ is approximately constant with τ, and $\langle p_T^2 \rangle_{pert}$ is proportional to s. The position of the peak of f slightly shifts to the right with growing M.

The resulting dependence of $p_T \equiv \sqrt{\langle \vec{p}_T^2 \rangle_{pert}}$ on s and M is plotted in Fig. 4.17 and 4.18, respectively. One can see in Fig. 4.17 that the evolution of perturbative p_T with s is almost logarithmic, in contrast to the naïve expectation of being proportional to $\sqrt{s}$. Furthermore, the slope of the logarithmic rise with s depends on M. Note that there is an interesting cross-over at about $s \approx 50$ GeV^2 (Fig. 4.17). While the perturbative $\langle p_T^2 \rangle_{pert}$ of Drell-Yan pairs increases with increasing M at high center of mass energy $\sqrt{s}$ (see Fig. 4.18(a)), it decreases with M at low s (for instance, at $s = 32$ GeV^2 relevant for the future PANDA experiment [23], Fig. 4.18(b)) due to phase-space limitations.

The transverse momentum distribution of Drell-Yan dileptons, *i.e.* the
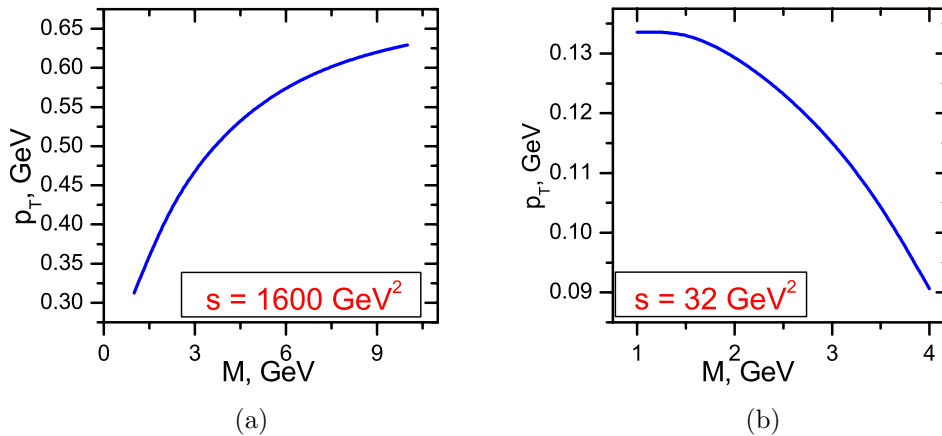
Figure 4.18: Perturbatively generated $p_T \equiv \sqrt{\langle \vec{p}_T^2 \rangle_{pert}}$.

triple differential cross section $d\sigma/dM^2 dx_F dp_T^2$, in the NLO perturbative QCD is singular at $p_T = 0$ [101, 106] and underestimates experimental data at high p_T [104, 107]. The average p_T of Drell-Yan pairs also cannot be reproduced in NLO. Indeed, the p_T calculated above is around 0.6 GeV at $s = 1600$ GeV^2 and $M \approx 7$ GeV (see Fig. 4.18(a)). This value is about a factor of 2 smaller than the width of the p_T distribution measured by the Fermilab experiment E866 [76]. We have to conclude that NLO pQCD is insufficient to describe present data on p_T of Drell-Yan pairs.

The natural approach to generate additional p_T is to take into account the primordial transverse momentum of quarks in the proton. The primordial quark transverse momentum is a non-perturbative effect and, from the uncertainty principle, averages at $\gtrsim 200$ MeV. On the other hand, we will show in Section 4.6 that the higher twist effect of the intrinsic k_T on the Drell-Yan cross section is of the same order as the effect of non-vanishing quark off-shellness in proton, which is caused by the interaction of partons of one hadron in the initial state. Therefore, both the intrinsic k_T and quark off-shellness have to be taken into account for the sake of consistency.

4.5 Double differential Drell-Yan cross section

In this section, we would like to make a consistent comparison of our model and NLO results. However, the triple differential cross section $Ed^3\sigma/d^3p$ is
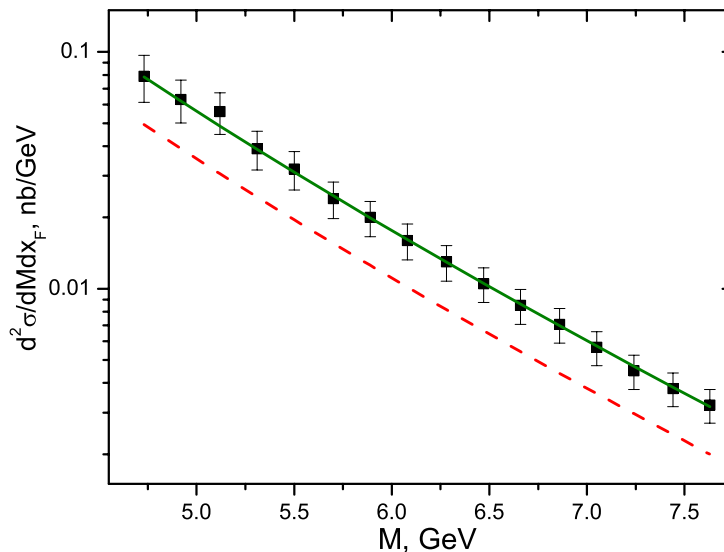
Figure 4.19: Result of LO collinear QCD for a double differential Drell-Yan cross section (dashed line) at $\sqrt{s} = 20$ and $x_F = 0.1$ as compared to experiment E439 [52]. Solid line is the LO result scaled up with a factor $K = 1.6$.

singular at $p_T \to 0$ in every fixed order of pQCD [69, 73]. We, therefore, apply our model now to the double differential cross section $d^2\sigma/dMdx_F$.

The K- factor, which is needed to increase the magnitude of the LO prediction for the double differential Drell-Yan process cross section so that it agrees with the data, can be decreased from 2 to 1.1 by taking into account NLO processes [108]. In order to determine, what part of this LO K-factor can be accounted for by the model with intrinsic k_T and off-shellness of quarks, we compare data to the double differential cross section calculated in our model. We use

$$\frac{d^2\sigma}{dM^2 dx_F} \equiv \int_0^{(p_T^2)_{max}} \frac{d^3\sigma}{dM^2 dx_F dp_T^2} dp_T^2, \qquad (4.12)$$

where the triple differential cross section is taken from (3.68). Note that the maximum transverse momentum of the Drell-Yan pair $(p_T^2)_{max}$ is fixed by the kinematics

$$(p_T^2)_{max} = \frac{(s + M^2 - M_R^2)^2}{4s} - x_F^2 \frac{(s - M^2)^2}{4s} - M^2, \qquad (4.13)$$

where M_R^2 is the minimal invariant mass of the undetected remnant.

In Fig. 4.19, the Drell-Yan process cross section $d^2\sigma/dMdx_F$ predicted
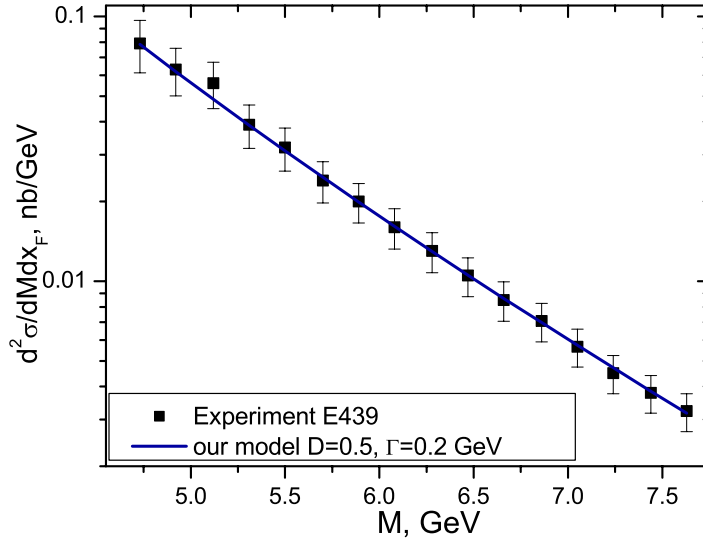
Figure 4.20: Drell-Yan cross section in our model at $D = 500$ MeV, $\Gamma = 200$ MeV compared to the data of experiment E439 [52]. $K = 1$.

at leading order of perturbative QCD (dashed line) is compared to the data of the Fermilab experiment E439 [52] on pW collision at 400 GeV incident energy, at $x_F = 0.1$. The LO prediction lies below the data. The solid line shows the LO curve scaled up with a factor $K = 1.6$. The K-factor depends somewhat on the parametrization of parton distributions used. We use here the parametrization [53]. If one assumes a larger contribution of sea quarks, the K-factor needed to describe the data is lower.

The double differential Drell-Yan process cross section in our model (4.12) is compared to data in Fig. 4.20. The data are reproduced well with $K = 1$. We conclude that in the experimentally relevant region the K-factor of the double differential Drell-Yan cross section can be explained by two alternative scenarios: either as an effect of higher orders of perturbative QCD as shown in [69, 108] or as an effect of non-collinearity and off-shellness of quarks in our phenomenological approach. The experimental cross section magnitude can be reproduced in NLO calculations by fitting the renormalization scale or in our model by fitting the parameters D and Γ. The latter explanation of the K-factor has the advantage that it can explain also the triple differential cross section.
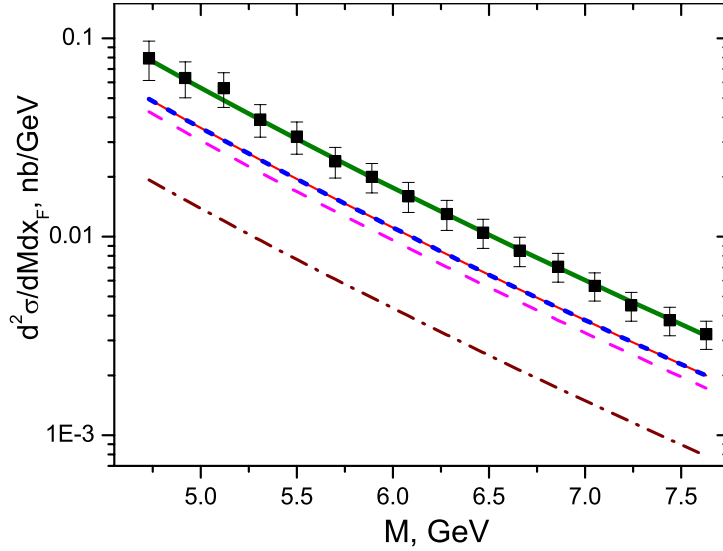
Figure 4.21: Drell-Yan cross section in a simplified intrinsic-k_T approach at $D = 50$ MeV (short dash), $D = 250$ MeV (dash), $D = 500$ MeV (dash-dot) compared to LO pQCD (thin solid line) and the data of experiment E439 [52]. The solid line gives the theoretical curves multiplied by D-dependent K-factors fitted to the data. Everywhere, $\Gamma = 0$.

In the following, we additionally study the relative importance of quark off-shellness and quark intrinsic transverse motion by comparing our result to that of the intrinsic-k_T approach. The intrinsic-k_T approach [12, 13, 21, 109] is a limiting case of our model at $\Gamma \to 0$. The factorization assumption in this case gives

$$\frac{d^4\sigma}{dM^2 dx_F d\vec{p}_T} = g(\vec{k}_{T1}) \otimes g(\vec{k}_{T2}) \otimes \frac{d^2\hat{\sigma}(\vec{k}_{T1}, \vec{k}_{T2})}{dM^2 dx_F} \delta(\vec{p}_T - \vec{k}_{T1} - \vec{k}_{T2}). \quad (4.14)$$

The formula is often simplified by neglecting the dependence of $\hat{\sigma}$ on $\vec{k}_{T1}$ and $\vec{k}_{T2}$, for example in [22] and in PYTHIA [24]. In this case, the p_T spectrum of Drell-Yan pairs $d^3\sigma/dM^2 dx_F dp_T^2$ is also simply a Gaussian in p_T^2. The cross section (4.14) has to be integrated over the azimuthal angle of the lepton pair and over p_T^2 according to (4.12). Because of the finite integration interval in (4.12), we do not recover the normalization of the k_T-distribution (3.70), but obtain a suppression that increases with D.

The double differential Drell-Yan process cross section in the intrinsic k_T approach with collinear sub-process cross section at three values of D is compared to the LO of pQCD and the data of the experiment E439 in Fig. 4.21.

The magnitude of the measured cross section cannot be reproduced in this leading order intrinsic k_T approach, in which the dependence of the partonic $d\hat{\sigma}$ on $\vec{k}_{1T}$ and $\vec{k}_{2T}$ are neglected. The part of higher-twist effects incorporated in the full intrinsic-k_T approach changes the distribution considerably compared to the result of leading twist, *cf.* Fig. 4.6 and its discussion in Section 4.2.

Just as in LO of pQCD, scaling with an overall K-factor ranging from 1.6 to 4 is necessary to describe the data. It is apparent from Fig. 4.21 that the K-factor extracted from the data is D-dependent. Therefore, this scaling factor should be understood as a phenomenological parameter and not as a measure of higher order corrections.

4.6 Twist decomposition of the phenomenological corrections due to intrinsic k_T and off-shellness of quarks

In the previous section we have shown that the double differential Drell-Yan cross section is reproduced by our model accounting for intrinsic k_T and off-shellness of quarks without a need for a K-factor. In addition, the p_T distribution of the Drell-Yan pairs can be explained in our model (see Sect. 4.3), but not in NLO of pQCD [73,104,107]. Therefore, the effects of quark off-shellness and intrinsic k_T do not arise solely from the diagrams of NLO pQCD. Instead, we will show that they parametrize higher twist processes. Some of the diagrams that contribute to the Drell-Yan cross section at higher twist are shown in Fig. 4.22. Gluon radiation in the initial state and gluon exchange between the active parton and spectators generate intrinsic k_T and virtuality of quarks in the proton in the Drell-Yan process. Some of these processes (for example, the gluon exchanges that connect factorized regions - the sub-process and a soft matrix element) are suppressed by powers of s in the scaling limit. However, the power-suppressed corrections give a sizable contribution to the transverse momentum spectrum of Drell-Yan pairs at finite s accessible in modern experiments.

In this section, we investigate the relationship of NLO and higher twist corrections to those calculated in our phenomenological approach by comparing their behaviour in the Drell-Yan scaling limit, in which $s \to \infty$ and $M^2 \to \infty$ with $\tau = s/M^2$ finite. The NLO corrections are proportional to α_S; therefore
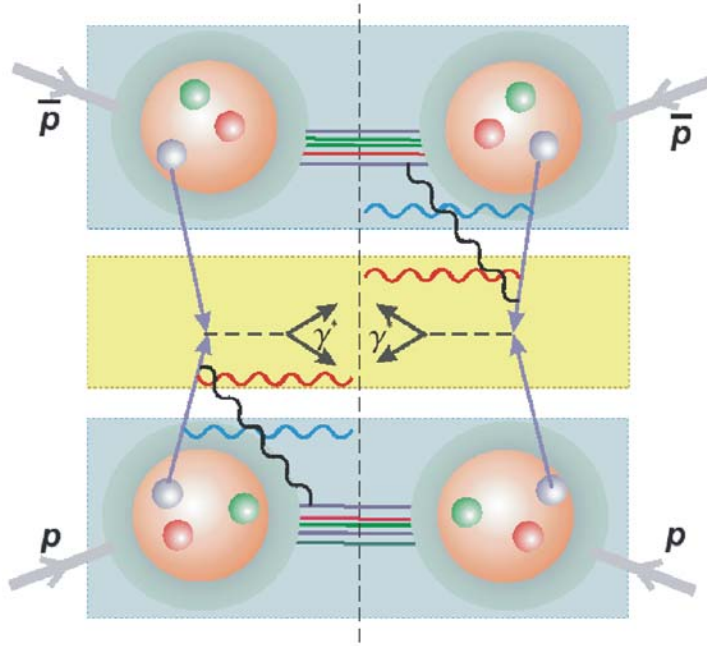
Figure 4.22: Example of gluon radiation diagrams generating intrinsic k_T and virtuality of quarks in the proton as probed in the Drell-Yan process.

we expect only a logarithmic dependence of these corrections on the hard scale $s \sim M^2$. On the other hand, higher twist contributions are suppressed in powers of s in the scaling limit. In order to determine whether the effects of quark virtuality and intrinsic k_T are leading twist, we study the behaviour of the Drell-Yan cross section calculated in our model in the scaling limit.

In the scaling limit ($s \rightarrow \infty$, s/M^2 =const), the spectral functions in (3.68) effectively drop out due to normalization (*cf.* discussion later), and the hadronic cross section goes to

$$\frac{d^3\sigma}{dM^2 dx_F dp_T^2} = \sum_q \Phi_q(x_1, x_2) \left(\frac{d^2\hat{\sigma}_q}{dM^2 dx_F} \right)_{LO} \frac{1}{8D^2} \exp\left(-\frac{p_T^2}{8D^2} \right), \quad (4.15)$$

where

$$\Phi_q(x_1, x_2) \equiv q^A(x_1)\bar{q}^B(x_2) + \bar{q}^A(x_1)q^B(x_2), \quad (4.16)$$

$$\left(\frac{d^2\hat{\sigma}_q}{dM^2 dx_F} \right)_{LO} = \frac{4\pi\alpha^2 e_q^2}{9M^4} \frac{x_1 x_2}{x_1 + x_2}(1 - x_1 x_2), \quad (4.17)$$

and the parton momentum fractions (x_1, x_2) are defined via

$$M^2 \;\; = \;\; x_1 x_2 s; \tag{4.18}$$

$$x_F \;\; = \;\; x_2 - x_1. \tag{4.19}$$

For comparison, note that the lowest order triple differential cross section is given by

$$\left(\frac{d^3\sigma}{dM^2 dx_F dp_T^2} \right)_{LO} = \sum_q \Phi_q(x_1, x_2) \left(\frac{d^2\hat{\sigma}_q}{dM^2 dx_F} \right)_{LO} \delta\left(p_T^2\right). \tag{4.20}$$

From (4.15) one observes that the corrections to the p_T distribution of the Drell-Yan pairs due to quark non-collinearity in the proton are not suppressed in the limit $s \to \infty$. The model taking into account the intrinsic k_T of partons therefore parametrizes some of the leading twist effects. This part of the model effects, i.e. the Gaussian smearing of p_T, is related to contributions of the higher order diagrams of the perturbative QCD series as is shown for deep inelastic scattering at small Bjorken x in [69].

On the other hand, the corrections to the LO cross section generated by the k_T dependence of the sub-process cross section $d\hat{\sigma}$ are suppressed by powers of the hard scale s. Therefore, they represent part of the higher twist effects. To study this in more detail, we expand the cross section (3.68) in a series in $1/s$ around $s = \infty$, keeping this time not only the leading term, as it has been done in (4.15), but all the terms that are suppressed by less than s^2. We analyze the cross section at the specific value of $x_F = 0$ to make the formulas less bulky.

Again, we start from the general formula (3.68). First, we expand the integrand of (3.68) in $1/s$. For this purpose not only $d\hat{\sigma}$ of (3.65) has to be evaluated at $s \to \infty$, but also the combination of parton distributions (3.69) that enters (3.68) has to be Taylor expanded around $(\xi_1 = \sqrt{\tau}, \xi_2 = \sqrt{\tau})$. The arguments of parton distributions ξ_1 and ξ_2 are fixed after integrating out the δ-functions in (3.65). As a result, the probed parton light cone momentum fractions depend on quark intrinsic transverse momentum and off-shellness. After integrating (3.68) over ξ_1, ξ_2 and angles, the quantity $\Phi_q(\tilde{\xi}_1, \tilde{\xi}_2)$ enters the hadronic cross section formula. Here, $\tilde{\xi}_1$ and $\tilde{\xi}_2$ are

$$\tilde{\xi}_1 \;\; = \;\; \sqrt{\tau}\left(1 + \frac{p_T^2/2 - m_2^2 - k_2^2}{\sqrt{\tau} s} + O\left(\frac{1}{s^2}\right)\right), \tag{4.21}$$

$$\tilde{\xi}_2 = \sqrt{\tau}\left(1 + \frac{p_T^2/2 - m_1^2 - k_1^2}{\sqrt{\tau}s} + O\left(\frac{1}{s^2}\right)\right). \tag{4.22}$$

Keeping the first two orders in the Taylor expansion of $\Phi_q(\tilde{\xi}_1, \tilde{\xi}_2)$ and in the $1/(\tau s)$-expansion of $d\hat{\sigma}$, we obtain:

$$
\begin{aligned}
\frac{d\sigma_q^3}{dM^2 dx_F dp_T^2}\bigg|_{x_F=0} &= \frac{\alpha^2 e_q^2(1-\tau)}{8\pi D^4 12\tau^2 s^3} \int_0^\infty dk_2^2 \int_{(k_1^2)_{min}}^{(k_1^2)_{max}} dk_1^2 \int_0^{(m_2)_{max}} dm_2 \int_0^{(m_1)_{max}} dm_1 \\
&\times \frac{A(m_1)A(m_2)\exp\left(-\frac{k_1^2+k_2^2}{4D^2}\right)}{\sqrt{k_1^2 k_2^2 - \frac{1}{4}(p_T^2 - k_1^2 - k_2^2)^2}} \left[G_1^q(\tau)\frac{\sqrt{\tau}}{8}\left(\frac{p_T^2}{2} - m_1^2 - k_1^2\right)\right. \\
&\left. + G_2^q(\tau)\frac{\sqrt{\tau}}{8}\left(\frac{p_T^2}{2} - m_2^2 - k_2^2\right)\right. \\
&\left. + T^q(\tau)\left(\frac{\tau s}{8} + \frac{p_T^2}{6} + \frac{k_1^2}{6} + F(m_1, m_2)\right) + O\left(\frac{1}{s}\right)\right], \tag{4.23}
\end{aligned}
$$

where

$$
\begin{aligned}
(k_1^2)_{min} &\equiv (p_T - k_2)^2; \tag{4.24} \\
(k_1^2)_{max} &\equiv (p_T + k_2)^2; \tag{4.25} \\
(m_1)_{max} &\equiv \sqrt{\tau s + p_T^2/2 - k_1^2}; \tag{4.26} \\
(m_2)_{max} &\equiv \sqrt{\tau s + p_T^2/2 - k_2^2}; \tag{4.27} \\
F(m_1, m_2) &\equiv \frac{1}{\tau}\left(2(m_1^2 + m_2^2)(\tau/8 + x_1^2/6 - x_1\sqrt{\tau}/6) + (m_1 + m_2)^2\tau/6\right. \\
&\quad + m_1^2\tau/6 + (m_1^2 - m_2^2)x_1\sqrt{\tau}/6 - m_1^2\tau\sqrt{\tau}/(6x_1) \\
&\quad \left. + \frac{\tau}{8}(m_1^2 - m_2^2 + k_1^2 - k_2^2)\right); \tag{4.28} \\
T^q(\tau) &\equiv \Phi^q(\sqrt{\tau}, \sqrt{\tau}); \tag{4.29}
\end{aligned}
$$

and

$$
\begin{aligned}
G_1^q(\tau) &\equiv \frac{\partial \Phi^q(x_1, x_2)}{\partial x_1}\bigg|_{(x_1=\sqrt{\tau}, x_2=\sqrt{\tau})}, \tag{4.30} \\
G_2^q(\tau) &\equiv \frac{\partial \Phi^q(x_1, x_2)}{\partial x_2}\bigg|_{(x_1=\sqrt{\tau}, x_2=\sqrt{\tau})} \tag{4.31}
\end{aligned}
$$

are the derivatives of the parton distribution product (4.16) at $(x_1 = \sqrt{\tau}, x_2 = \sqrt{\tau})$.

To further investigate the dependence of the integral (4.23) on s, we have

to specify the quark spectral function. Indeed, the integration variables m_1 and m_2 at $s \to \infty$ can be arbitrarily big, as can be seen from (4.26) and (4.27). Therefore, only after the integration over m_i has been performed can we judge whether any off-shellness generated term is sub-leading in s and how much it is suppressed. On the other hand, the integration over m_i provides additional terms $\sim k^2/s$, making the separation of off-shellness and intrinsic k_T effects involved.

In the following, we perform the analytical integration of (4.23), assuming different functional forms for the spectral function $A(m)$:

1. a Dirac delta-function $\delta(m)$,

2. a Breit-Wigner function (Lorentz distribution) with a constant parameter Γ, see (3.20).

In the former case, the model reduces to the intrinsic-k_T approach. Integrations over m_i drop out, while the remaining integrals over k_1^2 and k_2^2 can be done analytically via Bessel functions. As the result, one finds the leading term (4.15) plus $1/(\tau s)$ suppressed contributions.

Let us now consider the second, more general, case. The cross section for $A(m) = \delta(m)$ is the limiting case of the formulas given below for a Breit-Wigner distribution (3.20) at $\Gamma = 0$. Inserting the spectral function (3.20) into (4.23), performing all the integrations and keeping only the first few leading terms in $1/M$, we obtain (note that $M^2 = \tau s \to \infty$, as $s \to \infty$)

$$
\frac{d^3\sigma_q}{dM^2 dx_F dp_T^2}\bigg|_{x_F=0} = \frac{1}{8D^2} \exp\left(-\frac{\vec{p}_T^2}{8D^2}\right) \sum_q \left(\frac{d^2\hat\sigma_q}{dM^2 dx_F}\right)_{LO} [T^q(\tau)
$$

$$
+ \left\{4\,T^q(\tau) - \sqrt{\tau}\,(G_1^q(\tau) + G_2^q(\tau))\right\} \frac{1}{\pi}\frac{\Gamma}{M}
$$

$$
+ \left\{\sqrt{\tau}\,(G_1^q(\tau) + G_2^q(\tau)))\left(\frac{p_T^2}{4} - 2D^2\right) + \frac{8}{3}T^q(\tau)\left(\frac{5p_T^2}{4} + D^2\right)\right\}\frac{1}{M^2}
$$

$$
+ O\left(\frac{\Gamma}{M^3}\right)\bigg]. \quad (4.32)
$$

At leading twist, the Gaussian distribution of p_T (4.15) is recovered. However, it is modified by the higher twists, suppressed in the limit $s \to \infty$, but substantial at finite s accessible in experiment. The term proportional to $1/M = 1/\sqrt{\tau s}$ is p_T-independent and leads to an overall enhancement of the cross section, while the p_T-dependent terms proportional to $1/M^2$ additionally modify the shape of the p_T distribution.

The contribution of the off-shellness of quarks to (4.32) is given by the summands proportional to Γ. It is suppressed by powers of M and vanishes in the intrinsic k_T approach, in which $\Gamma = 0$. Thus, the model, which additionally accounts for quark off-shellness, parametrizes more higher twist effects than the intrinsic-k_T approach alone.

It is interesting that the effects due to the finite quark width Γ appear in the expansion at odd powers of $1/M$ in contrast to those due to the intrinsic-k_T. The first Γ-dependent correction is proportional to $1/M = 1/\sqrt{\tau s}$. Therefore, the corrections due to the virtuality of quarks seem to have a non-analytical dependence on s as $(\tau s)^{-1/2}$. In order to preserve analyticity of the cross section we have to assume that the quark spectral function width Γ has a particular scaling behavior at large hard scale of the probe $M = \sqrt{\tau s}$:

$$\Gamma(M) \sim \frac{1}{M}, \text{ as } M \to \infty. \tag{4.33}$$

Then, in (4.32), the terms proportional to Γ/M and the terms proportional to $1/M^2$ together constitute the dominant higher twist correction to the leading result (4.15) in the scaling limit.

We expect the formula (4.32) to give a good approximation to the Drell-Yan cross section (3.68) at large finite M and s. In order to illustrate this, we compare the result of the exact calculations, i.e. the numerical integration of (3.68), to the leading twist approximation (4.15) and to the next-to-leading twist result (4.32) in two regimes:

- at $M \approx 7$ GeV and $s = 1600$ GeV^2, see Fig. 4.23;

- at $M = 1$ GeV and $s = 30.25$ GeV^2 relevant for FAIR [77], see Fig. 4.24.

As expected, the sum of leading and next-to-leading terms of the power series (4.32) reproduces the full calculations quite well at M as high as 7 GeV. The approximate cross section has the same average magnitude and slope. Therefore, it is dominating the K-factor type corrections to the leading twist cross section. Only the bend of the cross section at low p_T, which is seen in the full calculations and in the data (Fig. 4.13), is not reproduced at the next-to-leading twist.

From the Fig. 4.24, one sees that our model predicts the higher twist effects to be very large at low M and s. The discrepancy between approximate and exact Drell-Yan cross sections is large in this regime, too, especially at low p_T.
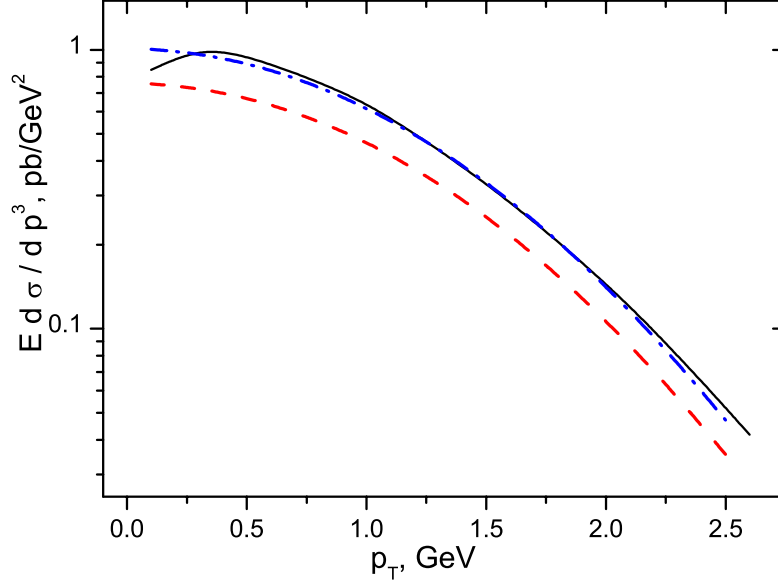
Figure 4.23: Cross section of $pp \to l^+l^-X$ at $M \approx 7$ GeV, $s = 1600$ GeV^2 in our model (solid), in the leading order in $1/M^2$ (dash), up to the next-to-leading order in $1/M^2$ expansion (dash-dot). $D = 650$ MeV, $\Gamma = 225$ MeV, $x_F = 0$.
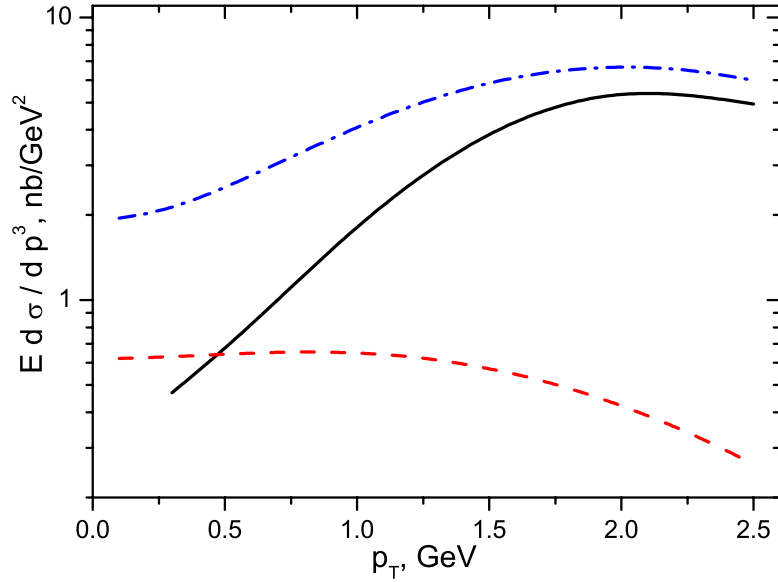

Figure 4.24: Cross section of $p\bar{p} \to l^+l^-X$ at $M = 1$ GeV and $s = 30.25$ GeV^2 in our model (solid), in the leading order in $1/M^2$ (dash), up to the next-to-leading order in $1/M^2$ expansion (dash-dot). $D = 600$ MeV, $\Gamma = 250$ MeV, $x_F = 0$.

We conclude that one needs to go beyond the next-to-leading twist at these low M and s. In this region, our model becomes indispensable, because it effectively sums higher orders and higher twists.

4.7 Prediction for the triple differential cross section of $\bar{p}p \to l^+l^- X$ at GSI-FAIR

Applying the model described in Section 3.5 and tested in Section 4.3 to calculate the triple differential cross section of the process $p\bar{p} \to l^+l^- X$ at the centre of mass energy $\sqrt{s} = 5.5$ GeV, we study a rather interesting, not yet experimentally explored kinematical regime. The planned experiment PANDA [23] at the future GSI facility is to probe the Drell-Yan process at this energy. We will predict the triple differential Drell-Yan cross section at $\sqrt{s}$ and M values, relevant for PANDA. We will find a cross section magnitude of up to 10 nb in the low mass region. A measurement with 10% accuracy is desirable in order to constrain the partonic transverse momentum dispersion D and the spectral function width Γ within ± 50 MeV. In this case, we will be able to extract the evolution of these parameters with M and $\sqrt{s}$.

The model was tested in Section 4.3 by comparing the triple differential cross section $d^3\sigma/dM^2dp_T^2dx_F$ of the processes $pp \to \mu^+\mu^- + X$ and $pd \to \mu^+\mu^- + X$ to the data of the experiments E866 [76] and E772 [98] at $\sqrt{s} = 40$ GeV. The two parameters of the model (D and Γ) should be extrapolated to the values of $M = (1 - 5.5)$ GeV and $\sqrt{s} = 5.5$ GeV relevant for PANDA. From the fits to experiments at different values of s and M, we estimate the parameter $D \approx 0.6 \pm 0.18$ GeV. The large uncertainty of the extrapolation is reflected in our estimate of the parameter error. The model parameter D should be understood as representing the summed effect of the transverse motion of partons inside the nucleon and of the perturbative corrections [22]: $D^2 = D_{\text{intr}}^2 + D_{\text{pert}}^2$. The transverse momentum coming from higher orders of collinear perturbation theory shows at constant $\tau \equiv M^2/s$ a linear dependence on s in addition to the logarithmic dependence on M^2 [101, 103]: $\langle p_T^2 \rangle_{\text{pert}} = s \, \alpha_S(M^2) \, f(\tau)$, see Section 4.4. On the other hand, the non-perturbative D_{intr} does not show a strong dependence on s. An analysis in event generator PYTHIA [24] has shown that the perturbative corrections constitute only 0.1% of the p_T-spectrum of Drell-Yan pairs with $p_T \neq 0$ at PANDA kinematics [110]. Thus, we set $D \approx D_{\text{intr}}$, using an s-averaged value for D_{intr}.
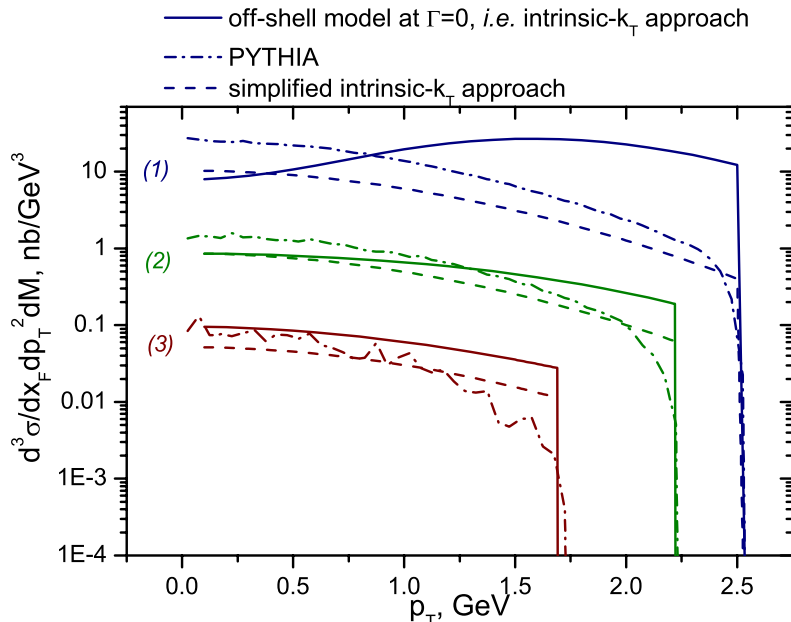
Figure 4.25: Comparison of the predictions of different models: (solid) intrinsic-k_T approach; (dash) intrinsic-k_T approach with collinear sub-process cross section; (dash-dot) PYTHIA generator. For all lines, $x_F = 0$, $D = 0.5$ GeV, $\sqrt{s} = 5.5$ GeV. The lines marked with *(1)* correspond to $M = 1$ GeV; *(2)*, $M = 2$ GeV; *(3)*, $M = 3$ GeV.

Fig. 4.25 presents a comparison of the predictions we have obtained in three different models: in our model at $\Gamma = 0$, $D = 0.5$ GeV, which is equivalent to the intrinsic-k_T approach (solid lines); in the widely used simplified version of the intrinsic-k_T approach, in which the dependence of $\hat{\sigma}$ on k_T is neglected (dashed line); by PYTHIA [24], taking into account QED and QCD initial state radiation and intrinsic-k_T (dash-dotted line). The models agree in the overall strength of the cross section within a factor of 3.

The demand of positive mass of the remnant M_R determines the maximum p_T according to (4.13). In PYTHIA, however, a stronger constraint is implemented: $M_R \geq 2m_{qq} \approx 1.6$ GeV, where m_{qq} is a diquark mass. While generating the plot under discussion, we used 1.6 GeV as the lower bound for the remnant mass in all the other models, too, for consistency. The dilepton mass bin width in the simulation was set to 100 MeV.

Note the qualitative difference of the cross section at the Drell-Yan pair mass $M = 1$ GeV in the intrinsic-k_T approach (solid lines). In contrast to the higher mass bins, the peak of the p_T-distribution for $M = 1$ GeV is not at zero in our model (solid line in Fig. 4.25). This behavior appears at $M \lesssim 2D$, *i.e.*
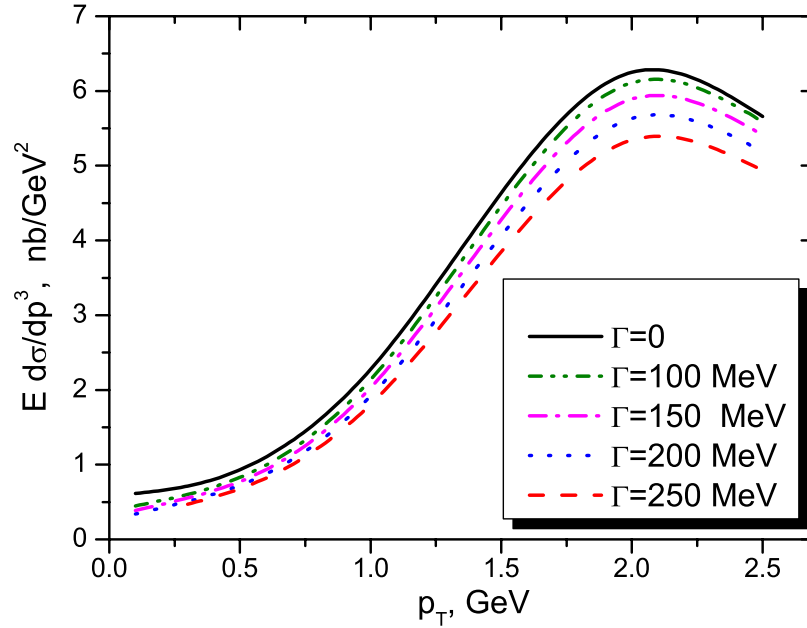
(a) $M = 1$ GeV
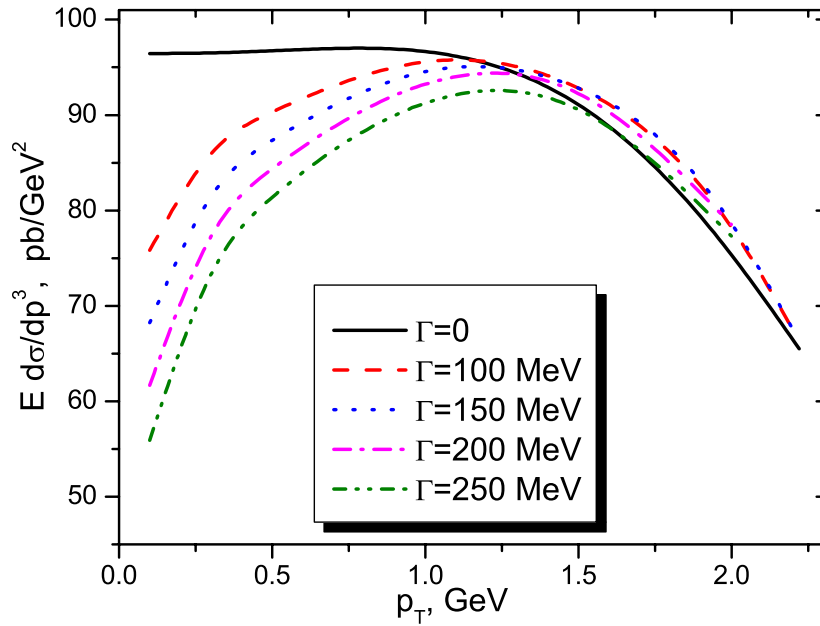
(b) $M = 2$ GeV

Figure 4.26: Prediction for the p_T-distribution of Drell-Yan lepton pairs at PANDA. Intrinsic transverse momentum dispersion $D = 0.6$ GeV. The solid line is the result of calculations in the intrinsic-k_T approach (width $\Gamma = 0$). The other curves are generated with Γ in the range that we have determined in Section 4.3. Note that the scale changes from nb in the subfigure (a) to pb in the subfigure (b). $\sqrt{s} = 5.5$ GeV, $x_F = 0.1$.
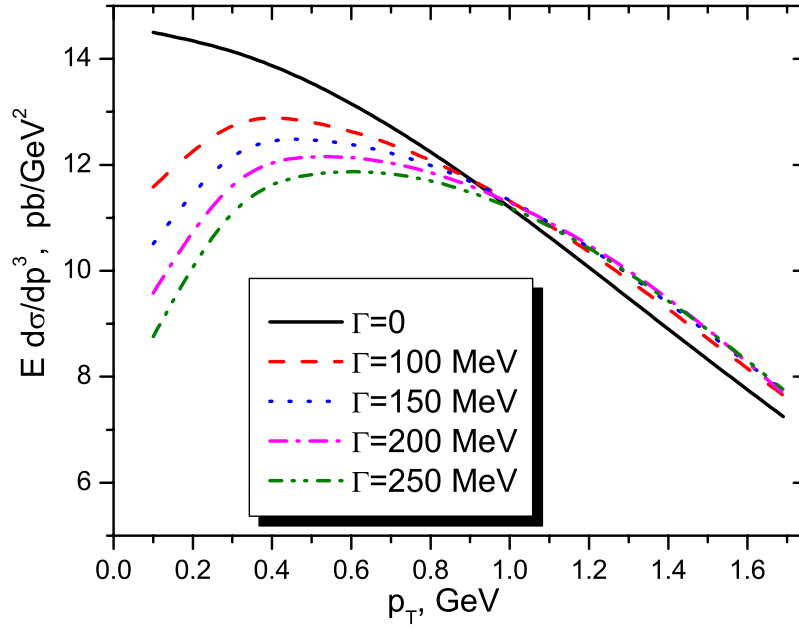
(a) $M = 3$ GeV
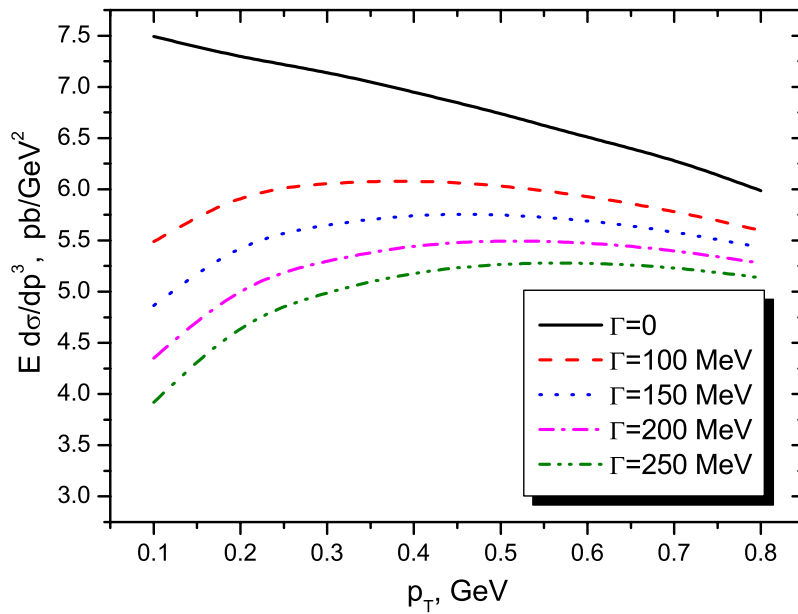
(b) $M = 4$ GeV

Figure 4.27: Same as Fig. 4.26, but for higher masses of Drell-Yan pairs.

in the distribution of the low virtuality photons, which can be produced by the partonic transverse motion alone. It is worthwhile to stress that this drastic change in the p_T-dependence of the cross section takes place for all values of Γ (see Fig. 4.26). An experimental verification of this effect would constitute a direct test for the transverse momentum distribution of partons.

Note, however, that this effect appears only if the k_T-dependence of the partonic cross section is not neglected (this is the difference between the solid and dashed lines in Fig.4.25). This big effect of the non-collinearity of the sub-process cross section is in accordance with the results of Section 4.2 (see the discussion of the plot 4.6) and Section 4.6.

Fig. 4.26 and 4.27 show several theoretical curves for the cross section (4.3) with $\Gamma = (100 - 250)$ MeV, which is the range determined from fitting E866 data. The results of our calculations in the intrinsic-k_T approach ($\Gamma = 0$) are plotted for comparison (solid lines). The evolution of the spectral function with the hard scale is unknown. It cannot be directly related to the evolution of the k_T-distribution, because the quark off-shellness depends also on k^-. One can see that the effect of the Γ variation on the cross section is of the order of 10%. On the other hand, the variation of the parameter D within theoretical uncertainty at fixed Γ (as presented in Fig. 4.28) also leads to considerable changes of the cross section. Though, as it was shown in Section 4.3, one can do a double fit and extract both parameters from the same data set.

The measurement of this cross section at $\sqrt{s}$ as low as 5.5 GeV will provide essential information on QCD in the regime where effects beyond leading order and leading twist are expected to be large [111]. The high amplitude of the predicted cross sections (up to 10 nb) indicates that PANDA at the design luminosity has a potential to measure the triple differential unpolarized cross section of $\bar{p}p \to l^+l^- + X$ with high statistics and an unprecedented accuracy.

The transverse momentum spectrum of Drell-Yan pairs at low $\sqrt{s}$ is generated predominantly by the non-perturbative primordial intrinsic transverse momentum of the partons. On the other hand, the distribution of the intrinsic k_T in this region is poorly known. PANDA data will be a valuable input that should allow one to pin down the quark transverse momentum distribution in the proton. Again, the $M = 1$ GeV mass bin shows the mentioned shift of the peak towards higher p_T.

The presented results also suggest that one can use the future PANDA data to gain information on the spectral function of partons bound in the
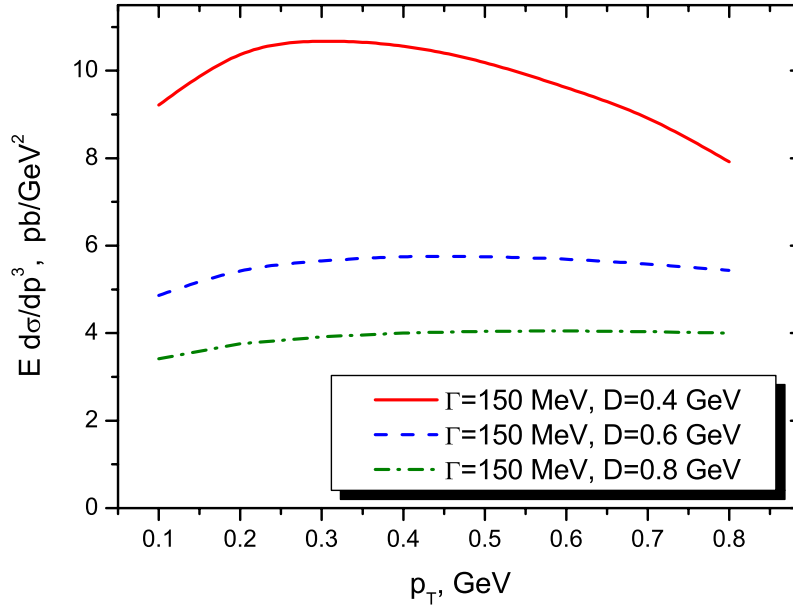
Figure 4.28: Variation of the cross section with D at fixed Γ. $\sqrt{s} = 5.5$ GeV, $x_F = 0.1$, $M = 4$ GeV.

nucleon. Indeed, as we see from Fig. 4.26 and 4.27, an experimental accuracy of 20-30% would be enough to answer the question of whether the cross section can be described by a model with on-shell quarks. The results of the earlier calculations at higher $\sqrt{s}$ together with the PANDA data can be used also to extract the dependence of the quark spectral function in the proton on the hard scales M and $\sqrt{s}$. For this purpose, we need an experimental accuracy of at least 10%, so that one can reliably extract the parameter Γ in different mass bins. Should the accuracy be even better, the data can be used to investigate the details of the quark spectral function shape.

Chapter 5

Conclusions and outlook

The research presented here reveals the importance of accounting for the parton off-shellness in addition to its intrinsic transverse momentum when studying the proton structure in high energy scattering processes. Both the off-shellness and intrinsic transverse motion are generated by the partonic interaction and gluon radiation in the initial state.

We have developed a formalism to study the quark structure of hadrons going further than the widely studied picture of collinear noninteracting partons. The parton off-shellness effects missed in the standard treatment were taken into account by dressing the parton lines with phenomenological spectral functions and using the factorization assumption. In this way, higher twist corrections to standard pQCD were modelled.

We have calculated the cross sections of deep inelastic ep scattering and the Drell-Yan process $pp \to l^+l^-X$, $pA \to l^+l^-X$ and $\bar{p}p \to l^+l^-X$ in the model allowing for a finite parton width. Off-shellness effects arise from the fact that the time-like lightcone momentum of the parton (p^-) is not fixed by an on-shell condition $(p^- = p_\perp^2/p^+)$ or by a collinearity condition $(p^- = 0)$. Since the partons in the proton interact, p^- is in fact distributed with some finite width. In order to disentangle the off-shellness effects from the effect of the parton primordial transverse momentum, we have additionally calculated the Drell-Yan cross section in the standard intrinsic-k_T approach. The obtained cross sections in both models were compared to the data on the triple differential cross section of the process $pp \to l^+l^-X$, $pA \to l^+l^-X$ and $\bar{p}p \to l^+l^-X$.

We have found a moderate effect of the initial state interaction in DIS in the region of small Bjorken x_{Bj} and low momentum transfer Q^2. For a parton width of 300 MeV, the cross section change due to the finite quark

width in the proton reaches 10% at $Q^2 = 1$ GeV^2. On the other hand, the effect is Q^2-suppressed. For values of Q^2 above 10 GeV^2, the initial parton off-shellness generates only at most 2% of the cross section. For most of the experimentally investigated values of Q^2, the difference between the off-shell result and the leading twist cross section is too small to be resolved by present experiments. We conclude that the value of the parton width in the nucleon cannot be extracted from the DIS data, because the DIS cross section is too inclusive. This is the result expected by the analogy to nuclear physics. On the other hand, DIS data do not contradict the assumption of the finite parton width in the proton.

In contrast, we discover a substantial contribution of the parton off-shellness to the transverse momentum distribution $d^3\sigma/dM^2dx_F dp_T^2$ of the high-mass virtual photons produced in hadron-hadron collisions in the whole range of hard scales, at which the cross section has been measured. The triple differential Drell-Yan cross section is a more exclusive observable than the DIS cross section. That is why the effect of the parton off-shellness was expected to be larger in the Drell-Yan case. Our results confirm this expectation.

Although the intrinsic-k_T approach alone can reproduce the slope of the experimentally measured distribution of dileptons, an overall K-factor is necessary to fit the data. Both the shape and magnitude of the cross section are much better reproduced by a model that allows for off-shell partons. In particular, one can fit the data without a K-factor. The parton width in the proton was estimated from the comparison to the data. For a mass of the Drell-Yan pair of $4.2 - 8.7$ GeV, the best fits were obtained with quark (antiquark) width of $50 - 250$ MeV and intrinsic transverse partonic momentum dispersion of $400 - 600$ MeV. This corresponds to a mean primordial transverse momentum of the parton inside a proton of $\sqrt{\langle \vec{p}_\perp{}^2 \rangle} = 0.8 - 1.2$ GeV.

Further, we have compared the double differential Drell-Yan cross section $d^2\sigma/dM^2dx_F$ and the p_T distribution of the Drell-Yan dileptons in the following approaches: collinear perturbative QCD at next-to-leading order and, again, our model, which makes use of phenomenological distributions for k_T and off-shellness of quarks in the proton. We find that the transverse momentum spectrum of the Drell-Yan pairs at NLO pQCD disagrees with experiment both quantitatively and qualitatively. In contrast, we find that the phenomenological model with off-shell non-collinear partons successfully describes both the double differential Drell-Yan cross section and the p_T spectrum of Drell-Yan

pairs without the need of a K-factor.

The analysis of the Drell-Yan process cross section in our model in the Drell-Yan scaling limit has shown that the phenomenological model parametrizes higher twist effects. Higher twist contributions were up to date usually considered to be small, because they are suppressed by powers of the hard scale. As a rule, they are neglected in pQCD calculations. However, the power suppressed effect can be large at realistic energies.

We have found that the intrinsic transverse momentum of quarks generates both leading twist and $1/(\tau s) = 1/M^2$ suppressed effects. This is in line with our analysis of section 4.15, which has shown that only part of observed $\langle p_T^2 \rangle$ can be explained by NLO effects. In addition, we have shown that next-to-leading twist corrections due to quark off-shellness lead to a cross section magnitude change and are, therefore, responsible for a part of the K-factor type discrepancy between leading order pQCD and the data.

If a Breit-Wigner parametrization for a quark spectral function is used, the next-to-leading contribution turned out to be proportional to $\Gamma/\sqrt{\tau s}$. This lead us to suggest that the quark spectral function width Γ scales as $\Gamma(M) \sim 1/M$ at large hard scale $M = \sqrt{\tau s}$.

The formula that we obtained for the Drell-Yan cross section at the next-to-leading twist level can be very useful for applications, for example, in an event generator. Indeed, it requires no numerical integration, while providing a good approximation to the full calculations at $M \gtrsim 5$ GeV. However, at $M \lesssim 5$ GeV, one has to go beyond the next-to-leading order in the power series and use our model.

The results show that the higher twist corrections to high energy processes can be large. Therefore, a detailed study and modelling of these effects is necessary, if one hopes to reliably extract quark and gluon properties from hadron scattering data.

Since the Drell-Yan process is expected to be one of the leading background contributions at the future high energy facilities, it is important to predict its cross section as precisely as possible. For example, it has been suggested [112,113] to use the Drell-Yan process and dijet production as centrality triggers in pp collisions at the Large Hadron Collider [114]. On the other hand, experiments PANDA [23] and PAX [115] will study the Drell-Yan process at the future FAIR facility [77]. Our prediction for the Drell-Yan process cross section in the kinematics relevant for PANDA has shown that the transverse

momentum spectrum of Drell-Yan pairs at low $\sqrt{s}$ is generated predominantly by the non-perturbative primordial intrinsic transverse momentum of the partons. The analysis in the Section 4.6 has proven that our model is indispensable in this low energy regime.

On the other hand, the distribution of the intrinsic k_T in this region is poorly known. PANDA data will be a valuable input that should allow one to pin down the quark transverse momentum distribution in the proton. We note again that the $M = 1$ GeV mass bin shows a shift of the peak of the distribution towards higher p_T. Observation of this peak shift is a clear test of the predictive power of our model.

The obtained triple differential cross section of the dilepton production in pp and $\bar{p}p$ collisions is also a necessary input for models, studying the nuclear medium via high energy dileptons, produced in pA, $\bar{p}A$ and AA collisions. In order to meet this demand and to consistently evaluate the ISI effects in high energy processes, we need to improve our knowledge of the parton off-shellness distribution in the nucleon.

In particular, it should be possible to reduce the sizable uncertainty in the width by analyzing additional data sets. Also, the evolution of Γ with M can be extracted from data. Firstly, this will serve as a test of our prediction of Γ falling at asymptotically large M. Secondly, known dependence of the parameters on s and M will give the model even greater phenomenological significance.

Also, the single-parameter Breit-Wigner parametrization might be insufficient. In order to pin down the quark (gluon) virtuality distribution, the study of other exclusive processes will be necessary, for example, jet production.

An important step towards understanding the underlying theory of our phenomenological approach can be made by going beyond the leading order in α_S while accounting for the off-shellness of the incoming (outgoing) partons. The NLO calculations of the triple differential Drell-Yan cross section is also important since calculations by different groups lead to different conclusions: the authors of [106] claim to have described the data at high Drell-Yan transverse momentum very well, while [107] has an opposite result.

Another issue to be addressed is the application of our model to single- and double-spin asymmetries, which is of enormous importance in light of the planned experimental efforts. It is also very interesting theoretically, because higher twist effects are expected to dominate some of the asymmetries [55].

Appendix A

Light cone coordinates

A four-vector in Cartesian coordinates is

$$a = (a_0, a_1, a_2, a_3), \tag{A.1}$$

and the scalar product, in Minkowski metric, is defined as

$$(a \cdot b) \equiv a_\mu b^\mu = a_\mu g^{\mu\mu} b_\mu \equiv a_0 b_0 - \vec{a} \cdot \vec{b} = a_0 b_0 - a_1 b_1 - a_2 b_2 - a_3 b_3. \tag{A.2}$$

We use the following definition for light cone coordinates

$$a = (a_+, a_-, \vec{a}_\perp), \tag{A.3}$$

with

$$a_+ = a_0 + a_3, \tag{A.4}$$
$$a_- = a_0 - a_3, \tag{A.5}$$
$$\vec{a}_\perp = (a_1, a_2), \tag{A.6}$$

the scalar product being

$$(a \cdot b) = \frac{1}{2}\left(a_+ b_- + a_- b_+ - 2\vec{a}_\perp \cdot \vec{b}_\perp\right). \tag{A.7}$$

The following relations are useful

$$a^2 = a_+ a_- - \vec{a}_\perp^2; \tag{A.8}$$

$$a_- = \frac{a^2 + \vec{a}_\perp^2}{a_+}. \qquad (A.9)$$

Note that an alternative convention exists:

$$
\begin{aligned}
a_+ &= (a_0 + a_3)/2, && (A.10) \\
a_- &= (a_0 - a_3)/2, && (A.11) \\
\vec{a}_\perp &= (a_1, a_2), && (A.12) \\
(a \cdot b) &= a_+ b_- + a_- b_+ - \vec{a}_\perp \cdot \vec{b}_\perp. && (A.13)
\end{aligned}
$$

Appendix B

Numerics

In order to calculate the triple differential Drell-Yan cross section, we need to take numerically a four dimentional integral - over the off-shellnesses (m_1, m_2) and momentum fractions (ξ_1, ξ_2). The difficulty is due to following points.The spectral functions (m_i distributions) are sometimes very narrow. There are integrable divergences at $\xi_1 = 0$ due to the properties of parton distributions (approximately $1/\sqrt{\xi_i}$), and additionally an integrable divergence on the upper limits of integrations arising from the analitical integration over the angle between the partonic transverse momenta. One needs many evaluation of the cross section during the double fit to the data in order to not only find the minimal χ^2 but also define the error bars for both parameters.

By a change of variables $(x \to x^2)$, the divergencies at 0 are softened. However, because the upper bounds of the inner integrals depend on the outer integration variables via a complicated system of inequalitites, achieving proper sampling is not so easy. The two courses of action are

1. finding analitically the upper bounds and programming a custon integration routine that takes into account the existence of divergencies in this region,

2. using a good library integration routine, which is able to determine divergencies at each step.

We used both approaches with the same interface enabling simply calculation of a cross section or a fit, with the output and input from/to an ASCII file or screen (of course, in case of a fit, the input is only from a file). In the first case, we programmed in C++ [116] a custom routine using adoptive sub-division method, explained, for example, in [117]. We inputs the desired cross section
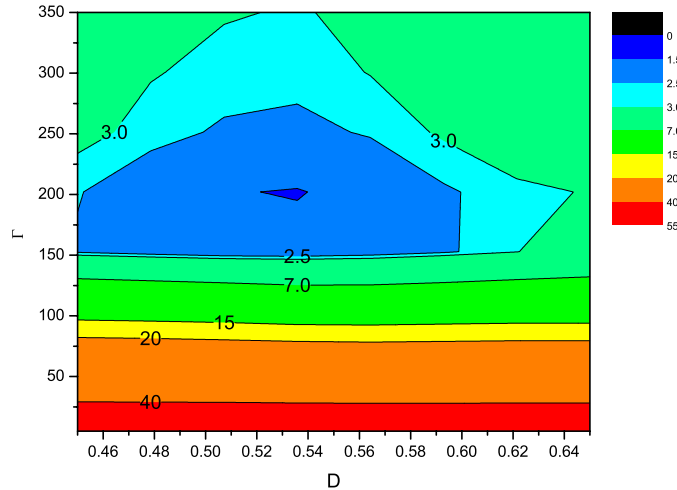
Figure B.1: χ^2 of the double fit corresponding to Fig. 4.12.

accuracy and the maximum recursion depth (usually, 50000). Relative and absolute accuracies for the sub-integrals are obtained automatically at each recursion step. This method is faster than others that we tried. The drawback, though, is that the error bars of the results are not calculated. In the second case, we used a deterministic adaptive routine from CUBA library [118]. This routine is a little slower, because the error bars of the result are also calculated. The results in both routines coincide within accuracy.

Neither method needs a lot of operating memory (<3MB). A calculation in the off-shell case at each (M, s, x_F, p_T, D, Γ) takes about 20-50 minutes on Athlon2400. The lower p_T, Γ, or D, the longer the calculation. The intrinsic-k_T approach is an order of magnitude faster. In calculating double differential cross section, as additional integration over p_T is performed, but it is smooth. The time compared to the triple differential case is about a factor of 5 more.

Two types of double fits are programmed: fitting the pair of parameters (D, Γ) in the off-shell case and fitting the pair (D, K-factor) in the intrinsic-k_T approach. In the first step, an approximate fit is done by a parabolic method. After that, one parameter (usually, D) is probed at equal intervals, while the golden section method is applied for fitting the second parameter. Thus, a detailed 3D plot of χ^2 can be built in order to determine the accuracy of parameter determination. Due to the quality of the data, the obtained minima of χ^2 were quite shallow (see Fig. B.1).

Bibliography

[1] K. Hagiwara *et al.*, Phys. Lett. **D66**, 010001 (2002).

[2] J. Lochner *et al.*, Imagine the universe: Dictionary, *http://imagine.gsfc.nasa.gov/docs/dict_ei.html*.

[3] H. M. Cuppen, O. Morata, and E. Herbst, Mon. Not. Roy. Astron. Soc. **367**, 1757 (2006), astro-ph/0601554.

[4] S. Weinberg, *The quantum theory of fields. Vol. 1: Foundations* (Cambridge: Univ. Pr., 1995).

[5] S. Weinberg, *The quantum theory of fields. Vol. 2: Modern applications* (Cambridge: Univ. Pr., 1996).

[6] O. Benhar, V. R. Pandharipande, and I. Sick, JLAB-TH-98-12.

[7] M. W. Paris and V. R. Pandharipande, Phys. Lett. **B514**, 361 (2001), nucl-th/0105076.

[8] J. D. Bjorken and S. D. Drell, *Relativistische Quantenfeldtheorie* (Mannheim: Bibliograph.Inst., 1967), in German.

[9] P. Hoyer, hep-ph/0307263, *unpublished*.

[10] P. Hoyer, hep-ph/0308019, *unpublished*.

[11] S. J. Brodsky, P. Hoyer, N. Marchal, S. Peigne, and F. Sannino, Phys. Rev. **D65**, 114025 (2002), hep-ph/0104291.

[12] X.-N. Wang, Phys. Rev. **C61**, 064910 (2000), nucl-th/9812021.

[13] Y. Zhang, G. I. Fai, G. Papp, G. G. Barnafoldi, and P. Levai, Phys. Rev. **C65**, 034903 (2002), hep-ph/0109233.

[14] U. D'Alesio and F. Murgia, hep-ph/0211454, *unpublished.*

[15] U. D'Alesio and F. Murgia, AIP Conf. Proc. **675**, 469 (2003), hep-ph/0211201.

[16] D. Boer, S. J. Brodsky, and D. S. Hwang, Phys. Rev. **D67**, 054003 (2003), hep-ph/0211110.

[17] S. J. Brodsky, D. S. Hwang, and I. Schmidt, Nucl. Phys. **B642**, 344 (2002), hep-ph/0206259.

[18] O. Linnyk, S. Leupold, and U. Mosel, Eur. Phys. J. **A19**, S203 (2004), hep-ph/0308265.

[19] O. Linnyk, S. Leupold, and U. Mosel, Phys. Rev. **D71**, 034009 (2005), hep-ph/0412138.

[20] G. I. Fai, J.-w. Qiu, and X.-f. Zhang, Phys. Lett. **B567**, 243 (2003), hep-ph/0303021.

[21] C.-Y. Wong and H. Wang, Phys. Rev. **C58**, 376 (1998), hep-ph/9802378.

[22] U. D'Alesio and F. Murgia, Phys. Rev. **D70**, 074009 (2004), hep-ph/0408092.

[23] PANDA, M. Kotulla *et al.*, Strong interaction studies with antiprotons: Technical progress report for PANDA, *http://www-panda.gsi.de/archive/public/panda_tpr.pdf*, 2005.

[24] T. Sjöstrand *et al.*, Comput. Phys. Commun. **135**, 238 (2001), hep-ph/0010017.

[25] A. I. Akhiezer and V. B. Berestetsky, *Quantum electrodynamics* (Moscow: Nauka, 1981), in Russian.

[26] A. I. Akhiezer, A. G. Sitenko, and V. K. Tartakovsky, *Electrodynamics of nuclei* (Kiev, Ukraine: Naukova Dumka, 1989), (in Russian).

[27] H. Feshbach, *Theoretical nuclear physics. Nuclear reactions* (John Wiley and Sons, inc, 1991).

[28] M. E. Peskin and D. V. Schroeder, *An Introduction to quantum field theory* (Addison-Wesley, 1995).

[29] R. Hofstadter, H. R. Fechter, and J. A. McIntyre, Phys. Rev. **49**, 978 (1953).

[30] V. B. Berestetsky, Y. M. Lifshits, and L. P. Pitaevsky, *Relativistic quantum theory, part 1* (Moscow: Nauka, 1968), in Russian.

[31] N. F. Mott, Proc. Roy. Soc. **A124**, 425 (1925).

[32] H. J. Bhabha, Proc. Roy. Soc. **164**, 257 (1938).

[33] L.-F. Li, Chineese Journal of Physics **35**, 4 (1997).

[34] C. Quigg, in Quarks, Quasars and Quandries, Ed. Aubrecht, G., American Association of Physics Teachers (1987).

[35] W. Lucha and F. F. Schöberl, *Die starke Wechselwirkung. Eine Einführung in nichtrelatiwistische Potentialmodelle* (Mannheim: Bibliograph.Inst., 1989).

[36] R. Frisch and O. Stern, Z. Phys. **85**, 4 (1933).

[37] I. Esterman and O. Stern, Z. Phys. **85**, 17 (1933).

[38] M. Breidenbach *et al.*, Phys. Rev. Lett. **23**, 935 (1969).

[39] Y. M. Lifshits and L. P. Pitaevsky, *Relativistic quantum theory, part 1* (Moscow: Nauka, 1971), in Russian.

[40] C. Möller, Ann. d. Phys. **14**, 531 (1932).

[41] X.-d. Ji, Phys. Rev. Lett. **91**, 062001 (2003), hep-ph/0304037.

[42] R. L. Jaffe, Lectures presented at the Los Alamos School on Quark Nuclear Physics, Los Alamos, N.Mex., Jun 10-14, 1985.

[43] L. D. Landau and Y. M. Lifshits, *Quantum mechanics. Nonrelativistic theory* (Moscow: Nauka, 1989), in Russian.

[44] J. D. Bjorken, Phys. Rev. **179**, 1547 (1969).

[45] Y. L. Dokshitzer, V. A. Khoze, A. H. Mueller, and S. I. Troian, *Basics of perturbative QCD* (Gif-sur-Yvette, France: Ed. Frontieres, 1991).

[46] C. Itzykson and J. B. Zuber, *International series in pure and applied physics: Quantum field theory* (New York: Mcgraw-hill, 1980).

[47] J. Collins, D. E. Soper, and G. Sterman, Adv. Ser. Direct. High Energy Phys. **5**, 1 (1988), hep-ph/0409313.

[48] V. N. Gribov and L. N. Lipatov, Yad. Fiz. **15**, 781 (1972).

[49] G. Altarelli and G. Parisi, Nucl. Phys. **B126**, 298 (1977).

[50] Y. L. Dokshitzer, Sov. Phys. JETP **46**, 641 (1977).

[51] S. D. Drell and T. M. Yan, Phys. Rev. Lett. **25**, 316 (1970).

[52] S. R. Smith *et al.*, Phys. Rev. Lett. **46**, 1607 (1981).

[53] M. Glück, E. Reya, and A. Vogt, Eur. Phys. J. **C5**, 461 (1998), hep-ph/9806404.

[54] E. V. Shuryak and A. I. Vainshtein, Nucl. Phys. **B199**, 451 (1982).

[55] P. G. Ratcliffe, AIP Conf. Proc. **675**, 176 (2003), hep-ph/0211232.

[56] J. P. Ralston and D. E. Soper, Nucl. Phys. **B152**, 109 (1979).

[57] X. Artru, (2002), hep-ph/0207309.

[58] R. L. Jaffe and X.-D. Ji, Phys. Rev. Lett. **67**, 552 (1991).

[59] A. D. Martin, W. J. Stirling, and R. S. Thorne, Phys. Lett. **B636**, 259 (2006), hep-ph/0603143.

[60] H. L. Lai *et al.*, Phys. Rev. **D51**, 4763 (1995), hep-ph/9410404.

[61] A. Sibirtsev, S. Krewald, and A. W. Thomas, J. Phys. **G30**, 1427 (2004).

[62] H.-n. Li, Phys. Rev. **D55**, 105 (1997), hep-ph/9604267.

[63] J. C. Collins and D. E. Soper, Nucl. Phys. **B194**, 445 (1982).

[64] A. Bacchetta, M. Boglione, A. Henneman, and P. J. Mulders, Phys. Rev. Lett. **85**, 712 (2000), hep-ph/9912490.

[65] M. A. Kimber, A. D. Martin, and M. G. Ryskin, Eur. Phys. J. **C12**, 655 (2000), hep-ph/9911379.

[66] Kuraev, L. N. Lipatov, and Fadin, Sov. Phys. JETP **44**, 443 (1976).

[67] Kuraev, L. N. Lipatov, and Fadin, Sov. Phys. JETP **45**, 199 (1977).

[68] Balitsky and L. N. Lipatov, Yad. Fiz. **28**, 822 (1978).

[69] R. K. Ellis, W. J. Stirling, and B. R. Webber, *QCD and collider physics* (Cambridge University Press, 1996).

[70] J. C. Collins, Acta Phys. Polon. **B34**, 3103 (2003), hep-ph/0304122.

[71] O. Benhar, nucl-th/0204042, *unpublished.*

[72] J. Collins and H. Jung, (2005), hep-ph/0508280.

[73] J. Raufeisen, hep-ph/0009358.

[74] V. V. Sudakov, Sov. Phys. JETP **3**, 65 (1956).

[75] A. Kulesza, G. Sterman, and W. Vogelsang, Phys. Rev. **D69**, 014012 (2004), hep-ph/0309264.

[76] J. C. Webb, *Measurement of continuum dimuon production in 800-GeV/c proton nucleon collisions*, PhD thesis, New Mexico State University, 2003, hep-ex/0301031.

[77] K. Peters, AIP Conf. Proc. **814**, 33 (2006).

[78] X. d. Ji, J. p. Ma, and F. Yuan, hep-ph/0304037.

[79] A. Lvovsky *et al.*, Gallery of Wigner functions, *http://qis.ucalgary.ca/quantech/wiggalery.html.*

[80] Z. Y. Ou *et al.*, Phys. Rev. Lett. **68**, 3663 (1992).

[81] L. D. Landau and E. M. Lifshitz, *Statistical physics* (Butterworth-Heinmann, 1999).

[82] Y. Miroshnychenko *et al.*, Nature **442**, 151 (2006).

[83] A. I. Lvovsky and J. H. Shapiro, Phys. Rev. A **65**, 033830 (2002).

[84] D. Leibfried *et al.*, Phys. Rev. Lett. **77**, 4281 (1996).

[85] N. N. Bogolubov and D. V. Shirkov, *Introduction to the theory of quantized fields* (Moscow: Gostekhizdat, 1957), in Russian.

[86] A. N. Sissakian, O. Y. Shevchenko, A. P. Nagaytsev, and O. N. Ivanov, Phys. Rev. **D72**, 054027 (2005), hep-ph/0505214.

[87] O. Benhar, S. Fantoni, and G. I. Lykasov, Phys. Lett. **B502**, 69 (2001), hep-ph/0011302.

[88] F. Frömel, S. Leupold, and U. Mosel, Phys. Rev. **C67**, 015206 (2003), nucl-th/0111004.

[89] I. M. Vinogradov (Ed.), *Mathematical encyclopedia* (Moscow: Sovetskaia Entsiklopedia, 1977), in Russian.

[90] S. Wolfram, *The Mathematica book* (Wolfram Research, Inc., 2003).

[91] M. Sawicki and J. P. Vary, Phys. Rev. Lett. **71**, 1320 (1993).

[92] U. Mosel, *Path integrals in field theory: An introduction* (Berlin, Germany: Springer, 2004).

[93] J. Raufeisen, J.-C. Peng, and G. C. Nayak, Phys. Rev. **D66**, 034024 (2002), hep-ph/0204095.

[94] CLAS, M. Osipenko *et al.*, hep-ex/0301033, published in *Genova 2002, Gerasimov-Drell-Hearn sum rule and the spin structure of the nucleon*.

[95] W. Melnitchouk, AIP Conf. Proc. **588**, 267 (2001), hep-ph/0010311.

[96] A. D. Martin, M. G. Ryskin, and G. Watt, Phys. Rev. **D70**, 091502 (2004), hep-ph/0406225.

[97] NuSea, J. C. Webb *et al.*, hep-ex/0302019, *unpublished*.

[98] E772, P. L. McGaughey *et al.*, Phys. Rev. **D50**, 3038 (1994), [Erratum-ibid. D **60** 119903 (1999)].

[99] G. Moreno *et al.*, Phys. Rev. **D43**, 2815 (1991).

[100] A. A. Molochkov and O. Linnyk, *work in progress*.

[101] G. Altarelli, G. Parisi, and R. Pretonzio, Phys. Lett. **B76**, 351 (1978).

[102] E. L. Berger, L. E. Gordon, and M. Klasen, Phys. Rev. **D58**, 074012 (1998), hep-ph/9803387.

[103] H. Fritzsch and P. Minkowski, Phys. Lett. **B73**, 80 (1978).

[104] E. Leader and E. Predazzi, *An Introduction to gauge theories and modern particle physics. Vol. 2: CP violation, QCD and hard processes* (Camb. Monogr. Part. Phys. Nucl. Phys. Cosmol., 1996).

[105] G. Altarelli, In *Geneva 1979, Proceedings, International conference on high energy physics, Vol.2*, 727-741.

[106] F. Halzen and D. M. Scott, Phys. Rev. Lett. **40**, 1117 (1978).

[107] S. Gavin *et al.*, Int. J. Mod. Phys. **A10**, 2961 (1995), hep-ph/9502372.

[108] R. Hamberg, W. L. van Neerven, and T. Matsuura, Nucl. Phys. **B359**, 343 (1991).

[109] M. Fontannaz and D. Schiff, Nucl. Phys. **B132**, 457 (1978).

[110] K. Gallmeister, *private communication.*

[111] R. Hamberg, W. L. van Neerven, and T. Matsuura, Nucl. Phys. **B359**, 343 (1991), [Erratum-ibid. B **644**, 403 (2002)].

[112] L. Frankfurt, M. Strikman, and C. Weiss, Dijet production as a centrality trigger for pp collision at LHC, talk given at the "DPG Fruhjahrestagung", Cologne, 2004, *unpublished.*

[113] L. Frankfurt, M. Strikman, and C. Weiss, Phys. Rev. **D69**, 114010 (2004), hep-ph/0311231.

[114] O. Bruning *et al.*, LHC design report. vol. I: The LHC main ring, CERN-2004-003-V-1, *http://ab-div.web.cern.ch/ab-div/Publications/LHC-DesignReport.html.*

[115] PAX, P. Lenisa, AIP Conf. Proc. **792**, 1023 (2005).

[116] B. Stroustrup, *Die C++ Programmiersprache* (Pearson Education Deutschland, 2000), in German.

[117] W. H. Press, B. P. Flannery, S. A. Teukolsky, and W. T. Vetterling, *Numerical Recipes in C Example Book* (Cambridge Univ. Pr., 1992).

[118] T. Hahn, Nucl. Instrum. Meth. **A559**, 273 (2006), hep-ph/0509016.